Summer 2019

Development of Amperometric Microbiosensors for Neurochemical Detection

Chao Tan

Louisiana Tech University

Recommended Citation

Tan, Chao, "" (2019). *Dissertation*. 835.
https://digitalcommons.latech.edu/dissertations/835

DEVELOPMENT OF AMPEROMETRIC MICROBIOSENSORS FOR NEUROCHEMICAL DETECTION

by

Chao Tan, M.S.

A Dissertation Presented in Partial Fulfillment
of the Requirements of the Degree
Doctor of Philosophy

COLLEGE OF ENGINEERING AND SCIENCE
LOUISIANA TECH UNIVERSITY

August 2019

LOUISIANA TECH UNIVERSITY

THE GRADUATE SCHOOL

JUNE 4, 2019
Date

We hereby recommend that the dissertation prepared under our supervision by

Chao Tan, M.S.

entitled **Development of Amperometric Microbiosensors for Neurochemical Detection**

be accepted in partial fulfillment of the requirements for the Degree of

Doctor of Philosophy in Engineering

Supervisor of Dissertation Research

Head of Department

Department

Recommendation concurred in:

Advisory Committee

Approved:

Director of Graduate Studies

Dean of the College

Approved:

Dean of the Graduate School

GS Form 13
(8/10)

ABSTRACT

Abnormal neurochemical signaling is often the underlying cause of brain disorders. Electrochemical microsensors are widely used to monitor neurochemicals with high spatial-temporal resolution. This research aimed to understand and develop high-performance microsensors to detect two types of neurotransmitters: glutamate and dopamine. This work included optimizing multiple parameters used to determine performance of an enzyme-based glutamate microsensor or carbon nanomaterials-based dopamine microsensor. The parameters included sensor surfaces, glutamate oxidase, interferent exclusive layers, storage methods, self-referencing, carbon nanotube coating, polymer exclusive layer applications *et al*. The developed sensor was also tested in animals.

Tuning key parameters allowed the developed microsensors to exhibit a sensitivity as high as 530±34 nA/cm^{2}µM (Mean ± SEM), an excellent ascorbic acid selectivity of 841±54 (Mean ± SEM) for *in vitro* beaker studies. The microsensor achieved excellent long-term stability in a wet storage method. A microsensor was also used successfully for real time measuring of glutamate *ex vivo* in brain slices with a fast response time and *in vivo* in a free-behaving rat after introduced status epilepsy.

As for dopamine sensor development, a carbon nanotube modified diamond microelectrode was developed for improved detection of dopamine. Modified microelectrodes were then characterized by cyclic voltammetry, scanning electron microscopy, x-ray photoelectron spectroscopy, and electrochemical impedance spectroscopy (EIS). With regard to implantable microsensors, the as-received platinum surface with a thin nafion coating has a comparatively low sensitivity to dopamine of 0.62±0.02 µA/cm^{2}µM, but a competitive selectivity of 670±50 and limit of detection of 25 nM. Furthermore, after carbon nanotube coating, we found a drastic increase in sensitivity (45.7±2.3 µA/cm^{2}µM), and limit of detection was reduced to 5 nM. With an additional ionic-exclusive layer of thick Nafion, we obtained a high selectivity of 683±17 at the cost of sacrificing sensitivity down to 13.5±0.6 µA/cm^{2}µM. This sensor was found to last for at least one month when dry stored in the box.

In summary, this dissertation formed a systematic study of electrochemical microsensors for neurochemical detection. Improved glutamate and dopamine microsensors have been developed; this work led to a comprehensive understanding of microsensor microarrays in brain chemical application.

APPROVAL FOR SCHOLARLY DISSEMINATION

The author grants to the Prescott Memorial Library of Louisiana Tech University the right to reproduce, by appropriate methods, upon request, any or all portions of this Dissertation. It is understood that “proper request” consists of the agreement, on the part of the requesting party, that said reproduction is for his personal use and that subsequent reproduction will not occur without written approval of the author of this Dissertation. Further, any portions of the Dissertation used in books, papers, and other works must be appropriately referenced to this Dissertation.

Finally, the author of this Dissertation reserves the right to publish freely, in the literature, at any time, any or all portions of this Dissertation.

Author ______________________________

Date ______________________________

DEDICATION

This dissertation is dedicated to my wife Bo and my parents, who stood by me and encouraged me throughout my graduate studies.

TABLE OF CONTENTS

LIST OF FIGURES

LIST OF TABLES

ACKNOWLEDGMENTS

I would like to thank Dr. Prabhu U Arumugam as my research advisor. He displayed a magnificent map of science and guided me step by step in a rigorous manner, with patience at training, and at a high standard. He has provided me great advice that is without a doubt the reason for this document.

I would also like to thank Dr. Teresa Murray and Dr. Shabnam Siddiqui for giving me guidance in experiments and help along the way.

Finally, I would like to thank Mr. Haocheng Yin, Phillip T. Doughty, and Gaurab Dutta for working with and helping me obtain the results.

CHAPTER 1

INTRODUCTION

1.1 Problem Statement

According to the Information Technology and Innovation Foundation, neurological, mental disorders and diseases cost the U.S. economy more than $1.5 trillion per year, which is 8.8 percent of the gross domestic product. Diseases of the nervous system pose a significant public health and economic challenge, and one in three Americans will be affected in his or her life. Neurochemical monitoring is a critical tool for identifying the neural basis of human behavior and treating brain disorders. Studies have shown that abnormal neurochemical signaling is often the underlying cause of brain disorders such as epilepsy, Parkinson's disease and drug addiction [1,2]. For example, there is a relationship between the three main monoamine neurotransmitters in the brain (i.e., dopamine (DA), norepinephrine (NE) and serotonin (5-HT)) and specific symptoms of major depressive disorder (characterized by a persistent feeling of sadness or a lack of interest in outside stimuli). Another example is glutamate. It plays a role in the initiation and spread of seizure activity. It also plays a critical role in epileptogenesis. Microdialysis studies show an increase in the extracellular concentration of glutamate and aspartate before or during seizure onset, suggesting that either enhanced amino acid release or impaired uptake contributes to seizure initiation. Symptoms usually come with the increase or decrease of specific neurotransmitters, which suggests that specific symptoms of disease could be assigned to specific neurochemical mechanisms [3, 4]. Hence, to treat such brain disorders, it is important to quantify the dynamics of neurochemicals like dopamine (DA), glutamate, gamma-aminobutyric acid (GABA), adenosine and serotonin (5-HT). Electrochemical microsensors are widely used to monitor neurochemicals with high spatial-temporal resolution. Microfabricated microsensor microarrays have the capability of taking measurements in multiple regions of the brain in real-time. Through different modifications, it is possible to simultaneously monitor the levels of different neurochemicals, e.g., glutamate, DA, hydrogen peroxide, ascorbic acid *et al.*

1.2 Research Objectives

This dissertation is a comprehensive study of glutamate and dopamine microsensors. The research objectives of this dissertation are:

1. To understand, develop and optimize a microsensor microarray with high sensitivity, high selectivity and a low limit of detection for glutamate sensing.
2. To study the long-term performance of a glutamate sensor for *in vitro* use.
3. To study the *ex vivo* brain-slice applications of a glutamate sensor.
4. To study the *in vivo*, free-moving animal application of a glutamate sensor.
5. To understand, develop and optimize a microsensor microarray with high sensitivity, high selectivity and a low limit of detection for dopamine sensing.
6. To study the long-term performance of a dopamine sensor for *in vitro* use.

1.3 Dissertation Structure

Chapter 2 provides a necessary review of the two neurotransmitters studied in this work: glutamate and dopamine. This chapter also mentions and compares up-to-date methods used in neurochemical sensing. The mechanism of amperometry used to detect the two chemicals is discussed in detail. Chapters 4 and 5 comprise the main discussion of sensor development for glutamate and dopamine, respectively. In chapter 6, results of *ex vivo* application in brain slices and *in vivo* study in free-behaving rats are shown. Finally, Chapter 7 presents the conclusions from this research and provides recommendations for future sensor development.

CHAPTER 2

LITERATURE REVIEW

2.1 L-Glutamate & Dopamine in the Mammalian Central Nervous System

Glutamate serves multiple functions in the central nerves system (CNS). Glutamate is not only the primary excitatory neurotransmitter that dominates depolarizing postsynaptic receptors; glutamate also serves as a precursor for the inhibitory neurotransmitter γ-aminobutyric acid (GABA) that acts by hyper-polarizing receptors. Glutamate plays an important role in the energy metabolism of the CNS and plays a role in the detoxification of ammonia. Normally, glutamate is involved in most aspects of normal brain functioning, including cognitive processes, the formation of memory and the plasticity of the CNS. More importantly, glutamate contributes to the pathophysiology of many neurological disorders such as epilepsy, Huntington’s chorea, Parkinson’s disease, Alzheimer’s disease and depression [5-8]. Intracellular concentrations of glutamate are in the millimolar range of 5-15 mM, but extracellular concentrations that leak from a synapse are in the micromolar range, and glutamate also presents a high concentration (5-100 μM) in the blood and tissue fluids [6, 9, 10]. In a synapse, high glutamate concentrations overexcite ionotropic glutamate receptors, and this leads to neuronal damage and death; the process is known as excitotoxicity [11]. Glutamate is not degraded by enzymatic activity in the synapse. It is removed from the synapse through diffusion by concentration gradient and by cellular uptake, such as through excitatory amino acid transporters (EAAT) expressed on astrocytes [6, 12]. Excitotoxicity is associated with seizure activity [13]. It has been suggested that impaired glutamate uptake contributes to epileptic seizures [13-15]. Another neurotransmitter, dopamine (DA), is also an important catecholamine in the mammalian central nervous system because it is a central player in the brain "reward" system and plays a critical role in various bodily functions, e.g., motor control, motivation, cognition and several debilitating neuropathologies [1]. Dopamine (3, 4-dihydroxyphenethylamine) is an important neurotransmitter in the human brain that controls emotions from the central nervous system, and their excess release makes people feel pleasure while their deficiency could possibly cause depression or even contribute to Parkinson's disease. Further symptoms of deficiency include loss of facial expressions and inability to complete movements caused by loss of midbrain substantia nigra neurons that produce the DA. Abnormal neurochemical signaling is often the underlying cause of brain disorders.

2.2 Methods for Studying Neurochemicals

Today, microdialysis followed by high performance liquid chromatography is commonly used to withdraw and analyze extracellular neurochemical concentration *in vivo*. The microdialysis probe consists of a semipermeable membrane that allows the release of perfused solution and then collects dialysate at certain time intervals for external analysis. However, microdialysis has a comparatively low temporal and spatial resolution, and because of probe insertion, responses like necrosis and inflammation require a long recovery time [16-18]. Optical sensors based on fluorescence markers in the tissue have emerged. A glutamate-binding protein and a fluorescent protein are introduced into cells and evaluated by multiphoton fluorescence microscopy [19-21]. The process yields millisecond temporal resolution, submicron-range spatial resolution and a submicromolar detection limit. But genetically encoded protein introduced to an organism needs complex engineering. A fluorescence signal provides intensity changes but not the exact concentration of analyte, and fluorescence imaging is non-linear. Optical access is also needed. Other methods like nuclear magnetic resonance or positron emission tomography are non-invasive or less invasive but require costly large equipment and have low temporal resolution (more than a minute). A detailed comparison of different methods for *in vivo* measurement has been included in ***Table 2-1*** [22].

Table 2-1. Comparison of different methods used for *in-vivo* measurement.

Method	**Advantages**	**Disadvantages**
Microsensors	High temporal resolution (<1s) High spatial resolution (<100 µm) Low limit of detection (<1 µM)	Invasive Limited lifetime Limited analytes
Microdialysis	Low limit of detection (<1 µM) Large number of analytes Powerful method	Invasive Low temporal resolution Fluidic set-up
Nuclear magnetic resonance	Non-invasive Direct detection of chemical structure Large number of analytes	Low precision (mM) High detection limit (mM) Low temporal resolution (min) Costly, large equipment
Positron emission tomography	Non-invasive Low limit of detection (<1 µM) Large number of analytes	Radiation exposure Tracer necessary Low temporal resolution (min) Costly, large equipment
Fluorescence Imaging	High temporal resolution (<1s) High spatial resolution (<100 µm) Low limit of detection (<1 µM)	Indirect via markers Complex engineering of markers Optical access need

Microsensors rely on electrochemical techniques to record currents. Various electrochemical techniques have been used to characterize microsensors and to detect analytes. Cyclic voltammetry (CV) has been widely used for detection of electroactive species such as dopamine and hydrogen peroxide, this process involves oxidation and reduction of chemicals at the electrode surface. CV comprises scanning the potential of a stationary working electrode operating under a triangular potential waveform and recording faradaic current at oxidation potential of a specific species. Another commonly used electrochemical technique is amperometry. The mechanism of amperometry is simple: monitor a gain or loss of electrons in the presence of a fixed potential. Amperometry provides highly quantitative data for the current-time relation, and signal current usually has a very low limit of detection. In the initial short time, amperometry recorded current follows the Cottrell equation:

$$\boldsymbol{i = \frac{nFACD^{0.5}}{\sqrt{\pi t}},} \qquad \textbf{\textit{Eq. 2-1}}$$

where *i* is recorded current (A); *n* is electron transferred (#); *F* is faraday constant (96485 C/mol); *A* is electrode area (m^2); *C* is substrate concentration (mol/m^3); *D* is mass transfer coefficient (m^2/s); *t* is time (S). After steady background charging current was obtained, due to a steady potential being applied in constant-voltage amperometry throughout the experiment, we expected a steady current in recordings because it was the oxidation of analyte on electrode surfaces, ***Figure 2.1.***

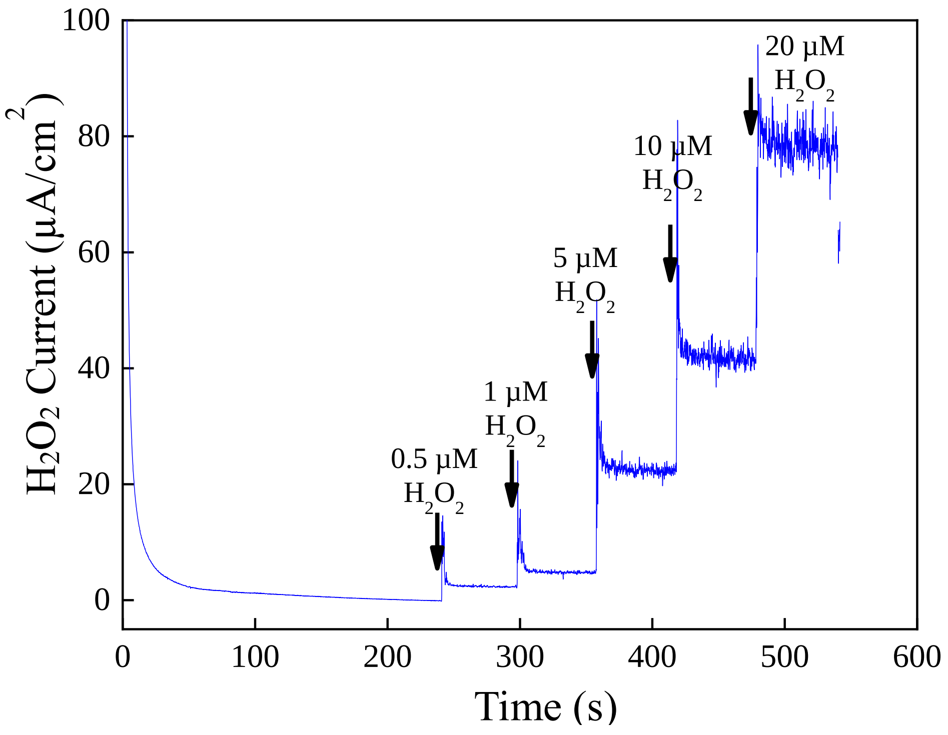

Figure 2-1. Full amperometry curve of H_2O_2 oxidation (concentrations after addition, left to right: 0.5, 1, 5, 10, 20 uM) in a stirred 1X PBS.

2.3 Microelectrodes for Neurochemical Sensing

In contrast to microdialysis, an electrochemical biosensor provides real-time detection of glutamate in a specified time window, a timeframe that can extend days. The sampling intervals vary from a few HZ to one thousand HZ, which provides excellent data acquisition capability for both *in vitro* and *in vivo* detections. The size of MEAs usually varies between 10's of microns to a few hundred microns in diameter, and the shape of electrodes is usually rectangular or circular. Enzyme-based electrochemical biosensors have proven to provide consistent, promising data with high selectivity to neurochemicals (through selective layer coating and a self-referencing technique) [23-26].

For chemical sensing, there are several metrics that should be used to evaluate a biosensor:

1. Sensitivity (faradaic current per unit molar of target analyte per unit electrode area, uA/uMcm2)
2. Selectivity (ability to distinguish the target analyte in the presence of other interference species such as ascorbic acid, uric acid *et al*.)
3. Detection limit (the lowest analyte concentration that can be detected and defined as a signal, uM)
4. Rise time T_{10-90} (the time needed to rise from 10% of signal to 90%, seconds)
5. Kinetics (the electrodes' ability to detect analyte with low overpotential, which ultimately decides the scan window in cyclic voltammetry, mV)
6. Stability and lifetime (the time a biosensor can be steadily used without obviously sacrificing performance)
7. Biocompatibility (ability to be compatible with living tissues or systems by not being toxic and not causing any immunological rejection)

Glutamate oxidase (GluOx) is the key element involved in the surface modification of enzyme-based glutamate sensors. The recombinant glutamate oxidase has a molecular weight ~140 KDa and has high substrate specificity to L-glutamate. The working mechanism of traditional GluOx-based glutamate sensors is that GluOx converts glutamate to α-ketoglutarate, hydrogen peroxide and ammonia at the presence of oxygen and water; the produced hydrogen peroxide can be detected using amperometry. The enzyme itself cannot bind to the probe surface; therefore, a good immobilization method should be able to retain the structure and functionality of enzymes after immobilization, leading to a stable enzyme matrix for long-term measurement. Crosslink, entrapment and electro-deposition are three main enzyme immobilization methods used in the literature [27-29].

Among the three methods, the more accepted method is crosslink, which uses glutaraldehyde (GDH) as the crosslinker between GluOx and stabilizing reagent bovine serum albumin (BSA). Specifically, glutaraldehyde is reactive to amine groups, which are enormously located on both GluOx and BSA surfaces. First generation glutamate sensors measure the products of enzymatic reactions that successfully diffuse to the electrode surface and give rise to faradaic current. This type of sensor relies on the enzymes to generate the electrochemical active species. The enzymes are usually classified into two categories: GluOx and glutamate dehydrogenase. For GluOx-based biosensors, GluOx is composed of an oligomeric dimer with each subunit containing α-, β-, γ- fragments, and it has two funnel-shaped inlets that allow the glutamate from the environment to reach active sites (prosthetic groups) deeply buried in the proteins [30, 31]. A co-factor flavin adenine dinucleotide (FAD) is the prosthetic group of enzymes. GluOx first converts glutamate to α-ketoglutarate, and then oxygen oxidizes reduced-form GluOx/$FADH_2$ to H_2O_2. GluOx-based biosensors monitor the concentration of glutamate by applying a constant positive potential (+0.7 V vs Ag/AgCl) to oxidize the byproduct H_2O_2. What needs attention in the mechanism is as follows: besides the main substrate glutamate, oxygen is the second most important substrate involved in the generation of H_2O_2. Therefore, this GluOx-based glutamate sensor is oxygen limited. As a result, one should expect the biosensor signal current to lose its linear relation with the substrate concentration when the analyte molarity exceeds millimolar range (oxygen depletion), ***Eq. 2-2***:

$$L - glutamate + H_2O \; + GluOx/FAD$$
$$\rightarrow \; \alpha - ketoglutarate \; + NH_3 + GluOx/FADH_2,$$

$$GluOx/FADH_2 + O_2 \rightarrow GluOx/FAD + H_2O_2,$$

$$H_2O_2 \rightarrow 2H^+ + O_2 + \; 2e^-, \qquad \textbf{Eq. 2-2}$$

Another type of first-generation glutamate sensor uses glutamate dehydrogenase (GDG) as the enzyme and nicotinamide adenine dinucleotide (NAD) as cofactor. The NADH concentration is directly proportional to the glutamate concentration, and NADH must present in the coating matrix to give rise to the signals, as given in ***Eq. 2-3***:

$$L - glutamate + H_2O + GDG + NAD^+ \rightarrow \; L - glutamate - GDG - NAD^+ + H_2O$$
$$\rightarrow \alpha - ketoglutarate \; + NH_3 + GDG + NADH + \; H^+,$$

$$NADH \rightarrow NAD^+ + H^+ + \; 2e^-, \qquad \textbf{Eq. 2-3}$$

Second generation glutamate sensors incorporated the use of a mediator, and the operation mechanism is as described below in ***Eq. 2-4***:

$$L - glutamate + H_2O \; + GluOx/FAD$$
$$\rightarrow \; \alpha - ketoglutarate \; + NH_3 + GluOx/FADH_2,$$

$$GOx/FADH_2 + 2M_{ox} \rightarrow GOx/FAD + 2M_{red} + 2H^+,$$

$$2M_{red} \rightarrow 2M_{ox} + \; 2e^-, \qquad \textbf{Eq. 2-4}$$

M_{red} and M_{ox} are the reduced and oxidative forms of mediator M and mediator will need to be pre-added to substrate or immobilized within the matrix of enzymes. Since the M_{red} is oxidized on the electrode surface and gives signal current, this method is no longer oxygen dependent and doesn’t need to apply a potential as high as +0.7 V. But the second-generation glutamate sensor is not as widely used as the first generation because of the low stability of the immobilized mediator [32-34]. Third generation biosensors rely on bio electrocatalysis, where there is direct electron transfer between enzyme and electrode. Because prosthetic groups are often well insulated and deeply buried within the active site of an enzyme, direct ET with a high rate is difficult to achieve. Nano-scale wiring elements are usually needed to ensure the signal propagation [35].

First generation glutamate sensors have been widely used for *in vitro* and *in vivo* studies using differently modified matrix, and they have proven to be very sensitive, highly selective and are usually characterized to be fast in response time [23-26,36-38]. Ammam *et al*. used electrical deposition throughout the preparation of a glutamate sensor. In this study, amperometry was used for coating of the permselective layer of polypyrrole at physiological PH and alternating current electrophoretic deposition (AC-EPD) was used for coating of both multi wall carbon nanotubes (MWCNT) (as the enzyme support) and diluted GluOx enzymes from ultrapure water. The resulting sensor turned out to be very thick (7-10 μm) and slow in response but exhibited a sensitivity as high as 384 nA/μMcm^2. With an additional outer layer of sprayed polyurethane, the sensor retained 70% activity even after 1-month of open-air storage [36].

In this work, we used electrochemical impedance spectroscopy (EIS), scanning electron microscope (SEM) and massive amperometry (AM) to characterize the glutamate biosensor. By cleaning the sensor surface and tuning the coating strategies, we developed a detailed understanding of sensor surface, glutamate oxidase, interferent exclusive layer, storage method and applied self-referencing for the *ex vivo* and *in vivo* environment. Thus, improved performance of a glutamate biosensor in terms of sensitivity, selectivity, limit of detection, lifetime *et al*. is reported here.

Neurochemicals like DA and 5-HT are electrochemically active. They are readily measured using electrochemical techniques such as fast-scan cyclic voltammetry (FSCV) and amperometry techniques with excellent spatial (micron range) and temporal (milli-second range) resolution *in vitro* and *in vivo* [39]. These methods routinely use carbon fiber microelectrodes (CFM) and glassy carbon electrodes (GCE) with sub-micromolar sensitivity [40, 41]. One of the grand challenges in this field is to develop a highly multiplexed microsensor microelectrode array (MEA)with a minimal footprint in order to detect many neurochemicals simultaneously with high sensitivity and high selectivity for a meaningful understanding of brain disorder mechanisms [42]. This requires the integration of multiple ultra-small microelectrodes into an array on a single chip. The main disadvantage of the use of ultra-small carbon fiber microelectrodes is that they have reduced electroactive surface area, with limited availability of DA adsorption sites and edge plane graphite sites, which results in poor sensitivity [43]. Several research groups have demonstrated high sensitivity by employing flame etching, laser ablation and electrochemical pretreatments (e.g., extended waveforms and overoxidation) that alter the microelectrode's surface charge [41,44–46]. However, the pretreatments are generally short-lived due to electrode loss from chemical etching [47]. Additionally, traditional electrode materials used to develop ultra-small microelectrodes lack selectivity. For example, DA and 5-HT have similar oxidation potentials (E_0) since their E_0 varies by less than 150 mV (i.e., E_0(DA)=200 mV, E_0(5-HT)=320 mV vs. Ag/AgCl), and many electrodes cannot distinguish them in the presence of ascorbic acid (AA), which is also present in the brain at much higher (100-1000 fold) concentrations [48–50]. Polymer coatings (e.g., Nafion) are now routinely used to block anionic molecules such as AA, but they increase the response time of analyte measurements [51]. This two-fold problem of achieving high sensitivity and high selectivity can be addressed by employing carbon nanotube (CNT)-enabled, three-dimensional microelectrode scaffolds that could significantly increase the electroactive/adsorption sites for higher sensitivity and electrocatalytic/defect-rich sites for higher selectivity detection. CNTs have been used to modify CFMs, graphite, GCE, carbon paste and diamond-like carbon (DLC) to increase DA adsorption sites, decrease oxidation overpotentials and improve sensitivity [41, 52-55]. For example, Sainio *et al.*, developed a complementary metal–oxide–semiconductor compatible DLC- multi walled carbon nanotube (MWCNT) macro composite electrode. The MWCNTs were grown directly on top of a DLC film and exhibited reversible charge transfer kinetics and 500 nM DA detection sensitivity as compared to a 10 µM sensitivity for a bare DLC electrode [52]. Other groups have used Nafion/CNT coatings on modified GCEs for detecting low concentrations of DA in the presence of AA and uric acid [41].

In this study, we have microfabricated and fully characterized a hybrid MWCNT film modified boron-doped ultrananocrystalline diamond (UNCD) microelectrode for DA detection in the presence of 5-HT and AA. The UNCD thin film was chosen as the bare microelectrode material because of its unique nanoscale structure–ultra-small equiaxed grains (2-5 nm diameter), inherently ultra-smooth surface (R_a of ~5-8 nm rms), excellent electrochemical properties, superior chemical inertness and dimensional stability, wide electrochemical potential window, extremely low background currents and exceptional biocompatibility for brain chemical sensing [1, 56, 57]. Several groups, including ours, have used microlithographic techniques to produce well-defined, reproducible microelectrode geometries on conductive diamond films and wires for *in vitro* and *in vivo* neurochemical measurements [50, 58–62]. MWCNT was chosen as a modifying layer for the UNCD because of its ballistic electronic properties, high surface area, excellent interfacial adsorption properties and enhanced electrocatalytic activity. Several techniques have been employed previously to modify surfaces with CNTs, namely, Chemical Vapor Deposition (CVD), drop casting and electrophoretic deposition (EPD) [63, 64]. CVD processes are quite expensive–involving cumbersome microfabrication processes, costly cleanroom equipment and high-temperature growth processes that severely limit the electrode and electrode substrate material choices [64–66]. Drop casting neither controls the thickness nor achieves a highly selective, uniform coating thickness on microelectrode surfaces [64]. However, EPD is well suited to deposit charged particles like CNTs with highly controllable coating thicknesses and precise integration of the coating on microelectrodes [67].

In this work, MWCNTs of varying thicknesses (100-500 nm) on 250-µm diameter UNCD microelectrodes were selectively deposited using EPD. For the first time, the effect of MWCNT film coatings on the electrochemical characteristics of a conductive UNCD microelectrode (sensitivity, selectivity, electrode-reaction kinetics, S/N ratio, limits of detection, film stability) have been quantitatively assessed via the detection of DA with this novel sensing technology. Cyclic voltammetry (CV), scanning electron microscopy (SEM), x-ray photoelectron spectroscopy (XPS) and electrochemical impedance spectroscopy (EIS) techniques were used to develop a detailed understanding of this new class of MWCNT-modified diamond microelectrodes for neurochemical detection. After characterization study, we applied this MWCNT coating technique to a commercial platinum-shank microelectrode and further coated it with Nafion to achieve selectivity in amperometry.

CHAPTER 3

MATERIALS AND METHODS

3.1 Reagents and Chemicals

All chemicals were reagent grade and purchased from Millipore-Sigma (St. Louis, MO, USA) unless otherwise specified. Glutamate oxidase, recombinant lyophilized powder (9.3 U/mg), was purchased from Cosmo Bio Co., LTD (Carlsbad, CA, USA). MWCNT suspension (1mg/mL) in DI water (PD15L-1-5, OD:15 ± 5 nm, Length: 1–5 µm, 5% COOH functionalized) was purchased from Nanolab, Inc (Waltham, MA). Deionized (DI) water was prepared using a three-filter purification system from Continental Water Systems (Modulab DI recirculator, service deionization polisher).

3.2 Microelectrode Array Design and Fabrication

3.2.1 8-TRK Platinum Microelectrode Array

Microsensors were prepared based on 8-TRK-type microelectrode arrays (Center for Microelectrode Technology, University of Kentucky, Lexington, KY, USA). 8-TRK MEA consisted of 4 pairs of side-by-side platinum sites (50 µm × 100 µm, 100 µm boundary-to-boundary spacing for sites within a pair and 1, 1, 2 mm distance for between pairs, ***Figure 3-1***) on a ceramic substrate (127 µm Al_2O_3) that employed a thin polyimide layer as insulation. The fabrication process is briefly described here. A photolithographic method was used for the mass fabrication of MEAs. Recording sites, connecting lines and bonding pads were patterned onto a photoresist-coated 2.5 cm × 2.5 cm ceramic substrate by exposing the photoresist with collimated UV light through a mask. Recording sites, connecting lines and bonding pads were defined by using a vacuum-sealed sputter chamber to sputter-coat the ceramic substrate with a 500 Å adhesion layer of titanium and 2300 Å layer of elemental Pt (Pt°). Besides the MEAs, all circuits were insulated with approximately 1.2 μm layer of polyimide to protect against aqueous environments and reduce crosstalk between connecting lines. Individual microelectrodes were sawed from patterned wafers using a computer-controlled diamond saw and were connected to printed circuit boards, ***Figure 3-1*** [68-70].

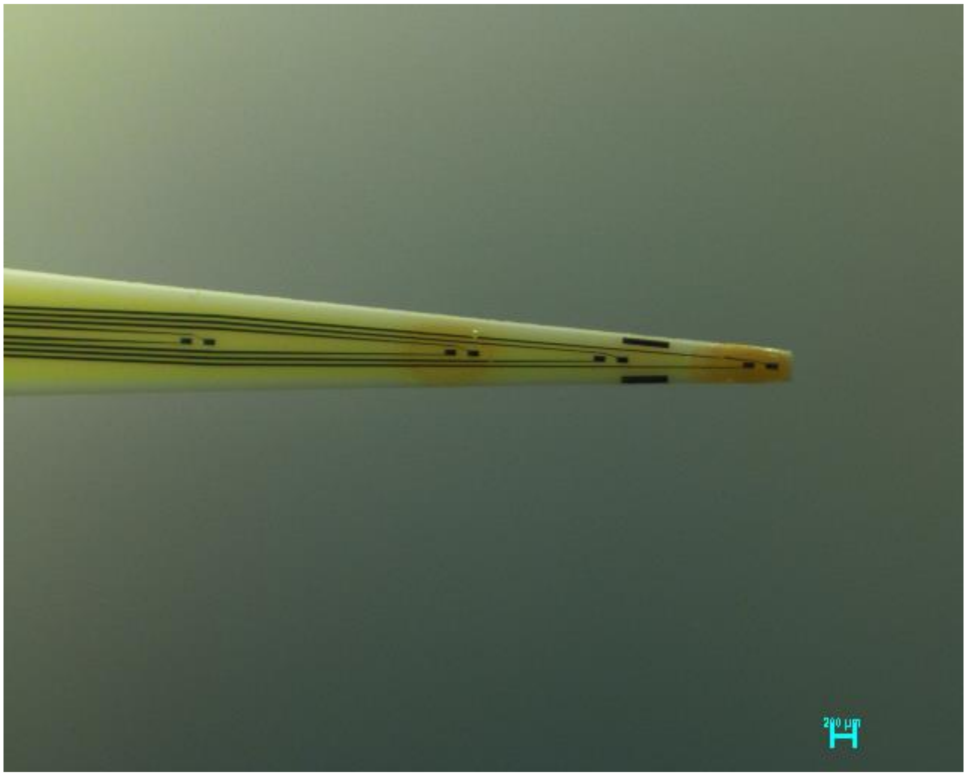

Figure 3-1. Optical picture of 8-TRK-type microelectrode arrays after enzyme coating; scale bar is 200 μm.

3.2.2 Lab on a Chip Diamond-based Microelectrode

The substrates employed for these microelectrodes were four-inch silicon wafers with a 1-µm thick thermal SiO_2 (Wafer World Inc.) surface coating. A 2-µm thick boron-doped UNCD film was then deposited with a Hot Filament Chemical Vapor Deposition (HFCVD) process from Advanced Diamond Technologies, Inc (Romeoville, IL, USA) [71-74]. The UNCD film resistivity was ~0.08 Ω·cm as measured by a 4-point probe from a witness wafer (Pro4, Lucas Labs, Gilroy, CA). The average roughness of the UNCD film was <10 nm rms based on AFM measurements (Digital Instruments, Santa Barbara, CA). Optical microlithography was used to pattern 21 chips per wafer. Each chip was micro patterned into nine individually electrically addressable 250-µm disk microelectrodes (~0.05 mm^2 geometrical area) in a 3×3 MEA format.

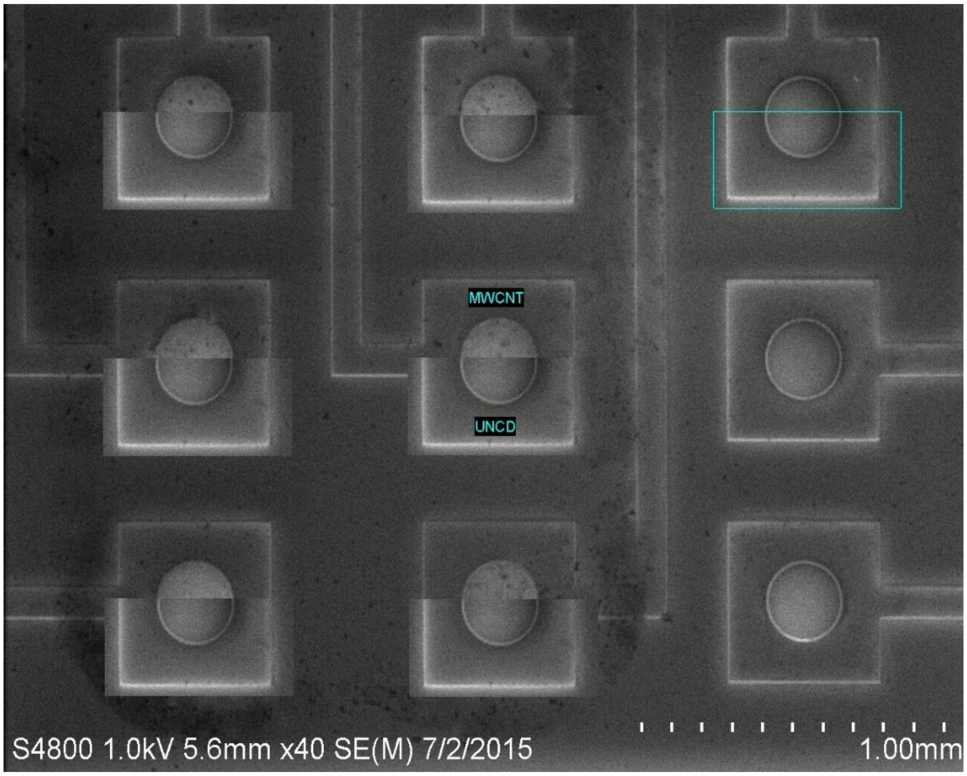

Figure 3-2. SEM picture of 3-by-3, 250 μm-diameter UNCD electrode array in a chip.

3.3 Biosensor Preparation

3.3.1 Glutamate Sensor Preparation

Prior to use, Pt MEAs were cleaned in methanol using a polymer swab. Afterward, they were electrochemically cycled in 0.05 M sulfuric acid ([–0.3 V, +1.0 V], 20 mV/s, 15 cycles) in a 2-electrode setup using a saturated calomel electrode as RE, and then they were rinsed with DI water and blown-dry with N_2. Finally, they were dried in an oven at 50 °C for 20 mins. Enzyme aliquot (1.0 U/μL) was mixed by adding GluOx in DI water upon arrival and stored as individual units under -80 °C. To immobilize the enzyme on platinum MEA, aliquot was transferred to the lab in an ice box and thawed to 4 °C in a fridge. Then it was thawed to room temperature. Stock solution was prepared by mixing 980 μL DI water with 13.3 mg BSA and then 6.7 μL of glutaraldehyde (25% in water). The prepared stock solution mixture was centrifuged 30s and kept still for 5 min, after which 1.5 µL of the mixture were added to 1 µL of GluOx (1.0 U/µL) and centrifuged to form the final enzyme solution. The final solution contains 0.8 wt% BSA, 0.1% v/v glutaraldehyde and 0.4 U/µL enzymes. A 2 µl micro syringe (Hamilton Co.) was used to manually drop cast the MEA recording sites with the enzyme solution under a Nikon stereomicroscope (Model SMZ18). One droplet of the solution (~ 0.05 µl) was suspended at the tip of the micro syringe and then applied to the paired recording sites. A 90 s interval was given if multiple drops were to be applied. All enzyme-coated MEAs were allowed at least 48 h curing before use. To avoid main interferents, 1,3-phenylenediamine (mPD) was electropolymerized onto sensor surfaces to create an exclusion layer and improve selectivity. The night before experiment day, 10 mM mPD was prepared in 1 M NaCl and then purged with nitrogen for 30 min before use. Cyclic voltammetry scans between +0.2 V and +0.8 V, using a saturated calomel electrode as a reference electrode, were performed to form a size-exclusive mPD layer. mPD coated MEAs were then rinsed with DI water and stored dry overnight.

3.3.2 Dopamine Sensor Preparation

MWCNT was diluted to 0.5 mg/mL by mixing a 1:1 ratio of as-received carbon ink with DI water. The MWCNT consisted of 98.92%wt carbon, 0.14% sulfur and 0.94% iron based on the EDAX data from the supplier. Before EPD, a 5 µM $MgCl_2 \cdot 6H_2O$ salt solution was added to the MWCNT suspension and sonicated for 30 min. This imparted a positive charge to the MWCNTs. Using a Gamry reference 600 workstation (Gamry instruments, Warminster, PA, USA), a stepwise voltage scan (−3 V to −9 V) was applied to the microelectrodes for various time durations (100 s to 500 s) until MWCNTs of desired thicknesses were deposited. After the EPD process was completed, the microelectrodes were soaked in DI water for 5 min and then gently rinsed for 30 s to remove any non-specifically bound MWCNTs and chloride salt residue. Finally, the MWCNT-modified microelectrodes were dried in an oven at 50 °C for 45 min. To increase selectivity, 8 drops of 5wt% Nafion (0.02µl per drop) were applied to paired Pt/MWCNT electrode surfaces and then cured at 165 °C for 5 minutes. Sensors were used from the second day.

3.4 Reference Electrodes

Teflon-coated Ag/AgCl wire was used as reference/counter electrode (wire diameter-200 µm bare, 280 µm coated; A-M Systems, Carlsberg, WA, USA). Preparation of the Ag/AgCl reference electrode followed this protocol: one side of the silver wire was exposed 2 mm using a scalpel and then soldered to a copper connection pin, and the other side of the silver wire was exposed approximately 1 cm. This silver wire was then used as an anode with the silver part immersed in saturated NaCl in 1 M HCl, and a platinum wire was used as a cathode. A +9 V potential was applied to this 2-electrode system using a Gamry reference 600 workstation for 20 minutes. Prepared Ag/AgCl wire was then rinsed with DI water before use. If not in use, the Ag/AgCl wires were socked in 3M NaCl solution.

3.5 Electrochemical Measurements

Measurements were performed using a FAST16mkII potentiostat system (Quanteon, LLC., Nicholasville, KY, USA) or Autolab potentiostat (PGSTAT 302N, Metrohm USA). Electrochemical impedance spectroscopy (EIS) was performed using a

3-electrode setup with a testing sensor as the working electrode (WE), a saturated calomel electrode as the reference electrode (RE) and a platinum wire as the counter electrode. The electrolyte was 5 mM Fe $(CN)_6^{3-/4-}$ in 1M KCL, 10 mV amplitude, OCP, 100 KHz- 0.1 Hz. Amperometry recordings were performed in a 2-electrode setup consisting of a testing sensor as the working electrode (WE) and a Teflon-coated Ag/AgCl wire as the reference electrode. All solutions were freshly prepared on the same day that the experiments were conducted. Experiments were carried out in a 50 mL 1X PBS solution. PH measured from 1X PBS was 7.3, and conductivity was 12.5 mS/cm. The solution was continuously stirred at 250 rpm, and temperature was maintained at 37 ± 0.2 °C using a water bath chamber, ***Figure 3-3.***

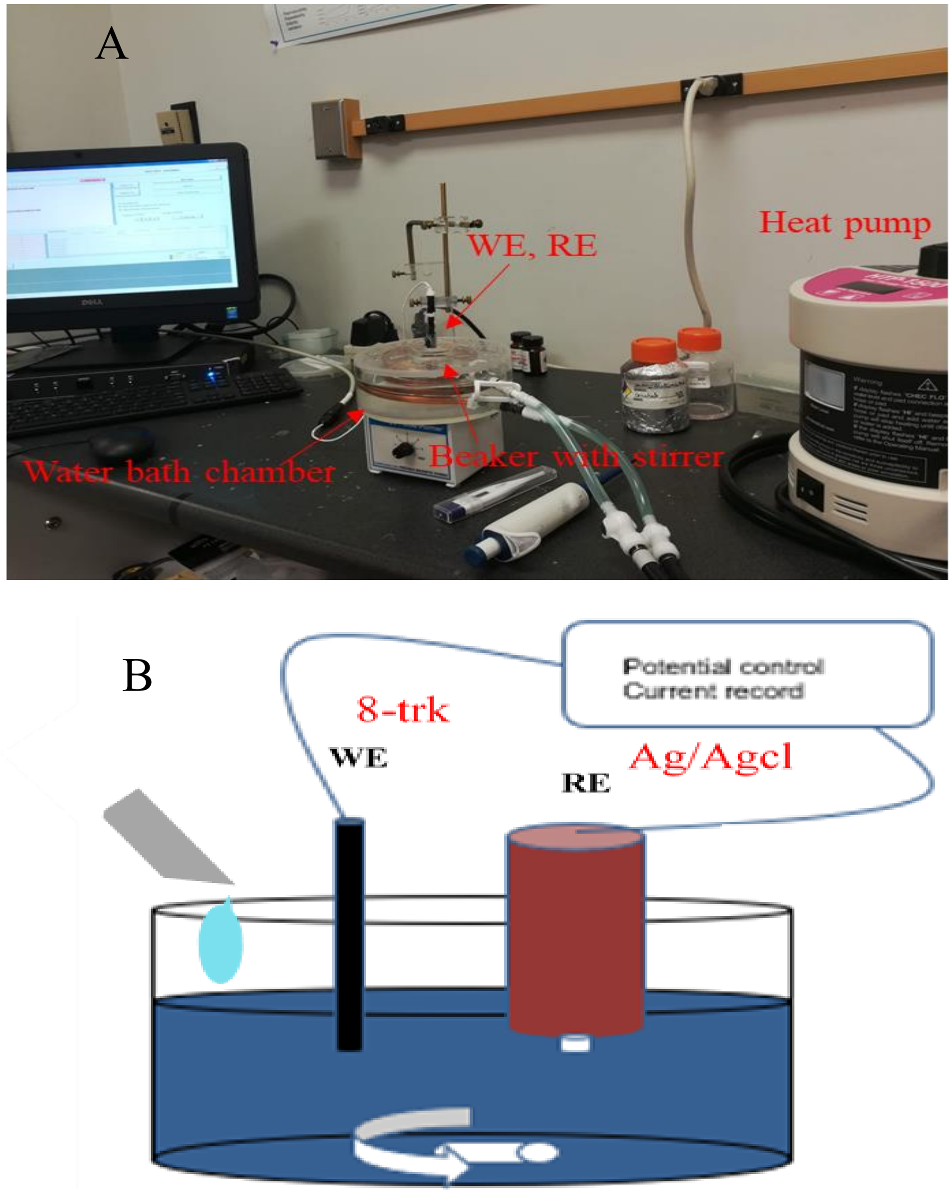

Figure 3-3. A General calibration set-up using 8-TRK-type sensor in FAST16mkII potentiostat. ***B*** Schematic diagram of in-beaker, two-electrode system consisting of an 8-trk as working electrode (WE) and a Silver/Silver chloride as reference electrode (RE).

Sensitivity (SS, nA/µMcm^2) was calculated from the slope of current density (µA/cm^2) to concentration plot at linear range. Limit of detection (LOD) was calculated as 3.3σ/SS (σ was standard deviation calculated from 20 points from the baseline when no electroactive analyte was present in the solution). Recordings were plotted and analyzed using OriginPro 2018 or Microsoft Excel. A two-tailed student's t-test was performed at two different confidence intervals to verify the difference was significant: 99.9% ($P < 0.001$) or 95% ($P<0.05$).

In amperometry calibration for the glutamate sensor, 15 mins was usually given to obtain a stable baseline. A small amount of analyte stock solution of 20 mM serotonin, 2 mM dopamine, 20 mM ascorbic acid, 360 µM uric acid and 20 mM L-glutamic acid was added to the stirred beaker, so the final concentrations after each addition of the analytes were 10 µM serotonin, 1 µM DA, 200 µM AA, 10 µM UA, 1 µM, 5 µM, 10 µM, 20 µM and 40 µM glutamate). As for the dopamine sensor, 15 min was given to obtain a stable baseline. A small amount of analyte stock solution of 2 mM dopamine and 20 mM ascorbic acid was added to the stirred beaker, so the final concentrations for all the analytes were: 5 nM, 25 nM, 50 nM, 100 nM, 200 nM, 400 nM DA and 200 µM AA.

3.6 Brain Slice Experiments

For *ex vivo* experiments, brain slices from male adult Sprague Dawley rats were used, and rats were housed in a 12 h on – 12 h off cycle room with food and water provided *ad libitum*, according to a Louisiana Tech University IACUC protocol, the *Guide for the Care and Use of Laboratory Animals*, and the AVMA Guidelines on Euthanasia. Hippocampal slices were prepared from a rat that was anesthetized using 5% isoflurane gas prior to decapitation. The brain was rapidly removed and immediately placed into ice cold artificial cerebral spinal fluid (aCSF) containing (in mM): 135 NaCl, 3 KCl, 16 $NaHCO_3$, 1 $MgCl_2$, 1.25 NaH_2PO_4, 2 $CaCl_2$, and 10 glucose, bubbled with 95% O_2/5% CO_2 (carbogen) [75]. The slicing chamber of an OTS-5000 tissue slicer (Electron Microscopy Sciences) was filled with cold aCSF, and then several pieces of 500 µm-thick coronal sections were cut and transferred to a holding chamber using a transparent transfer pipette. The holding chamber was prefilled with aCSF maintained at 35°C and bubbled with carbogen, ***Figure 3-4***. Slices were incubated for at least 60 min prior to recording. Thereafter, one slice was transferred to a liquid-air interface of a BSC1 chamber (Scientific Systems Design, Inc.) with the slice suspended on a nylon net at the liquid-air interface with continuously dripping aCSF (37°C) bubbled with carbogen. Waste products were removed by continuous suction from the recording chamber.

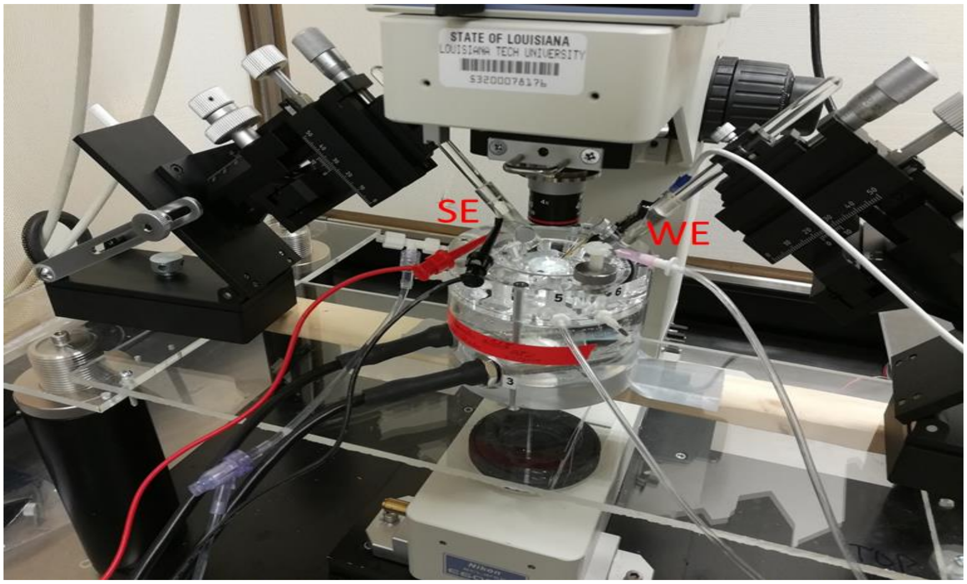

Figure 3-4. A picture of *ex vivo* experiments in a working chamber consisting of modified 8-TRK probe, Ag/AgCl wire as working, referencing electrode (WE/RE) and tungsten wire as stimulus electrode (SE).

3.7 Awake Free-Behaving Recordings

For *in vivo* experiments, 2-month-old adult male Sprague Dawley rats were used, and the rats were housed in a 12 h on – 12 h off cycle room with food and water provided *ad libitum*, according to a Louisiana Tech University IACUC protocol, the *Guide for the Care and Use of Laboratory Animals* and the AVMA Guidelines on Euthanasia. The rats were anesthetized using 5% isoflurane gas and placed on a thermal pad before any surgery operation. A 1 mm hole was drilled from the skull under the stereotaxic rat adaptor. 8-TRK probes and reference wire were implanted to the dentate/Cornu Ammonis-1 (CA1 area). Liquid polymethyl methacrylate (PMMA) was freshly prepared and dipped surround the probe shank to protect the sensor, seal the skull and avoid any further infections. Rats were sent back to the cage after surgery. Three days were usually given for optimal recovery and rewiring before the experiment.

CHAPTER 4

GLUTAMATE SENSOR DEVELOPMENT

4.1 Surface Cleaning Study

The as-received 8-TRK sensors went through microfabrication and were supposed to be cleaned before use. As for the development of an H_2O_2 (glutamate) sensor, we need to maximize the sensitivity towards hydrogen peroxide before moving on to further steps such as enzyme applications. To study the effect of cleaning on hydrogen peroxide sensitivity, electrodes (n=4) were treated step by step and calibrated using 1-40 µM hydrogen peroxide. For an as-received sensor site, the H_2O_2 sensitivity was 2443 ± 78 nA/µMcm^2; however, this number increased approximately 27% to 3113 ± 118 nA/µMcm^2 when the sensor was cleaned using only methanol. Interestingly, the sensitivity was further improved to 3845 ± 120 nA/µMcm^2 after a 30-min electrochemical cleaning in 0.05 M sulfuric acid (cyclic voltammetry, [–0.3 V, +1.0 V], 20 mV/s, 15 cycles) in a 2-electrode setup using a saturated calomel electrode as the RE, ***Figure 4-1.*** Through this two-step cleaning process, an overall improvement of around 57.4% was observed for a platinum microsensor towards sensing H_2O_2 in the linear range of 1-40 µM, and a statistically significant difference was found between sensitivity in uncleaned and two-step cleaned electrodes (student's t-test, $P<0.001$, n=4).

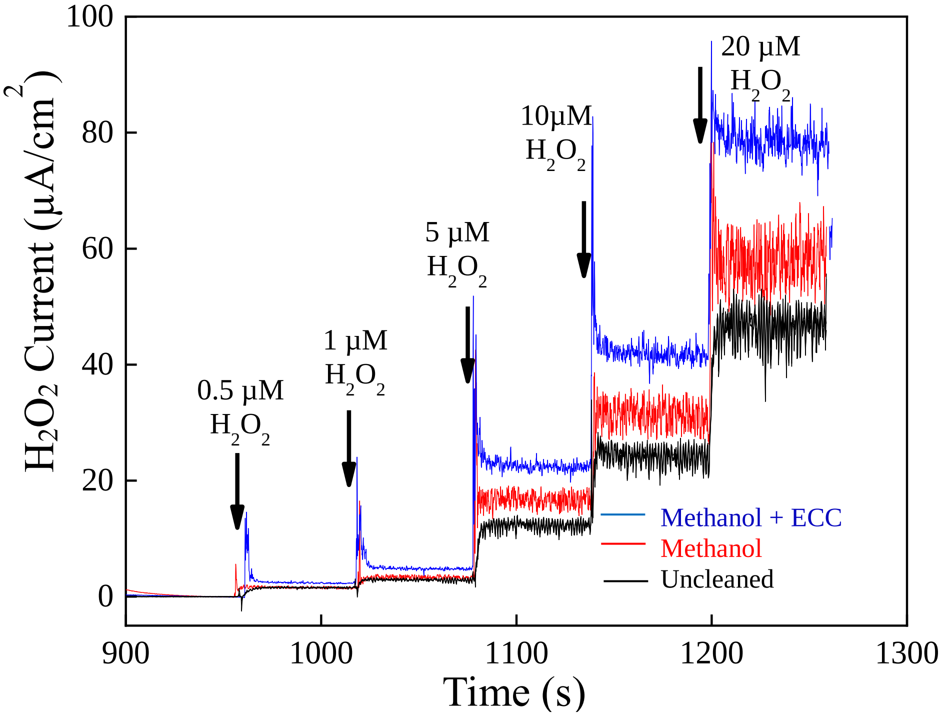

Figure 4-1. Calibration of differently cleaned bare platinum surfaces with 0.5, 1, 5, 10, 20 µM H_2O_2 (concentrations after addition, left to right), uncleaned (black), methanol cleaned (red) and methanol, electrochemically cleaned (blue). Amperometry**:** + 0.7 V *vs* Ag/AgCl wire in a stirred 1X PBS beaker; the stir rate was 250 rpm.

To help explain what has changed the surface and contributed to this increase, the EIS spectrum of an uncleaned sensor and a sensor that went through the methanol, ECC cleaning were plotted, and surface impedance models were built in ***Figure 4-2***. The solid line represents fitting to the circuit; an equivalent circuit of [$R_s(R_{ct1}Q_1)(R_{ct2}Q_2)$] was also fitted. The elements in the equivalent circuit are solution resistance (R_s), charge transfer resistance from grain boundary (R_{ct1}), charge transfer resistance from grain (R_{ct2}) and constant phase element (Q); the values are shown in ***Table 4-1***.

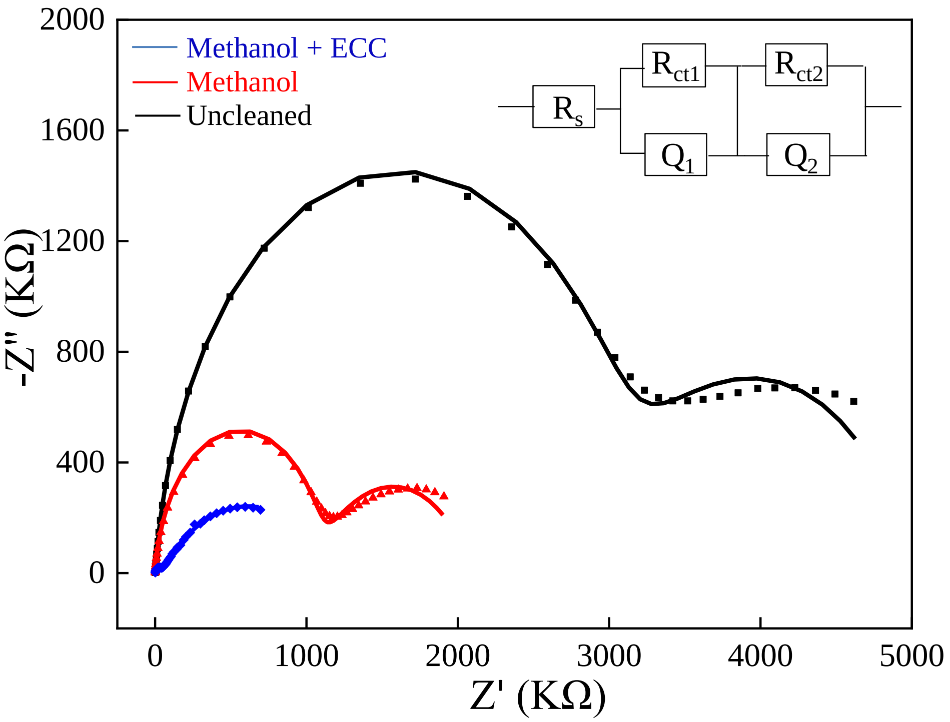

Figure 4-2. Nyquist plots and the equivalent circuit of uncleaned (black), methanol cleaned (red), methanol, electrochemically cleaned (blue) platinum microelectrodes. The electrolyte was 5 mM Fe $(CN)_6^{3-/4-}$ in 1M KCL. 10 mV amplitude, OCP, 100 KHz- 0.1 Hz.

The Nyquist plot of the EIS data of the above microelectrode depicts two arcs. The arc at lower frequencies is much broader than the arc at higher frequencies. The Bode amplitude plot shows maximum impedance of 4.6 MΩ at the lowest frequency of 0.1 Hz, and lowest impedance of 1.1 kΩ at the highest frequency of 100 kHz. The Bode phase plot shows broad phase peak for frequencies from 100 Hz to 100 kHz. The equivalent circuit model fitted to the EIS is inserted in ***Figure 4-2***. The circuit is comprised of two constant phase elements (CPE) in parallel with two charge transfer resistances together in series with a solution resistance. In general, the existence of CPE is attributed to dispersion of time constants due to surface adsorption, presence of atomic-scale inhomogeneities, various crystal planes or defects [76, 77]. The value of the 'n' parameter in CPE describes an ideal capacitor for n=1, ideal resistor for n=0, and presence of inhomogeneities for $0 < n < 1$ [78]. The circuit is comprised of two distinct parts. The first part is comprised of a constant phase element (Y_1, n_1) in parallel with a charge transfer resistance (R_{ct1}). The n_1 value of the CPE suggests the presence of atomic scale inhomogeneities [79, 80]. The grain boundaries of typical platinum electrodes are comprised of a mixture of different atoms than the grains. This suggests that the first part of the circuit corresponds to the impedance of the grain boundaries. The second part is comprised of another CPE (Y_2, n_2) element in parallel with a charge transfer resistance (R_{ct2}). The n_2 value of this circuit suggests less inhomogeneities, and such surfaces correspond to the grains of the platinum microelectrode [81]. Therefore, this part of the circuit corresponds to impedance due to grains.

The mathematical expressions of the impedances due to grain boundaries and grains can be written as

$$Z_{GB} = \frac{R_{ct1}}{1+A_1\omega^{n_1}(Cos\left[\frac{n_1\pi}{2}\right]+i\ Sin\left[\frac{n_1\pi}{2}\right])}, \qquad \textbf{\textit{Eq. 4-1}}$$

$$Z_G = \frac{R_{ct2}}{1+A_2\omega^{n_2}(Cos\left[\frac{n_2\pi}{2}\right]+i\ Sin\left[\frac{n_2\pi}{2}\right])}, \qquad \textbf{\textit{Eq. 4-2}}$$

where $A_1 = R_{ct1}Y_1$ and $A_2 = R_{ct2}Y_2$.

The coefficients A_1 and A_2 are key parameters for determining the impedances of the grains and grain boundaries. or an unclean microelectrode, the value of the coefficient A_2 for the grains is almost 100 times smaller than that of the grain boundaries. This implies that the impedance of the grain boundaries is much smaller than the impedance of the grains. Hence, grain boundaries are more conductive than the grains of an unclean microelectrode [81]. However, after methanol cleaning, the values of the parameters changed minimally for the grain boundaries but significantly for the grains. The charge transfer resistance of the grain boundaries reduced by half, and A_1 and n_1 parameters changed minimally. The charge transfer resistance of the grains reduced by three times, and the coefficient A_2 also reduced by almost three-fold. However, the n_2 parameter changed minimally. This implies that the methanol cleaning enhanced the conductivity of the grains much more than grain boundaries. But the surface heterogeneity of the grains and grain boundaries remained the same. Further, CV cycling performed for cleaning the microelectrode brought about significant changes in the values of the circuit elements. ***Table 4-1*** provides a comparison between the circuit element values and coefficients for the microelectrodes before and after CV cycling.

Table 4-1. Comparison of the circuit element values and coefficients for the microelectrodes before and after cleaning. The % errors for the circuit elements are 0–9%.

	Grain boundaries			***Grains***		
	R_{ct1}(MΩ)	***n_1***	***A_1***	***R_{ct2}(MΩ)***	***n_2***	***A_2***
Uncleaned	1.91	0.763	0.531	3.09	0.935	0.714×10^{-2}
Methanol Cleaned	0.976	0.717	0.435	1.09	0.945	0.170×10^{-2}
CV cycling cleaned	0.981	0.546	0.753	0.0374	0.973	0.0056×10^{-2}

After CV cycling, the charge transfer resistance of the grain boundaries remained almost the same, but the n_1 value further reduced. This implies that CV cycling has etched the grain boundaries' surface, which has caused atomic-scale heterogeneity. The charge transfer resistance of the grains was reduced by almost 30-fold, and the A_2 parameter became almost negligible. Such a reduction in charge transfer resistance may also be due to an increase in the kinetic constant of the electron transfer between the electrode and the electrolyte, which means the electron transfer between the electrode and electrolyte became a kinetically fast process. The n_2 value of the grains suggests the grains behave more like an ideal capacitor. Thus, CV cycling of the Pt microelectrode makes grains far more conductive than the grain boundaries. Also, it decreases the grains' deviation from an ideal capacitive behavior and enhances CPE behavior of the grain boundaries. Interestingly, such a process of cleaning the electrode surface brings clear distinction between the atomic-scale electrochemical behavior of the grains and grain boundaries.

4.2 Enzyme Concentration Study

Sensitivity is one of the key factors taken into consideration when designing a microsensor. To determine the best enzyme concentration with the highest reaction rate, the GluOx concentration study was performed. Results are presented in this section. Different concentrations of GluOx (0.05, 0.1, 0.2, 0.4, 0.6 and 0.8 U/µL) were mixed in a protein matrix and then coated on the 8-TRK probes' surface. When preparing these small solutions, we only changed the GluOx concentrations. BSA and glutaraldehyde percentages in each matrix were kept the same (0.8 wt% BSA and 0.1% v/v glutaraldehyde). Four drops were coated on paired sensors for each GluOx concentration using a micro syringe and approximately 0.05 µL for each drop. After coating, the sensors were cured at room temperature for two days. These microsensors were then calibrated in a glutamate range of 1-40 µM in a stirred beaker containing 50 mL 1X PBS. The amperometry curve is shown in ***Figure 4-3.A,*** and a glutamate sensitivity to enzyme concentration relation was plotted in ***Figure 4-3.B***. Interestingly, within the concentration range from 0.05 to 0.8 U/µL, the sensitivity of the glutamate sensor started from a very low value of 41.9 ± 2.5 nA/µMcm^2 (0.05 U/µL) and reached a peak of 555.9 ± 19.0 nA/µMcm^2 at 0.4 U/µL. But the sensitivity did not continue increasing after 0.4 U/µL. Instead, sensitivity decreased between 0.4-0.8 U/µL and finally dropped to 379.2 ± 20.6 nA/µMcm^2 when the enzyme concentration was as high as 0.8 U/µL. Thus, an optimized enzyme concentration found here was 0.4 U/µL. Experiment were measured and averaged from six sets of data and sensitivity differences with 0.4 U/µL were significant (student's t-test, $P<0.05$, $n=6$).

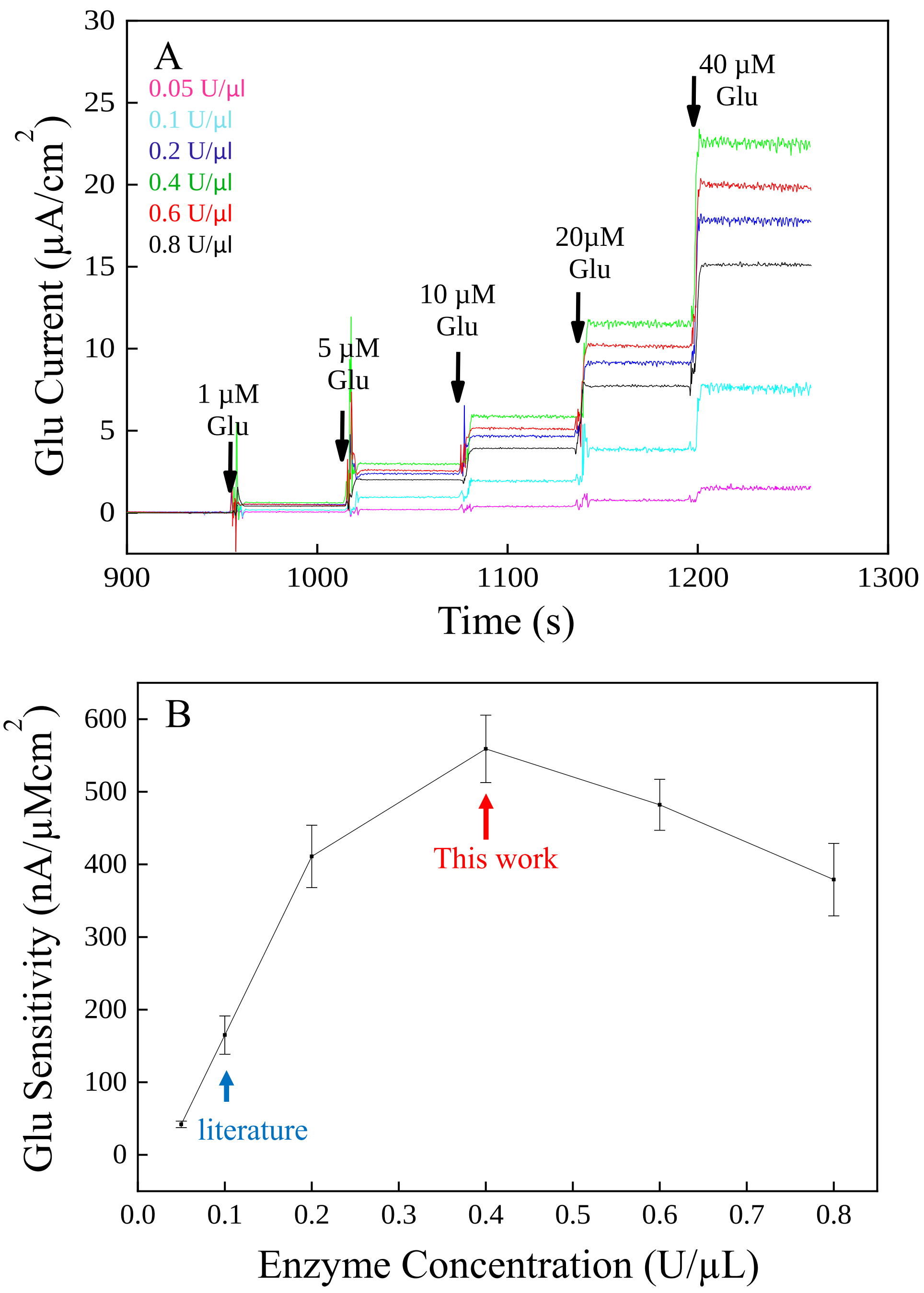

Figure 4-3. A) Calibration of enzyme-modified platinum surfaces with 1, 5, 10, 20, 40 µM glutamate (concentrations after addition, left to right). The platinum surfaces were coated with different concentrations of enzymes, unit in U/µL: 0.05 (magenta), 0.1 (cyan), 0.2 (blue), 0.4 (green), 0.6 (red), 0.8 (black); 4 drops were used for each concentration, approximately 0.05 µL for each drop. Amperometry: + 0.7 V *vs* Ag/AgCl wire in a stirred 1X PBS beaker; the stir rate was 250 rpm. ***B)*** Dependence of glutamate sensitivity on enzyme concentrations.

This result indicates a bell-shaped curve of sensitivity with the increasing concentration of GluOx, which can be explained by Michaelis Menten theory in low GluOx concentrations and by thickness and ionization state influence in high GluOx concentrations. In Michaelis Menten theory, the reaction rate is proportional to the enzyme concentrations; therefore, higher current density is expected from a comparatively higher enzyme concentration. But when the GluOx concentration exceeds 0.4 U/µL, the reaction rate decreased rather than saturated afterwards. One explanation is that as the concentration of GluOx increases (BSA and glutaraldehyde remained same), the thickness of the protein finally stays on the sensor surface after curing increases, and this thicker layer should cause some difficulty for H_2O_2 diffusion (***Figure 4-4.*** would better support this). Another explanation is that when there is concentrated GluOx in the enzyme matrix, electrostatic repulsions between negatively charged glutamate molecules and negatively charged GluOx (isoelectric point PH(I)=6.2) may reduce the access of glutamate to the enzyme matrix, and thus reduce resulting current density [82]. A similar study has never been reported in the literature, and unfortunately, commonly used GluOx concentrations as described in many papers were usually 0.1 U/µL [23-25, 28, 36, 38].

4.3 Enzyme Thickness Study

Another experiment was performed to study the behavior of the sensor as the loading of enzymes changes. In this section, microsensors were modified with 1-16 drops of enzymes (0.41 µm-8.83 µm). Thicknesses were measured and averaged from six sets of data (n=6) using a Keyence 3D Laser Scanning Confocal Microscope (model VK-X150). The drop-casted enzyme used the optimized GluOx concentration from previous study: 0.4 U/µL. The amperometry curves are shown in ***Figure 4-4. A,*** and sensitivity calculated from a linear glutamate range 1-40 µM was as plotted in ***Figure 4-4.B***. It was found that the sensitivity keeps decreasing when a thicker layer is applied. From 837.3 ± 30.4 nA/µMcm^2 (0.41 µm), it dropped to 288.7 ± 19.7 nA/µMcm^2 (8.83 µm). An increase in rise time $T_{10\text{-}90}$ was also observed from 1.9 s (2.23 µm) to 8.0 s (8.83 µm) with 20 µM glutamate in the beaker, ***Table 4-2***.

Table 4-2. Sensitivity and thicknesses of surfaces coated differently with enzymes.

Surface types	**Thickness (µm)**	**Sensitivity (nA/cm^{2}µM)**
Pt/1GluOx	0.41±0.03 µm	837.3 ± 30.4
Pt/2GluOx	0.86±0.11 µm	771.7 ± 24.0
Pt/4GluOx	2.25±0.11 µm	563.7 ± 17.9
Pt/8GluOx	4.79±0.37 µm	369.8 ± 14.5
Pt/16GluOx	8.83±0.73 µm	288.7 ±19.7

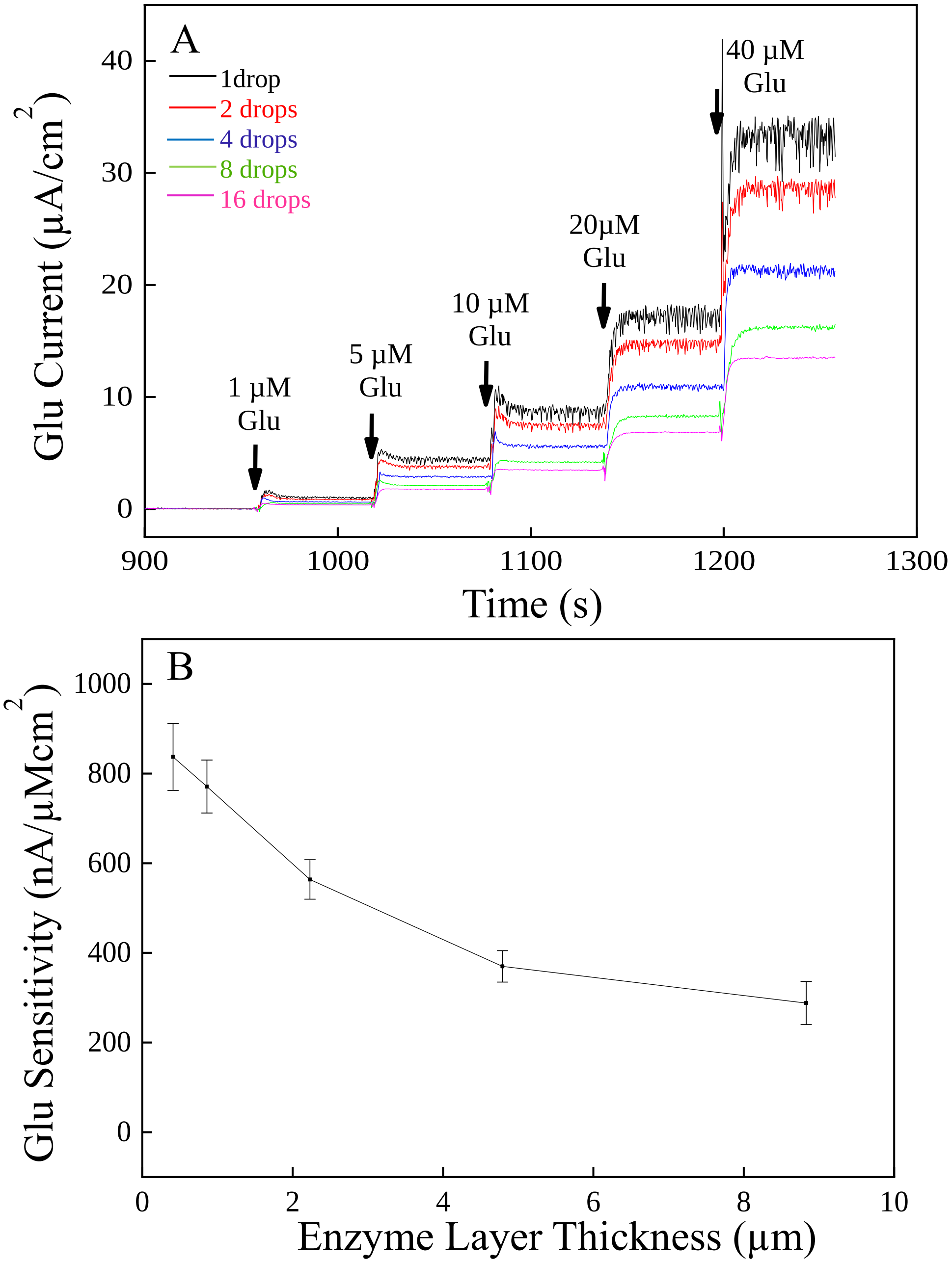

Figure 4-4. A) Calibration of enzyme-modified platinum surfaces with 1, 5, 10, 20, 40 µM glutamate (concentrations after addition, left to right). The platinum surfaces were coated with 0.4 U/µL, vary enzyme loadings, unit in drops: 1 (black), 2 (red), 4 (blue), 8 (green), 16 (magenta), approximately 0.05 µL each drop. Amperometry: + 0.7 V *vs* Ag/AgCl wire in a stirred 1X PBS beaker; the stir rate was 250 rpm. ***B)*** Dependence of *g*lutamate sensitivity on enzyme thickness.

This decrease in sensitivity with increase in enzyme thickness indicates that even in a stirred-beaker experiment, enzymes from different layers (with respect to a platinum surface) have access to different amounts of glutamate due to the diffusion barrier. In other words, enzymes that are coated at inner layers and closer to the platinum surface turn out to have less enzymatic reaction with glutamate. Then, the decrease in sensitivity when a thicker layer is applied would be explained by less generated H_2O_2 from the inner-layer enzymes and the difficulty to diffuse H_2O_2 that is generated from the outer layers. This diffusion barrier of enzyme matrix is further confirmed by detecting H_2O_2 directly in beaker. The H_2O_2 signal currents were found to decrease as coating thickness increased, ***Figure 4-5.*** Though H_2O_2 is a small molecule, as the enzyme matrix barrier was stacked from 0.41 µm to 8.83 µm, the sensor gradually lost the amount of H_2O_2 that could diffuse to the platinum surfaces: 3240 ± 43 nA/µMcm^2 (bare) to 740 ± 36 nA/µMcm^2 (16 drops). The same principle applied to H_2O_2 generated from enzymes. Though there were more enzymatic reactions in the matrix as the loading of enzymes increased, the enzymes in the inner layer accessed less glutamate and contributed less to the signal current. Though enzymes in the outer layer still accessed enough glutamate and generated lots of H_2O_2, the H_2O_2 generated faced a greater barrier before diffusing to the platinum surface and contributing to signal current. Therefore, with loading of thicker enzymes, the signal current decreases.

From this set of experiments, the relation between glutamate biosensor sensitivity and enzyme thicknesses was well established, and one can tune the thickness of the enzyme matrix according to need. A thinner enzyme layer has advantages over a thicker layer in terms of higher sensitivity, and it provides a faster response for acute experiments. However, for chronic or *in vivo* studies, too thin a layer of enzymes is not desired because enzyme layers will foul in those conditions due to adsorption of proteins, tissue inflammation, bacteria *et al*., thus losing their functionality.

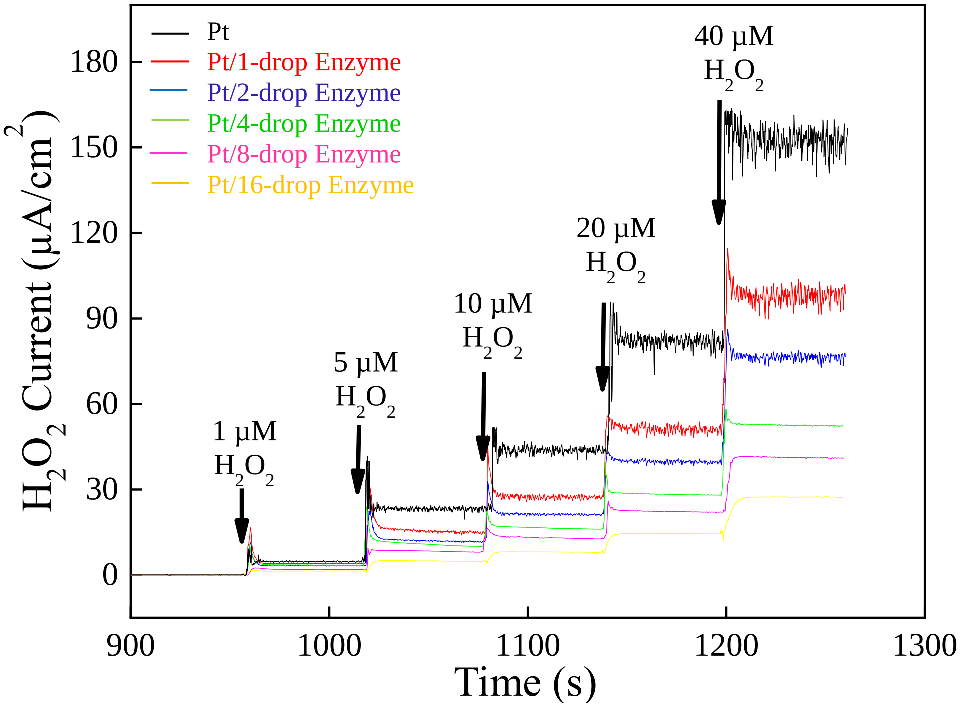

Figure 4-5. Calibration of enzyme-modified platinum surfaces with 1, 5, 10, 20, 40 µM H_2O_2 (concentrations after addition, left to right). The platinum surfaces were coated with 0.4 U/µL, vary enzyme loadings, unit in drops: 0 (black), 1 (red), 2 (blue), 4 (green), 8 (magenta), 16 (orange), approximately 0.05 µL each drop. Amperometry: + 0.7 V *vs* Ag/AgCl wire in a stirred 1X PBS beaker; the stir rate was 250 rpm.

4.4 Applied Potential Study

A simple but fundamental question that needs be addressed is what potential should be applied to sense glutamate (H_2O_2). To scientifically answer this question, different potentials were chosen in glutamate calibration, and resulting currents were compared. In this set of experiments, glutamate sensitivity under different potentials (+0.5, +0.6, +0.7, +0.8, +0.9 V) was calculated. Results showed clear and consistent data from three sensors that the highest sensitivity is from +0.7 V, and a bell-shaped relationship exists between sensitivity percentage ($SS/SS_{+0.7\ V}$) and applied voltage range, ***Figure 4-6***. Therefore, we conclude here that the optimal potential is +0.7 V.

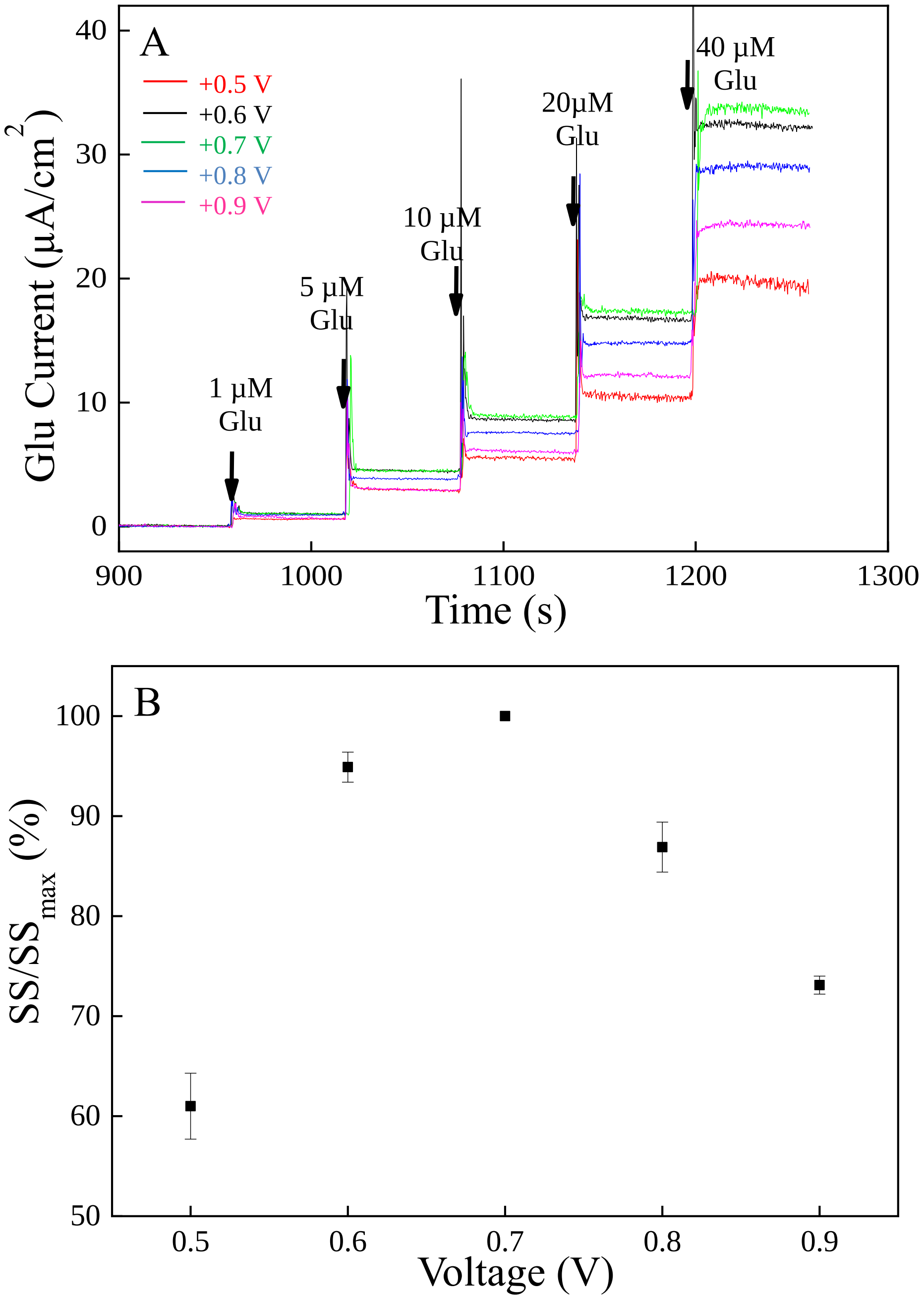

Figure 4-6. A) Calibration of enzyme-modified platinum surfaces with 1-40 µM glutamate (concentrations after addition, left to right). The platinum surfaces were coated with GluOx: 0.4 U/µL, 1 drop, approximately 0.05 µL per drop. Amperometry: + 0.5 to + 0.9 V *vs* Ag/AgCl wire in a stirred 1X PBS beaker; the stir rate was 250 rpm. ***B)*** Dependence of sensitivity/maximum sensitivity ratio on applied voltage with maximum sensitivity always obtained from +0.7 V.

4.5 Long-Term *In Vitro* Stability Study

In this section, stability of microsensors with two different enzyme coatings 0.1, 0.4 U/µL (4 drops, 0.05 µL/drop) were explored through a long-term use study. The differently coated microsensors were calibrated with 1-40 µM glutamate for an entire one month. Thirty days of recordings (1-hour of use per day, 30 days) showed how the sensitivity towards glutamate changed with time and indicated the *in vitro* lifetime of those differently coated biosensors. Amperometry curves for each microsensor from day 1, 10, 20 and 30 were plotted in ***Figure 4-7***. There was an obvious sensitivity loss for 0.1 U/µL after 30 days (81±10%, averaged from 4 long-term studied sensors, n=4) while sensitivity was retained well for higher loading of 0.4 U/µL GluOx. In short, the optimized microsensors (0.4 U/µL, 4 drops) had a long-lasting lifetime, and data was in the best range compared with related works from other literature [25, 28, 36].

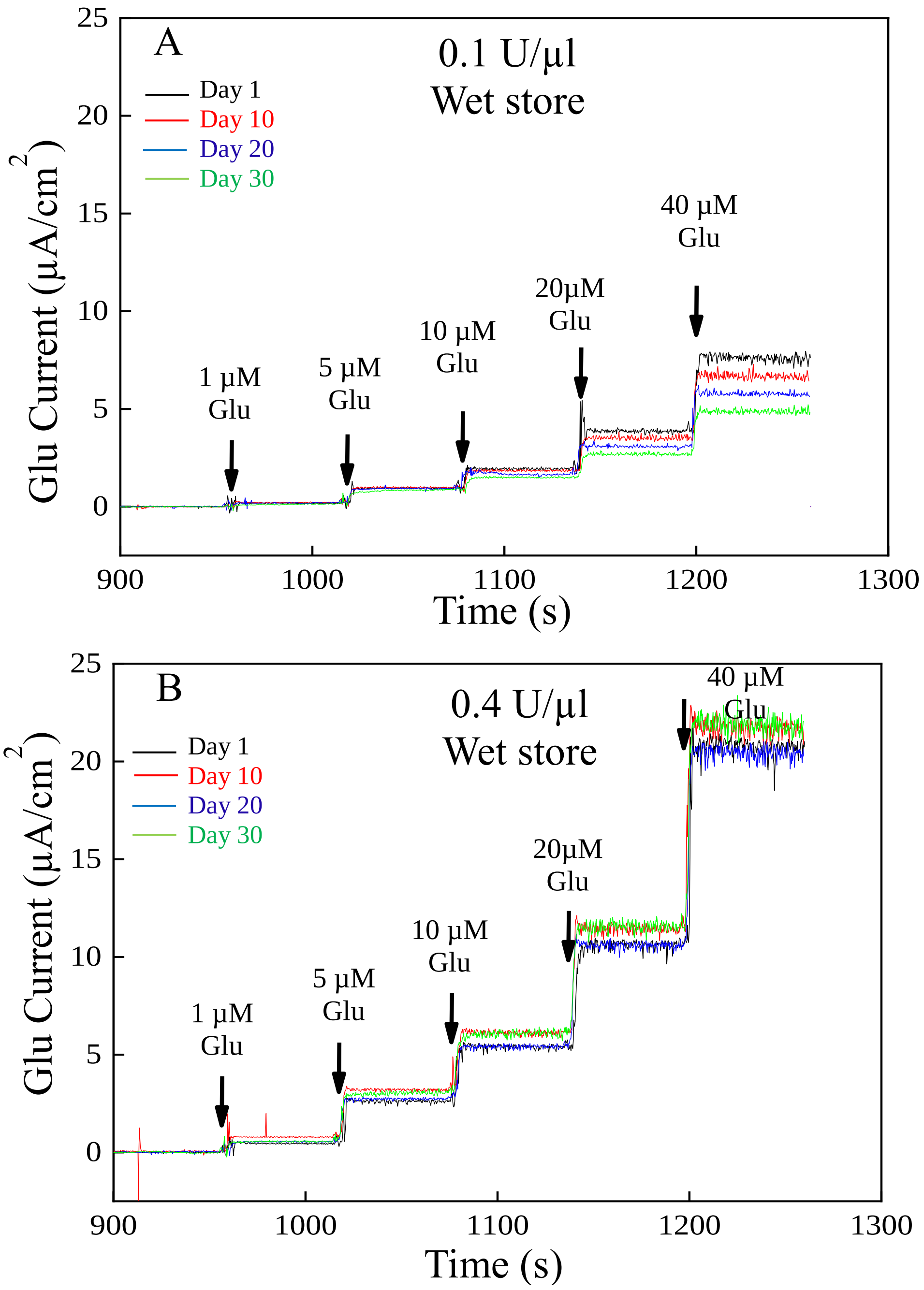

Figure 4-7. 30 days' calibrations of enzyme-modified platinum surfaces with 1, 5, 10, 20, 40 µM glutamate (concentrations after addition, left to right). The platinum surfaces were coated with two different concentrations of enzymes: ***A.*** 0.1, ***B.*** 0.4 U/µL, 4 drops for each concentration and approximately 0.05 µL per drop. Amperometry: + 0.7 V *vs* Ag/AgCl wire in a stirred 1X PBS beaker.

Interestingly, microsensors with an enzyme loading of 0.4 U/µL even showed a slight sensitivity increase at the end of one-month experiments ($SS_{30} > SS_1$, 111±5%, averaged from 4 long-term studied sensors, n=4), which might be attributed to several reasons described below: 1) the intrinsic properties of the GluOx enzyme—the active sites are prosthetic groups deeply buried in the enzyme, leading to the assumption that the enzymes were well protected and stabilized through the cross-link reaction with BSA and glutaraldehyde; 2) a higher concentration of enzyme matrix ensured enough enzymatic reaction with glutamate molecules throughout the one-month experiments; 3) the microsensors were stored in DI water in a dark place and at room temperature unless being used in experiments. Storing the sensors continuously in DI water keeps this enzyme healthy (fresh DI water supplied every 4 days). From this set of data, storing the sensors in a 4-8 °C fridge seems to be avoidable for glutamate sensor because thawing of the enzymes is commonly believed to be harmful to enzyme activity. It was also found that sensors that were dry stored after use experienced a drastic decay in sensitivity with time. (***Figure 4-8*** plots indicate the glutamate sensitivity change over days on this surface: day 1 (red), day 3 (black), day 6 (blue), day 9 (green), day 12 (magenta). Statistics show a 70±2 % decrease after 12 days. Sensors were used half an hour every day and dry stored at RT in the dark when not in use)

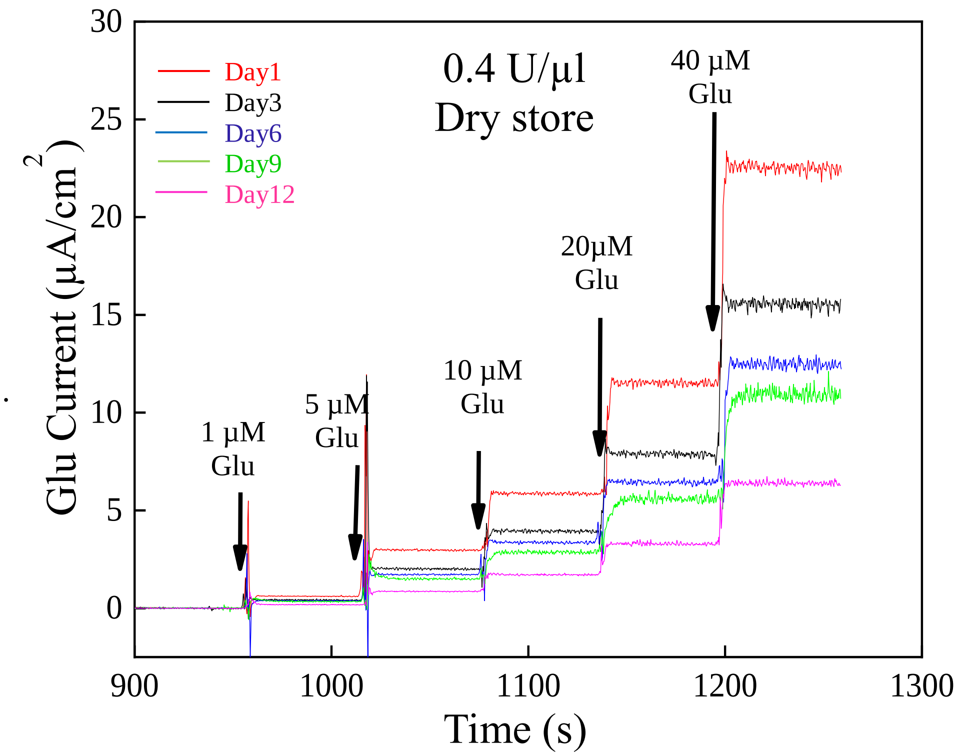

Figure 4-8. Calibration of enzyme-modified platinum surfaces with 1, 5, 10, 20, 40 µM glutamate (concentrations after addition, left to right). The platinum surfaces were coated with 0.4 U/µL, 4 drops of enzymes, approximately 0.05 µL per drop; This sensor was dry stored if not in use. Amperometry: + 0.7 V *vs* Ag/AgCl wire in a stirred 1X PBS beaker; the stir rate was 250 rpm.

4.6 Exclusive Layer Study

Selectivity of a neurochemical biosensor is vital for the sensor's performance because it indicates the accuracy of *ex vivo* and *in vivo* data. A sensor without a coating of perm-selective layer will detect all the chemicals that could be oxidized on its surface, e.g., serotonin (5-HT), dopamine (DA), ascorbic acid (AA), uric acid (UA) and norepinephrine (NE) are electroactive species that could contribute to obvious faradaic current when present on the platinum surface. To screen those interferents, two different types of strategies are usually applied: size-exclusive film or charge-exclusion coating. A size-exclusive layer such as cellulose acetate or polyphenol is commonly used as the perm-selective layer to impede large interferents while still allowing the penetration of small analytes like H_2O_2 or NO. A charge-exclusion coating relies on the repulsive force between ions; e.g., Nafion, polypyrole, polyaniline and polythiophene are all negatively charged polymers that could block negatively charged ions like ascorbic acid. In this work, the night before experimental day, 10 mM 1,3-phenylenediamine (mPD) was prepared in 1 M NaCl and then purged with nitrogen for 30 min before use. Cyclic voltammetry scans between +0.2 V and +0.8 V, using a saturated calomel electrode as a reference electrode, were performed to form a size-exclusive mPD layer. mPD coated MEAs were rinsed with DI water and stored dry overnight. ***Figure 4-9*** gives the electropolymerization formula of mPD and shows the reduced signal in glutamate after coating of mPD.

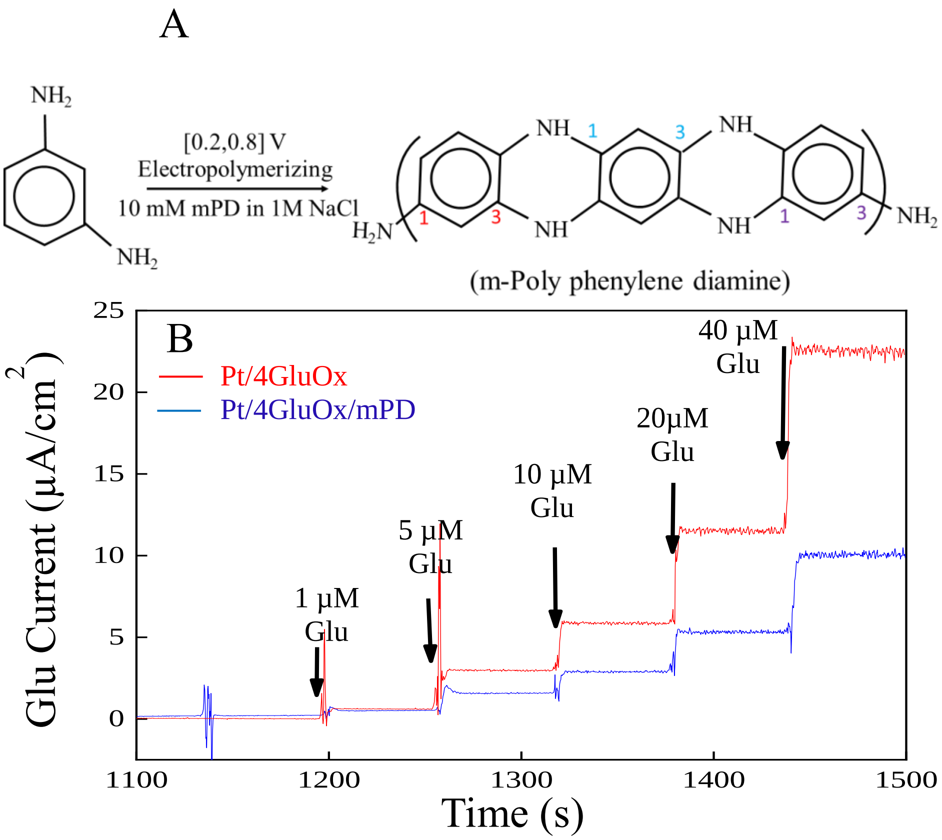

Figure 4-9. A) Electro-polymerization of mPD to poly-mPD. ***B)*** sensing of 1-40 µM glutamate (concentrations after addition, left to right): Pt/Enzyme (red), Pt/Enzyme/mPD (blue) coating uses a concentration of 0.4 U/µL, 4 drops and approximately 0.05 µL per drop; mPD was deposited between [0.2, 0.8V] with a scan rate of 50 mV/s. Amperometry: + 0.7 V *vs* Ag/AgCl wire in a stirred 1X PBS beaker; the stir rate was 250 rpm.

First, we can see a decrease in glutamate sensitivity of approximately 60 %. This finding has been reported in many papers because mPD screens molecules by size [29]. Second, the coating-like enzyme layer could only reduce interferent currents but not eliminate them, ***Figure 4-10***. The resulting interferent currents are still significant compared to the glutamate signal without mPD coating, ***Table 4-3***. But with mPD coating, it was found that at this moment our sensor gave no signal to 5-HT, DA and UA, GABA, NE, choline and acetylcholine. In addition, only a minimal leak current was seen from the main interferent ascorbic acid, thus, a high selectivity to those 8 interferents.

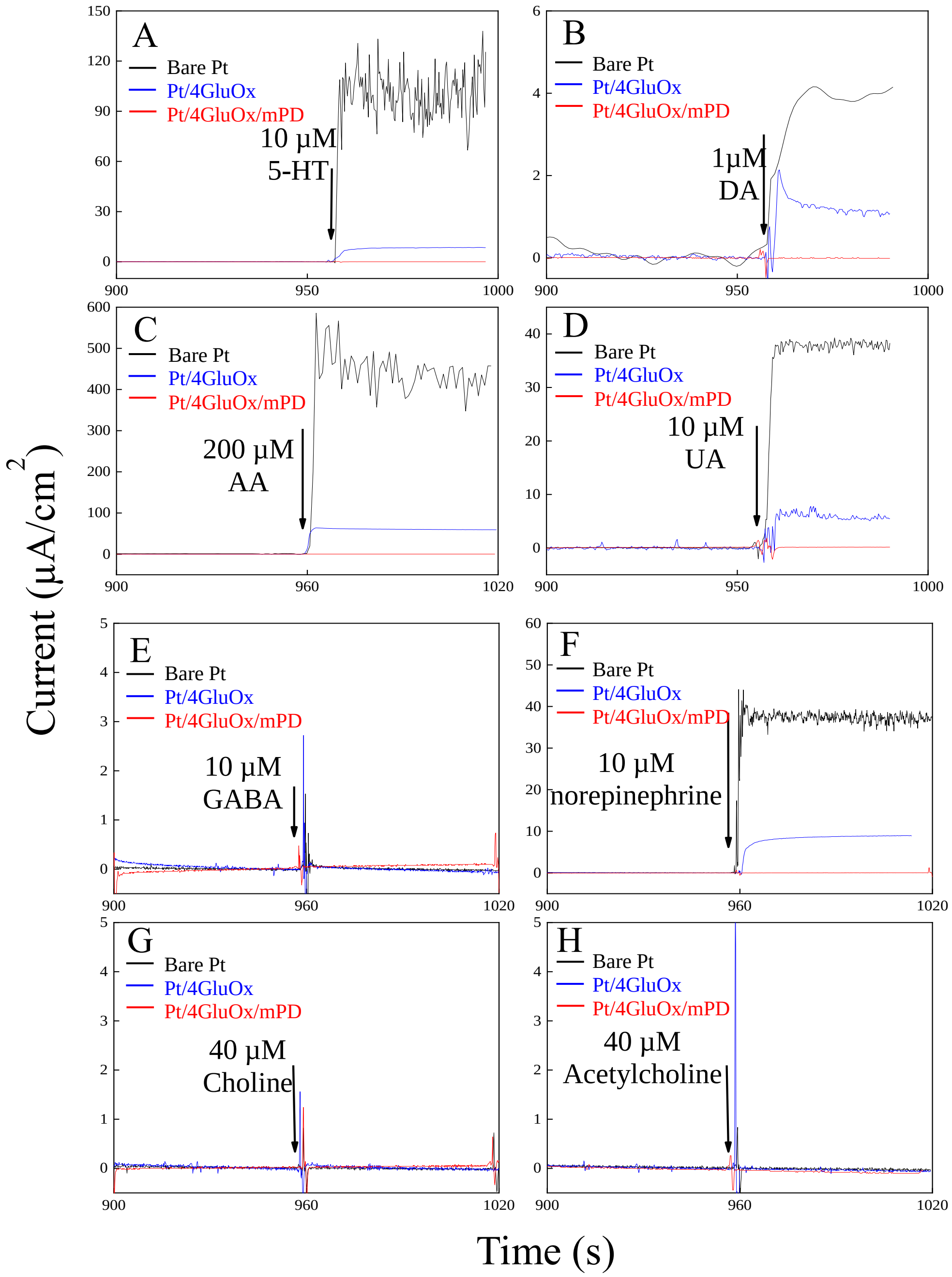

Figure 4-10. Calibrations of enzyme-modified platinum surfaces with 10 µM 5-HT, 1 µM dopamine, 200 µM ascorbic acid, 10 µM uric acid, 10 µM GABA, 10 µM norepinephrine, 40 µM choline, 40 µM acetylcholine (concentrations after addition, top to down): Pt (black), Pt/Enzyme (blue), Pt/Enzyme/mPD (red); enzyme coating used a concentration of 0.4 U/µL, 4 drops and approximately 0.05 µL per drop, Amperometry: + 0.7 V vs Ag/AgCl wire in a stirred 1X PBS beaker; the stir rate was 250 rpm.

Table 4-3. Effect of enzyme and mPD coating to interferent currents on a platinum surface. 4 drops enzymes, 0.4 U/µL and approximately 0.05 µL each drop. mPD coating uses CV [0.2, 0.8 V], 5 mV/s, 40 min. Amperometry: + 0.7 V vs Ag/AgCl wire in a stirred 1X PBS beaker, the stir rate is 250 rpm.

Analyte	**Pt/4GluOx Sensitivity (nA/µMcm^2)**	**Pt/4GluOx Glu/Inter Selectivity**	**Pt/4GluOx/mPD Sensitivity (nA/µMcm^2)**	**Pt/4GluOx/mPD Glu/Inter Selectivity**
1-40 µM Glutamate	564±18		240±7	
10 µM 5-HT	800±45	0.71±0.04	0	infinite
1 µM DA	1000±100	0.57±0.04	0	infinite
200 µM AA	257.5±23.5	2.22±0.16	0.8±0.2	300.4±9.4
10 µM UA	530±10	1.07±0.03	0	infinite
10 µM GABA	≈0	infinite	0	infinite
10 µM NE	873±37	0.65±0.03	0	infinite
40 µM Choline	≈0	infinite	0	infinite
40 µM Ach	0	infinite	0	infinite

Two different mPD electropolymerization parameters were used here: 50 mV/s (mPD parameter 1) and 5 mV/s (mPD parameter 2), 40 min, 10 mM mPD in 1 M NaCl. Here, mPD was firstly coated by scanning platinum surfaces between [0.2, 0.8 V] with the two parameters, separately. Then, 1 or 4 drops of enzymes were drop cast on mPD, respectively. The coating and curing followed the protocol described in Chapter 2**.** After standard calibrations, comparing those sensors that were coated with same mPD parameter but different enzyme thicknesses in ***Figure 4-11. A & B*** showed that the Pt/mPD/Enzyme sensors exhibit 1) excellent selectivity because the interferent current is ignorable compared to the signal current, and no drastic difference in interferent current was observed from those sensors, which was expected since mPD has superiority in impeding large molecules; 2) sensitivity decreased with the increase in enzyme thickness, specifically from 530±34 nA/cm^{2}μM (Pt/mPD1/Enzyme, one drop) to 362±14 nA/μMcm^2 (Pt/mPD1/Enzyme, four drops) and from 446±18 nA/μMcm^2 (Pt/mPD2/Enzyme, one drop) to 256±22 nA/μMcm^2 (Pt/mPD2/Enzyme, four drops). A student's t-test was performed with a $P<0.001$, $n=6$. This decrease in sensitivity with the loading of thicker enzyme corresponds with our thickness study in previous plots in ***Figure 4-4.*** The decrease in sensitivity as enzyme thickness is increased will also change Glu/AA selectivity because glutamate sensitivity from a thicker enzyme-coated sensor (four drops) is lower than a thin layer (one drop). Thus, AA selectivity as high as 841±54 was observed for a Pt/mPD1/Enzyme (one drop) and as low as 406±35 for a Pt/mPD2/Enzyme (four drops). What needs mention here is that those numbers are among the best when compared to other literature, ***Table 4-4***. A limit of detection calculated from our best sensitivity of 530±34 nA/cm^{2}μM (Pt/mPD1/Enzyme, one drop) is 69±5 nM. If we compare the sensors coated with same enzyme thickness but different mPD parameters (mPD1 & mPD2), we find that for both thicknesses (one or four drops enzymes), the mPD1 always gives higher sensitivity than mPD2. Specifically, 530±34 nA/cm^{2}μM (Pt/mPD1/Enzyme, one drop, red) decreased to 446±18 nA/μMcm^2 (Pt/mPD2/Enzyme, one drop, black) in ***Figure 4-11.A,*** and 362±14 nA/μMcm^2 (Pt/mPD1/Enzyme, four drops, red) decreased to 256±22 nA/μMcm^2 (Pt/mPD2/Enzyme, four drops, black) in ***Figure 4-11.B***. A student's t-test showed significance of $P<0.05$ for both thicknesses. Similar findings also apply to Pt/Enzyme/mPD matrix in ***Figure 4-11*** as blue and green traces. This could be due to a more smooth and thicker structure of mPD layer formed at mPD2 than at mPD1.

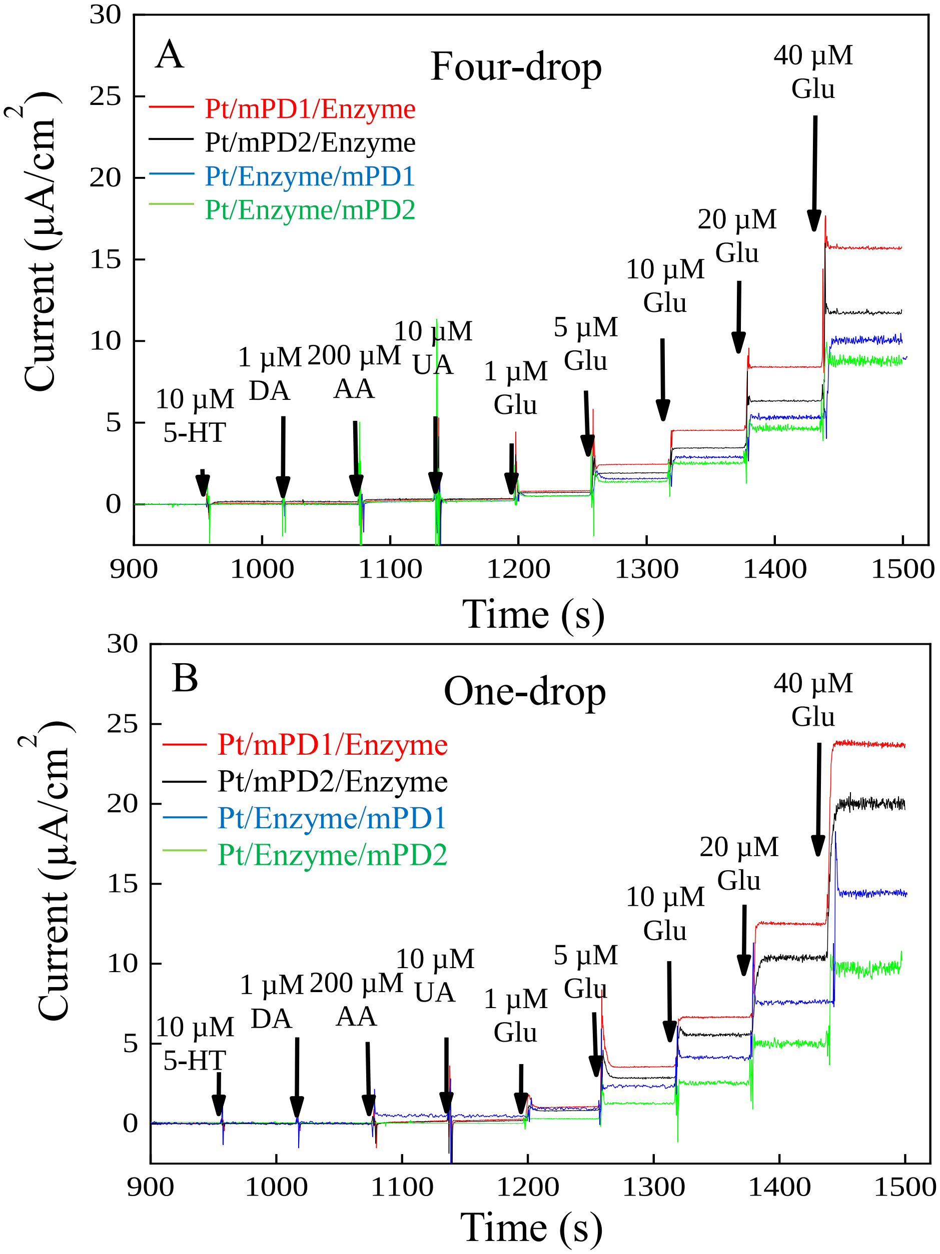

Figure 4-11. Calibration of enzyme- and mPD-modified platinum surfaces with (concentrations after addition, left to right):10 µM 5-HT, 1 µM dopamine, 200 µM ascorbic acid, 10 µM uric acid and 1, 5, 10, 20, 40 µM glutamate. The platinum surfaces were modified differently: ***A.*** four drops of enzyme. ***B.*** one drop of enzyme, 0.4 U/µL, approximately 0.05 µL per drop; Pt/mPD1/Enzyme (red), Pt/mPD2/Enzyme (black), Pt/Enzyme/mPD1 (blue), Pt/Enzyme/mPD2 (green). mPD1,2 indicates two different electric parameters during mPD coating, 50 mV/s and 5 mV/s. Amperometry: + 0.7 V *vs* Ag/AgCl wire in a stirred 1X PBS beaker; the stir rate was 250 rpm.

Table 4-4. Related work of 1st generation glutamate biosensor.

Sensor type	Coating method	Sensitivity (nA/µMcm^2)	Selectivity (Glu/AA)	LOD (nM)	Stability
Pt/Nafion/GluOx-BSA-GDH	0.2U/µL, 5 drops, 0.1µL/drop	63±9.6	389±153	980±90	Dry @-4 °C, store in PBS[23]
Pt/Nafion/GluOx-BSA-GDH	0.1U/µL, 4 drops, 0.1µL/drop	320±20	100±14	1820±170	Not mentioned[24]
Pt/mPD/GluOx-BSA-GDH	0.1U/µL, 4 drops, 0.1µL/drop	216±8	143	220	In PBS, 28 days, 75%[25]
Pt/mPD/GluOx-Silica	0.1U/µL, [-0.9V, -1.2V], 10-40 s	279±2	109	5	Dry @-4 °C, 4 months, 95%[28]
Pt/PPY/MWCNT/GluOx/PU	0.1U/500µL, AC-EPD 30mins 250 V_{pp}	250	Infinite	<300	Air dry @ RT, 1 month, 100%[36]
Pt/GluOx-BSA-GDH/mPD	0.1 U/µL, dropcast, 0.1µL/drop	110±10	161±34	N.A.	N.A.[38]
Pt/GluOx-BSA-GDH/mPD Pt/mPD/GluOx-BSA-GDH	0.4 U/µL, dropcast, 0.05µL/drop	212-530	244-841	69-173	In water & avoid light, 2months, 100%, this work

Another factor when designing a sensor matrix is more interesting: whether to coat with mPD before or after enzyme applications. This is a question that is important for all enzyme-based sensors but not yet well understood and properly explained. In this section, Pt/Enzyme/mPD and Pt/mPD/Enzyme (four and one drops of enzymes) were studied and compared in terms of sensitivity and selectivity. We have not found significant differences in rejecting interferent current from the Pt/Enzyme/mPD or the Pt/mPD/Enzyme design because they both give very low current to the main interferent AA ($<0.2\ \mu A/cm^2$ for 200 µM AA). But we did observe a higher sensitivity from the Pt/mPD/Enzyme than the Pt/Enzyme/mPD, 21±7% higher for mPD2 (black *vs* green) and 51±6 % higher for mPD1 (red *vs* blue); all used 4 drops of enzymes in ***Figure 4-11. A.*** Similarly, sensitivity was 74±8% higher for mPD2 (black *vs* green) and 39±7% higher for mPD1(red *vs* blue); all used one drop of enzymes in ***Figure 4-11. B***. To better understand those differences, a list of experiments was performed, and we only used 4 drops of enzymes and the mPD1 parameter in these experiments. Some additional data are shown in ***Figure 4-12***.

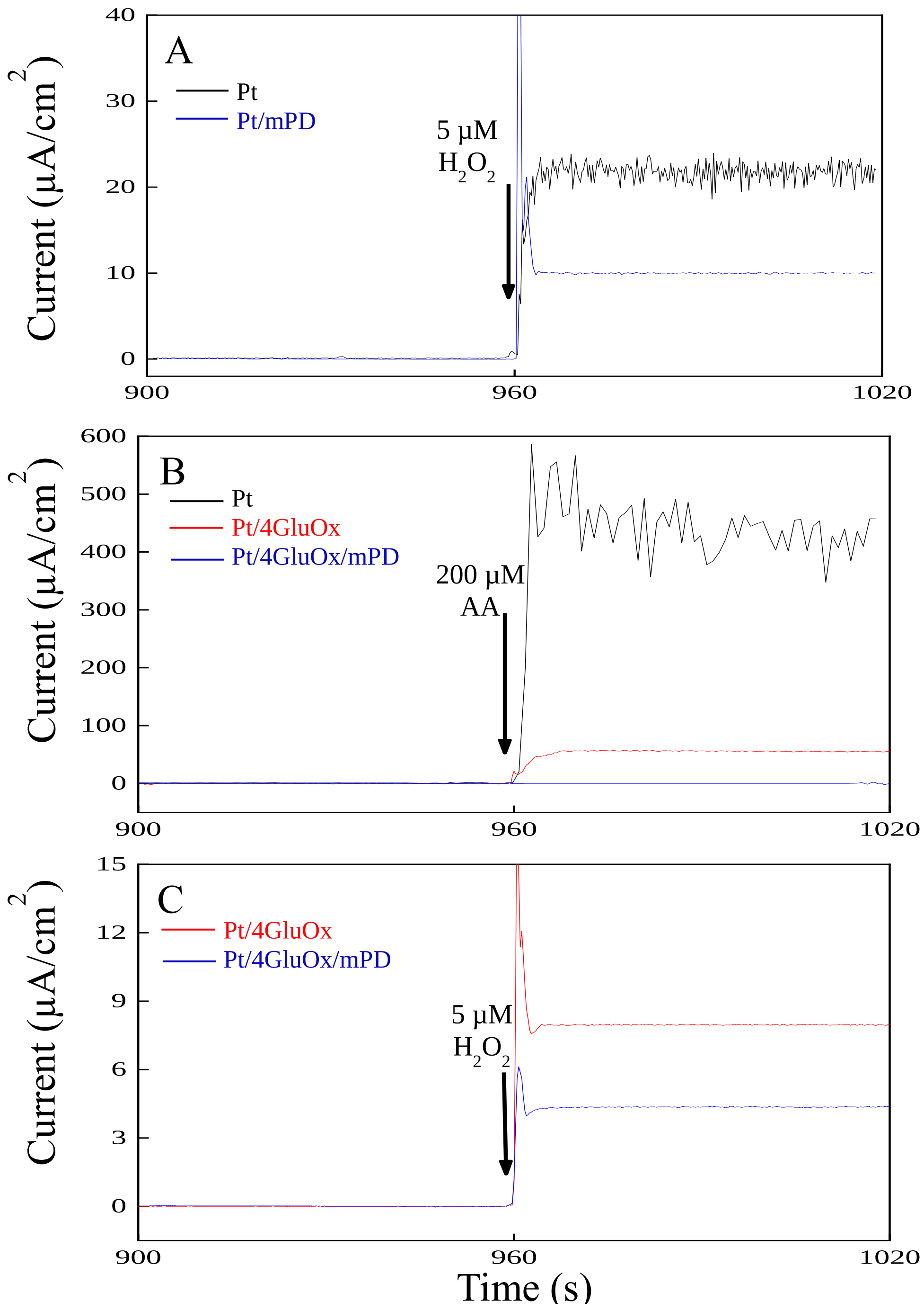

Figure 4-12. Calibrations of differently modified platinum surfaces with ***A).*** 5 µM H_2O_2: Pt (black), Pt/mPD1 (blue); ***B).*** 200 µM AA: Pt (black), Pt/Enzyme (red), Pt/Enzyme/mPD1 (blue), ***C.*** 5 µM H_2O_2: Pt/Enzyme (red), Pt/Enzyme/mPD1 (blue), enzyme coating used a concentration of 0.4 U/µL, 4 drops and approximately 0.05 µL per drop; mPD was deposited between [0.2, 0.8V] with a scan rate of 50 mV/s. Amperometry: + 0.7 V *vs* Ag/AgCl wire in a stirred 1X PBS beaker; the stir rate was 250 rpm.

We think three reasons together contribute to higher sensitivity when mPD was chosen as the inner layer. The first reason is size-exclusive theory. In accordance with this theory, mPD as a size-exclusive layer rejects more glutamate (five-carbon molecule) than H_2O_2 (small molecules). In other words, in a Pt/Enzyme/mPD1 matrix, using mPD1 as the outer layer would impede a greater amount of glutamate from accessing enzymes. This was further confirmed by observing a 57±2 % current loss when the mPD1 layer was coated (compared to the Pt/Enzyme data shown in ***Table 4-5***); but in the Pt/mPD1/Enzyme matrix, the mPD layer does not impede the outer glutamate from reaching the enzymes, but it built barriers for the byproduct H_2O_2 to reach the platinum surface (only a 35±3 % loss in glutamate current, if comparing Pt/mPD1/Enzyme to Pt/Enzyme, ***Table 4-5***). Therefore, due to H_2O_2's small size, a size-exclusive layer of mPD rejects more glutamate than H_2O_2, ***Figure 4-13***. That might explain why in many papers exclusive materials were used as the inner layer and why high sensitivity (>200 nA/µMcm^2) was reported [24, 25, 28, 36].

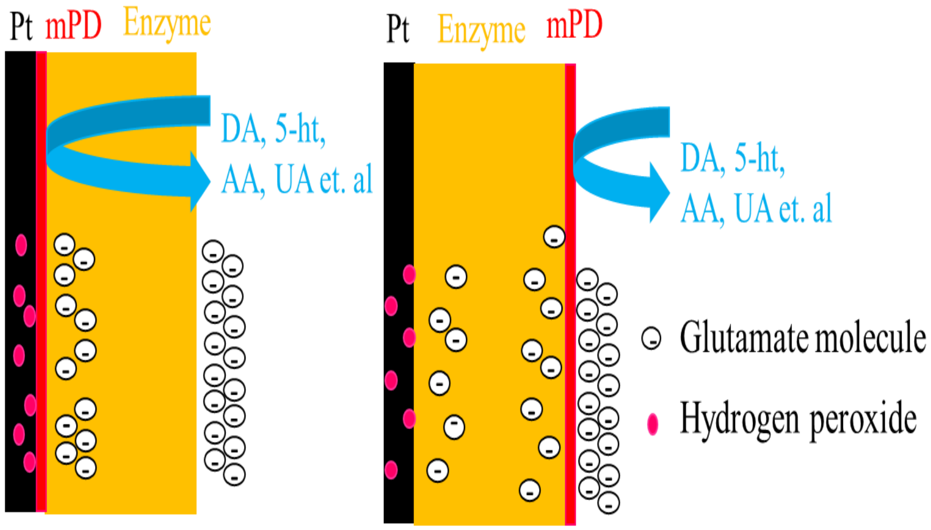

Figure 4-13. Schematic diagram of effect of mPD coating before and after enzyme loading.

However, this size-exclusive theory cannot explain everything. In ***Table 4-5*** and ***Figure 4-12.A***, for a Pt sensor with only mPD1, we found there was only a 40±3 % H_2O_2 signal current left compared to bare, cleaned Pt surfaces; but we also know that in the Pt/mPD1/Enzyme, the glutamate current is still as high as 65±3 % of the Pt/Enzyme when mPD was placed directly on the Pt, the signal current did not reduce to 40±3 % as direct oxidation of H_2O_2 does. Similarly, for direct detection of 5 μM H_2O_2 or 200 μM AA in ***Figure 4-12.B&C***, the Pt/Enzyme/mPD1 blocks 45±4 % of the H_2O_2 current and 97±1 % of the AA current when compared with currents from Pt/Enzyme (see ***Table 4-5)***. If we only apply size-exclusive theory, glutamate's molecule size is between AA and H_2O_2 but more close to AA; thus, glutamate should be impeded more than 70% when mPD is coated on GluOx, but the fact is that we still got a 43±2 % glutamate signal after the mPD coating. For both cases, the resulting currents were higher than the expected value, if only size-exclusive theory is applied. We think the extra currents came from an accumulation of H_2O_2 after introducing the mPD layer. In the Pt/Enzyme/mPD, after the mPD blocked a great amount of glutamate, another thing changed. The generated H_2O_2 was hard to diffuse outside the matrix to the beaker, whereas before the mPD coating, H_2O_2 generated could diffuse either to the Pt surface or to the solutions. The same principle applied with the Pt/mPD/Enzyme as with the additional mPD layer: diffusion of the generated H_2O_2 to the Pt surface became hard, the consumption rate was slower, and there was accumulation of H_2O_2 close to the surface. 3) We think hydrate use and dehydrate storage of the microsensor resulted in decreased enzyme activity. The coating of mPD as an outer layer requires enzyme layers to go through such a process because mPD layer was chemically coated in mPD solution and again dry stored overnight before the experiment. We think such a process would make some reduction in sensitivity as shown in ***Figure 4-8***.

Table 4-5. Glutamate and H_2O_2 sensitivity from different types of sensors, used a concentration of 0.4 U/µL, 4 drops and approximately 0.05 µL per drop, mPD1 protocol cyclic between [0.2, 0.8V] with a scan rate of 50 mV/s.

Sensor Type	**Glu Sensitivity (nA/µMcm^2)**	**Sensor Type**	**5 µM H_2O_2 Current (nA/cm^2)**
Pt/4Enzyme	555.9±19.0	Pt	23±1.24
Pt/mPD1/4Enzyme	362±14.0	Pt/mPD1	9.2±0.65
Pt/4Enzyme/mPD1	240±8.0	Pt/4Enzyme	7.7±0.68
		Pt/4Enzyme/mPD1	4.2±0.15

Though microsensors coated using mPD as the inner layer did show higher sensitivity, leaving the enzyme layer exposed to the *ex vivo* or *in vivo* environment did not seem wise because the enzymes could decay due to adsorption of proteins, tissue inflammation, bacteria *et al*., thus losing their functionality. Therefore, we decided to coat mPD on top of the enzymes. In the short term, mPD2 did not seem to have advantages in sensitivity compared to mPD1, but we did find its superiority in impeding interferents for the long-term. When using a Pt/Enzyme/mPD matrix (four drops of enzymes) for a two-month *in vitro* stability study, we found sensors employing mPD1 as the exclusive layer failed faster, thus leaking more interferent current during this long-term use (***Figure 4-14.***). After two months of use (1-hour use every two days, 60 days), overall interferent current increased from 0.2±0.01 µA/cm^2 to 1.6±0.17 µA/cm^2 (mean ± SEM, n=4) for the microsensor that used the mPD1 parameter while it only increased from 0.19±0.02 µA/cm^2 to 0.6±0.14 µA/cm^2 for microsensor that used the mPD2 coating parameter. This is probably because mPD2 has a thicker layer than mPD1 because mPD2 on bare platinum is 83 ± 4.2 nm, and mPD 1 on bare platinum is only 37±2.4 nm thick. Glutamate sensitivity for both types of sensors still retained well at $SS_{60} > SS_{1}$, ***Figure 4-15,*** which is consistent with our study as shown in ***Figure 4-7***. Thus, for consideration of more reliable data from an *ex vivo* environment or any long-term *in vitro* use of sensors, we would recommend choosing mPD2 (5 mV/s) as the electrical parameter for the mPD coating because the environment in those situations is more challenging.

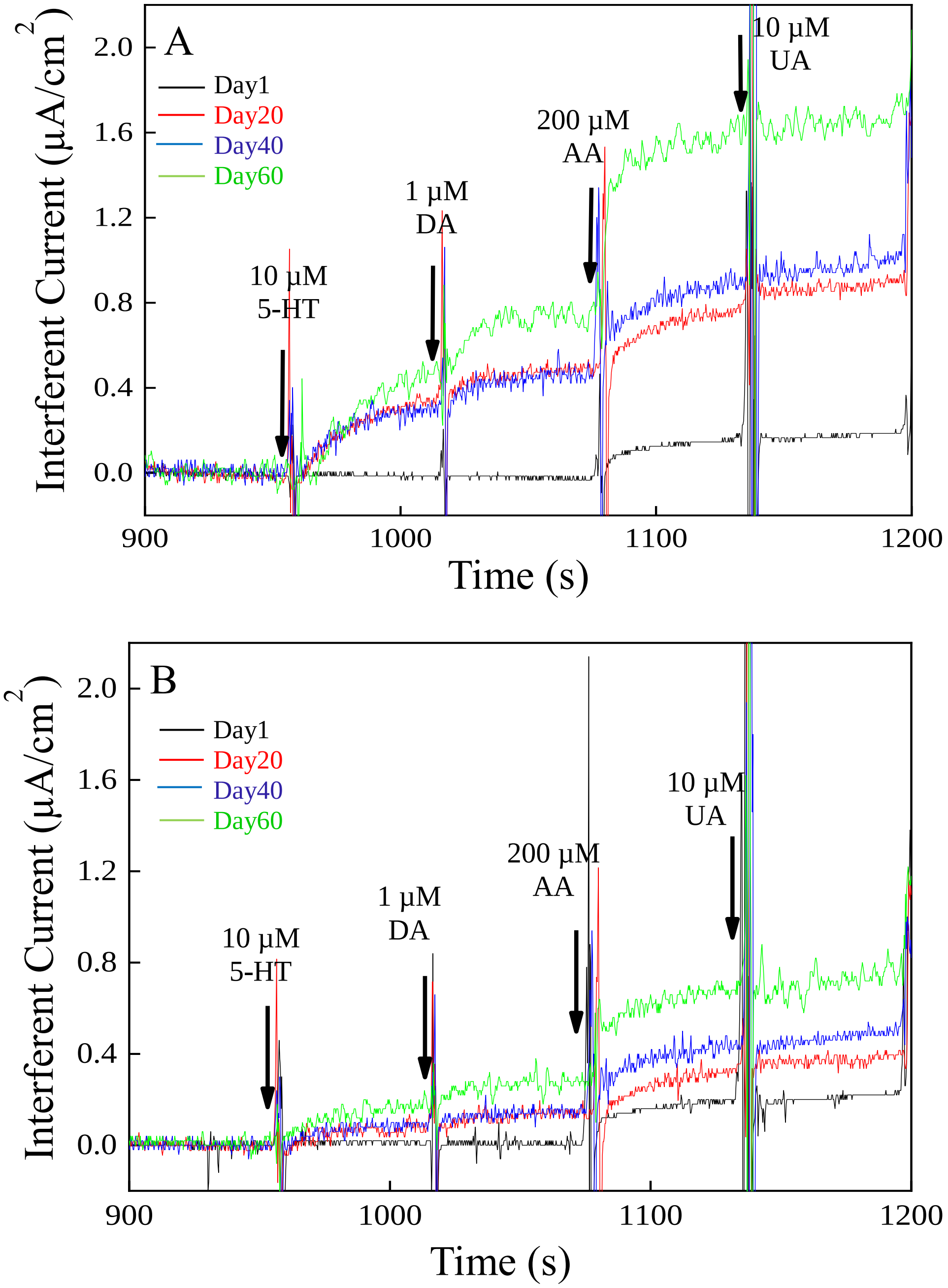

Figure 4-14. 60 days' calibrations of enzymes and mPD-modified platinum surfaces with (concentrations after addition, left to right) 10 µM 5-HT, 1 µM dopamine, 200 µM ascorbic acid, 10 µM uric acid. The platinum surfaces were coated with 0.4 U/µL, 4 drops of enzymes (approximately 0.05 µL per drop), and mPD coating used two different electrical parameters ***A).*** 50 mV/s and ***B).*** 5 mV/s. Plots indicate the trend of interferent currents over time from the two mPD parameters: day 1 (black), day 20 (red), day 40 (blue), day 60 (green); sensors were used one hour every day and stored in DI water and dark when not in use. Amperometry: + 0.7 V *vs* Ag/AgCl wire in a stirred 1X PBS beaker; the stir rate was 250 rpm.

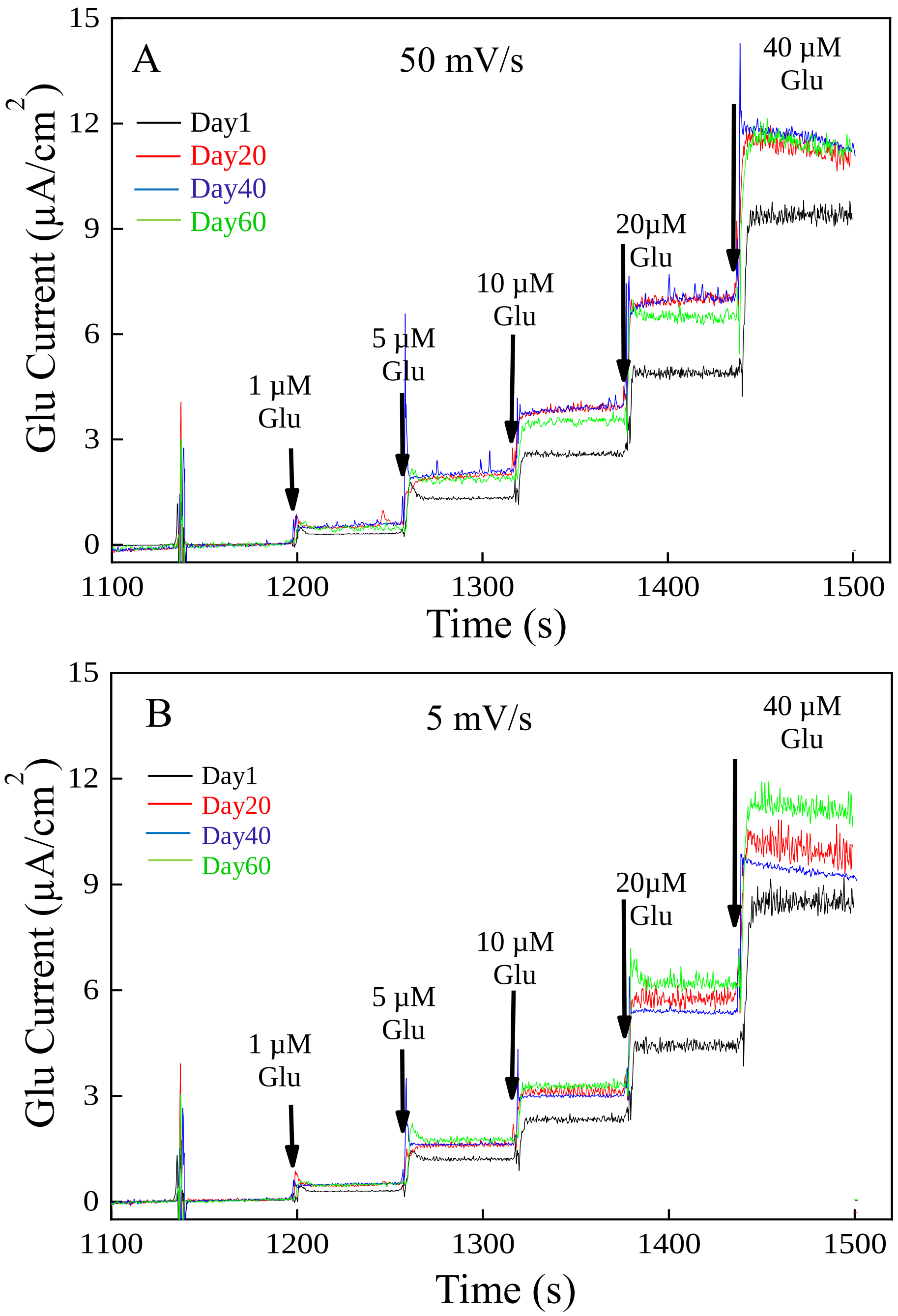

Figure 4-15. 60 days' calibrations of enzymes and mPD-modified platinum surfaces with 1, 5, 10, 20, 40 µM glutamate (concentrations after addition, left to right). The platinum surfaces were coated with 0.4 U/µL, 4 drops of GluOx (approximately 0.05 µL per drop), and mPD coating used two different electrical parameters ***A)*** 50 mV/s and ***B)*** 5 mV/s. Plots indicate the trend of glutamate sensitivity over time from the two mPD parameters: day 1 (black), day 20 (red), day 40 (blue), day 60 (green); sensors were used one hour every day and stored in DI water and dark when not in use; after two months of use, the sensor sensitivity was even higher, SS_{60}>SS_1. Amperometry: + 0.7 V *vs* Ag/AgCl wire in a stirred 1X PBS beaker; the stir rate was 250 rpm.

4.7 Working Range Study

In this study, a Pt/1 drop Enzyme/mPD2 sensor was prepared and calibrated within a wide-range of glutamate, 1-8000 µM. Current-analyte concentration relation was established based on Michaelis Menten fitting. We found a linear range between 1-600 µM, and data fit well into the Michaelis Menten equation from 600-8000 µM, ***Figure 4-16***. That is to say, for a sensor with a 10 pA/ µM sensitivity and a signal current that does not exceed 6000 pA, we can easily come up with the glutamate concentration by dividing current by sensitivity; if the signal current exceeds 6000 pA, then we have to fit it into the Michaelis Menten equation.

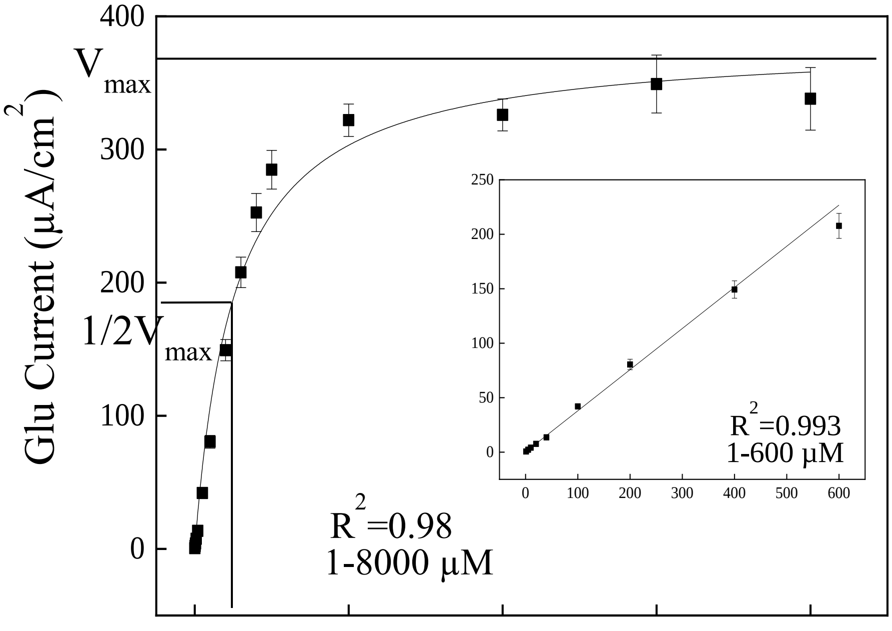

Figure 4-16. Calibration of enzymes and mPD-modified platinum surfaces with 1, 5, 10, 20, 40, 100, 200, 400, 600, 800, 1000, 2000, 4000, 6000, 8000 µM glutamate (concentrations after addition, left to right). The platinum surfaces were modified with one drop of enzyme, 0.4 U/µL, approximately 0.05 µL per drop, electric parameters during mPD coating used 5 mV/s. Amperometry: + 0.7 V *vs* Ag/AgCl wire in a stirred 1X PBS beaker; the stir rate was 250 rpm.

4.8 Platinum Surface Etching Study

As described in ***Section 4.1***, we cleaned the platinum sensor surface using methanol and electrochemical cycling, and we found a drastic hydrogen peroxide sensitivity increase from 2443 ± 78 nA/µMcm^2 (uncleaned) to 3845 ± 120 nA/µMcm^2 (methanol + ECC). In this section, we discuss how we further modified our sensor surface using a different method to enhance sensitivity to H_2O_2. 4000 HZ +1.2/-0.25 V pulses (OWON AG 4121 Single-channel Arbitrary Waveform Generator) were applied to the platinum microelectrode using an SCE as the reference electrode for 100s duration with a duty cycle of 1:3, ***Figure. 4-17 A***. After the pulse-assisted process, a -0.2 V amperometry in 0.5 M $HClO_4$ applied to reduce the surfaces.

This pulse contains a positive part and a negative part as shown in ***Figure 4-17***. The chemistry reactions happened, as explained previously, based on potential range in cyclic voltammetry. For a cycling between [-0.3 V, 1.4 V], the first step occurred at $0.25 \leq E \leq 0.85$V. It was the interaction of H_2O molecules with the Pt electrode at this point, ***Figure. 4-17 B & Eq 4-1***. In this potential region, the Pt surface had a partial positive charge that attracted the negatively charged oxygen end of the water molecules. In the second step, ***Figure. 4-17 C***, the discharge of about half a monolayer of H_2O molecules took place and resulted in formation of ∼0.5 monolayer of chemisorbed oxygen (Ochem) and ∼0.5 monolayer of H_2O molecules. This process initiated at + 0.85V and ended at ∼1.15V, ***Eq 4-1***. The third step (***Figure. 4-17 D***) involved the discharge of the second half-monolayer of H_2O molecules that experienced strong interfacial interactions with the Pt electrode surface (as the platinum surfaces were already covered by ∼0.5 monolayer of O_{chem}). As the second half-monolayer of O_{chem} began to build up (in addition to the already existing 0.5 monolayer of O_{chem}), the strong dipole-dipole lateral repulsive interactions set in, driven by the dipole moment of the $(Pt–Pt)^{\delta+}– O_{chem}{}^{\delta+}$ surface compound. In order to minimize these repulsions, the initial half-monolayer of O_{chem} adatoms underwent an interfacial place-exchange process with the Pt surface atoms, leading to a surface PtO lattice. The place exchange was accompanied by completion of the charge transfer from Pt to O_{chem}, thus leading to a quasi-3D surface lattice comprising Pt^{2+} and O^{2-} moieties (***Figure. 4-17 E, Eq 4-3***) [83]. Finally, when applying negative potential, the platinum surfaces were reduced to pure platinum as the oxygens were gone, ***Eq 4-4***. At this point, the etching of platinum was complete.

$$Pt\ + H_2O \rightarrow Pt^{\delta+}O^{\delta-}H_2, \qquad 0.25 - 0.85\,V \qquad \textbf{\textit{Eq. 4-3}}$$

$$(Pt - Pt)H_2O \rightarrow (Pt - Pt)^{\delta+}O_{chem}{}^{\delta-} + 2H^+ + 2e^-, \qquad 0.85 - 1.15\,V \qquad \textbf{\textit{Eq. 4-4}}$$

$$PtO_{chem} + H_2O \rightarrow (Pt^{2+}O^{2-})_{3D\ lattice} + 2H^+ + 2e^-, \qquad 1.15 - 1.40\,V \qquad \textbf{\textit{Eq. 4-5}}$$

$$(PtO) + 2H^+ + 2e^- \rightarrow Pt + H_2O, \qquad -0.3V \qquad \textbf{\textit{Eq. 4-6}}$$

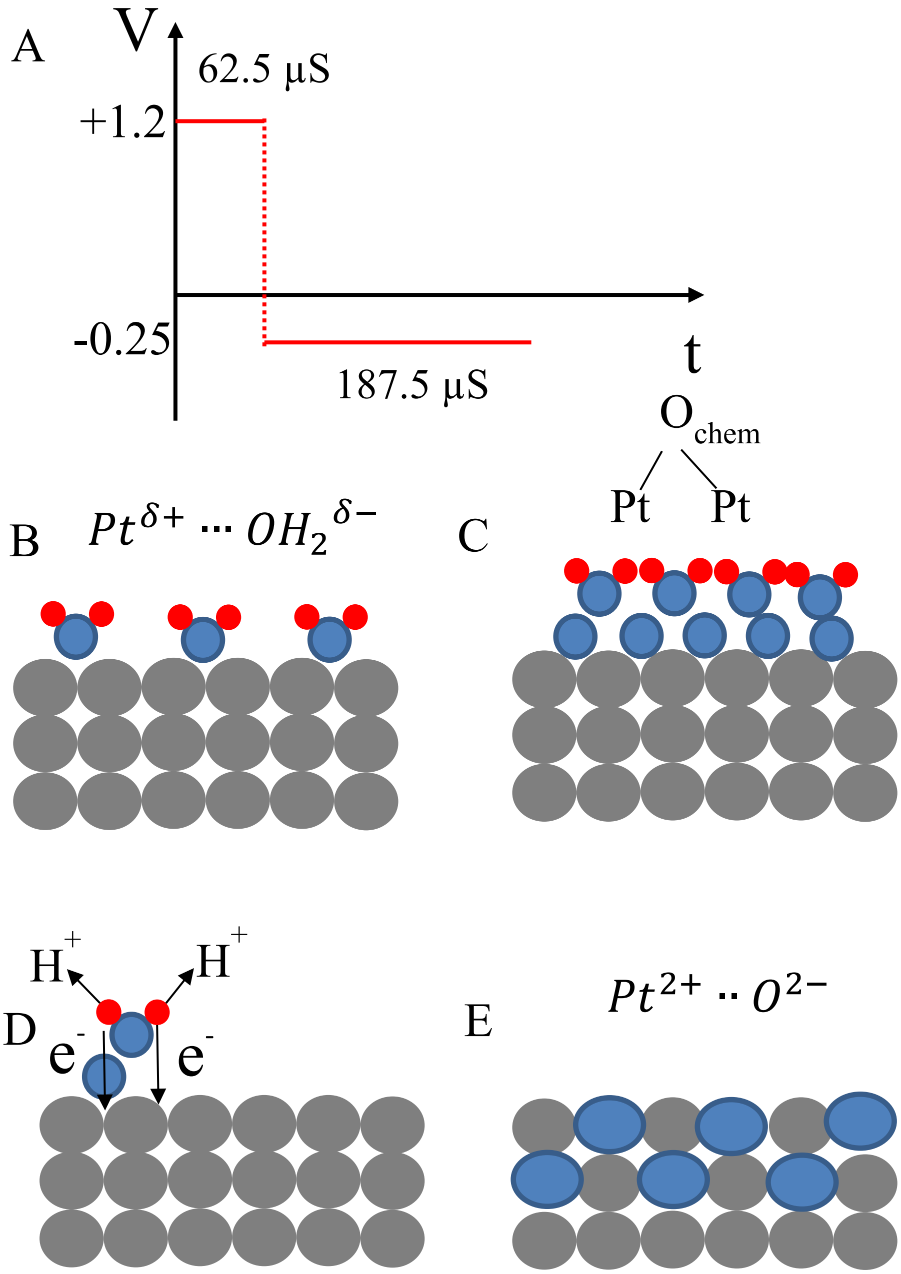

Figure 4-17. Representation of the platinum-oxide growth mechanism: ***A)*** applied pulse ***B)*** interaction of H_2O molecules with the Pt electrode that occurs in the $0.25 \leq E \leq 0.85$V range; ***C)*** discharge of half a monolayer of H_2O molecules and formation of chemisorbed oxygen (Ochem); ***D)*** discharge of the second half-monolayer of H_2O molecules; the process was accompanied by the development of repulsive interactions between $(Pt–Pt)^{\delta+}$–$O_{chem}{}^{\delta-}$ surface species that stimulated an interfacial place exchange of O_{chem} and Pt surface atoms; ***E)*** quasi-3D surface PtO lattice comprising Pt^{2+} and O^{2-} moieties that formed through the place-exchange.

Confocal images were taken under a laser-optical mode before and after the facile pulse process. The two surfaces looked completely different because the untreated platinum was very smooth and shiny while the pulse-treated surfaces were very rough, ***Figure. 4-18***. The arithmetic mean roughness increased from 9.0±0.5 nm to 116.3±7.4 nm, a 13-fold increase in roughness. The texture aspect ratio was also increased from 0.49±0.07 to 0.87±0.01, which indicates an ununiform surface. Further evidence to improve understanding of surface areas is that $I_{charging}$ in 1X PBS when running CV also increased. The charging current reflects exposed surface areas. Charging current has increased from 0.765±0.015 nA to 1.168±0.024 nA, a 53% increase. An advantage of doing pulse etching is that it can expose more platinum surfaces without increasing geometric area. This boosts the sensitivity of biosensors that function by detecting H_2O_2.

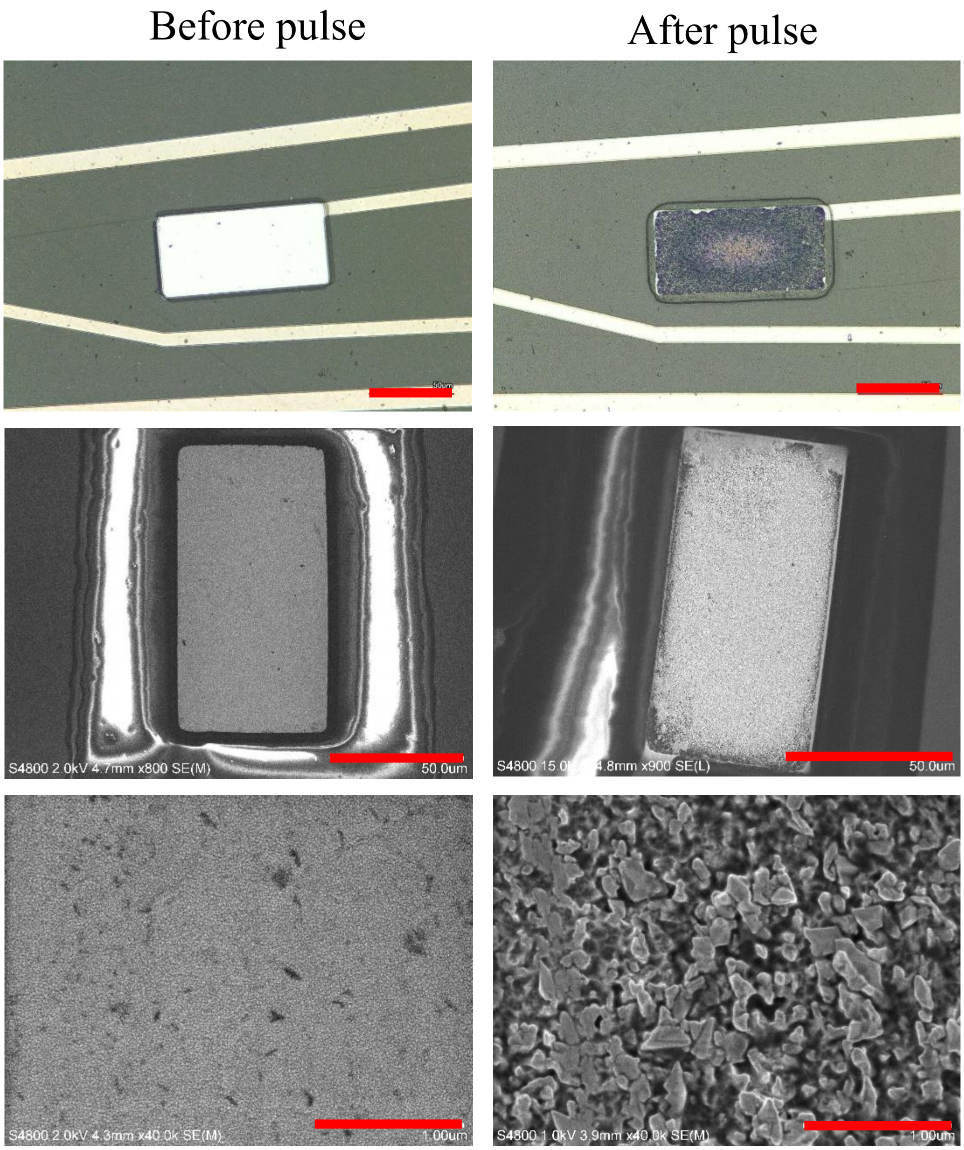

Figure 4-18. Confocal microscope (***A & B***) and SEM (***C-F***) images of an 8-TRK platinum microelectrode surface, before (***A, C, E***) and after (***B, D, F***) pulse treatment. ***A-D*** scale bar is 50 µm; ***E&F*** scale bar is 1 µm.

The increase in platinum surface areas contributes to hydrogen peroxide sensing, resulting in a sensitivity increase from 3845±120 nA/µMcm^2 (methanol + ECC) to 5893±182 nA/µMcm^2 (methanol + ECC+ Pulse), a 53% increase that agrees exactly with $I_{charging}$ changes, ***Figure. 4-19.***

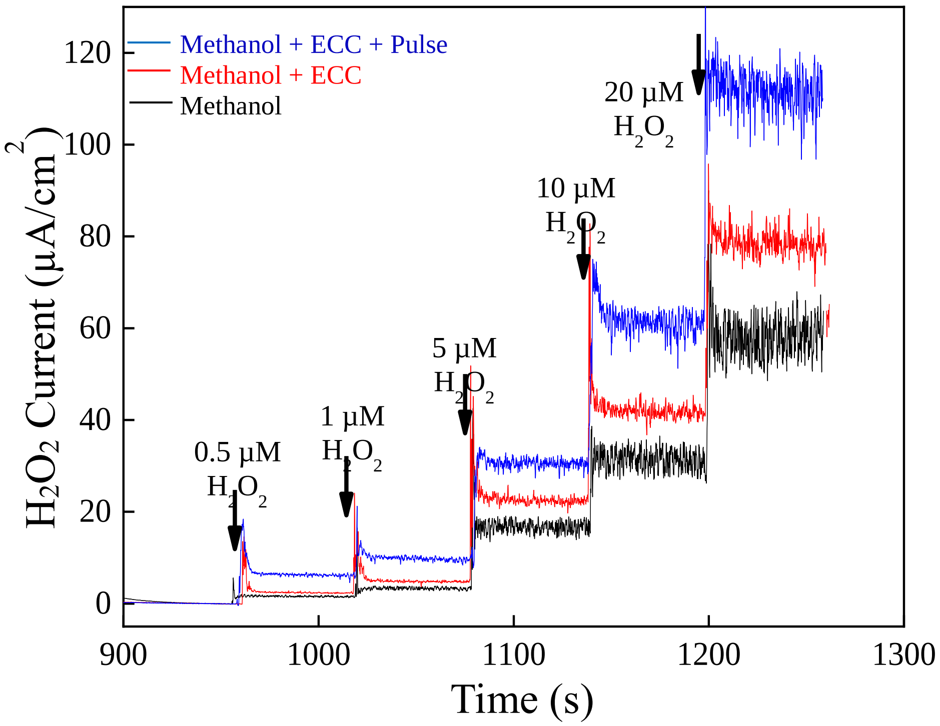

Figure 4-19. Calibration of differently cleaned bare platinum surfaces with 0.5, 1, 5, 10, 20 µM H_2O_2 (concentrations after addition, left to right), methanol cleaned (black), methanol + ECC cleaned (red) and methanol + ECC + pulse cleaned (blue). Amperometry**:** + 0.7 V *vs* Ag/AgCl wire in a stirred 1X PBS beaker; the stir rate was 250 rpm.

However, this indirectly illustrated that the platinum surface increase aided glutamate sensing. To see if this porous surface really contributes to a higher sensitivity in neurochemical detection, the next step was to apply 4 drops of 0.4 U/µL glutamate oxidase and mPD1 to the treated surfaces and perform glutamate calibrations. In this experiment, we saw an appreciable 25% increase of 240±7 nA/µMcm^2 to 299±13 nA/µMcm^2, ***Figure. 4-20***. This number is not as high as what we see from direct oxidation of H_2O_2, but it is still encouraging data that proved the importance of a porous surface, and through this study, we provided a method of surface treatment for porous biosensors.

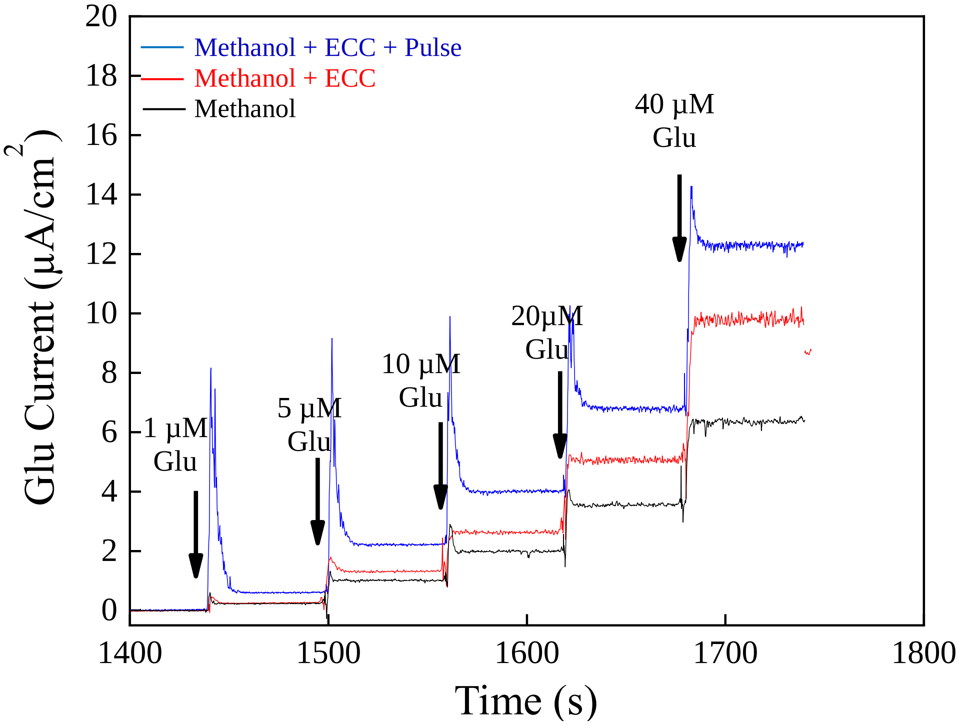

Figure 4-20. Calibration of differently cleaned bare platinum surfaces with 1, 5, 10, 20, 40 µM glutamate (concentrations after addition, left to right), methanol cleaned (black), methanol + ECC cleaned (red) and methanol + ECC + pulse cleaned (blue). Amperometry**:** + 0.7 V *vs* Ag/AgCl wire in a stirred 1X PBS beaker; the stir rate was 250 rpm.

CHAPTER 5

DOPAMINE SENSOR DEVELOPMENT

5.1 Lab on a Chip: MWCNT/UNCD Hybrid Electrode

5.1.1 Optimization of EPD Parameters

In my master's work, an MWCNT/UNCD hybrid electrode was developed and studied. Three EPD parameters – voltage (–3V to –9V), deposition time (up to 500 s) and MWCNT concentration (0.5 mg/mL and 1 mg/mL) were controlled to study the MWCNT film coverage, film uniformity and film thickness on a UNCD surface (see ***Table 5-1***). In brief, excellent film coverage and film uniformity was observed at low MWCNT concentration (0.5 mg/mL), low voltage (–4.5 V) and longer deposition times (300 s to 500s). High voltage (–9 V) and high MWCNT concentration (1.0 mg/mL) resulted in thick, nonuniform films. Since a highly uniform continuous coverage of MWCNTs with a controllable thickness is important to reliable functioning of the microelectrode, lower voltage values (i.e., slower deposition rates), longer deposition times and low MWCNT concentration (i.e., better surface coverages) were selected for detailed characterization of the modified microelectrode.

Table 5-1. Effect of EPD parameters on the surface characteristics of MWCNT film modified UNCD microelectrode. Film thickness was measured using a surface profilometer (Dektak150). The variation in the film thickness was ±10%.

Process Parameters	***Surface characteristics of MWCNT-modified microelectrode***
None	250 µm-diameter unmodified UNCD (control)
0.5 mg, –4.5 V, <120 s	Low surface coverage, non-uniform, ultra-thin MWCNT film (~50 nm)
0.5 mg, –4.5 V, 500 s	High surface coverage, uniform "thin" MWCNT film (~100 nm)
0.5 mg, –6.0 V, 500 s	High surface coverage, uniform "thick" MWCNT film (~250 nm)
1.0 mg, –4.5 V, 500 s	High surface coverage, non-uniform "thickest" MWCNT film (~500 nm)

Figure 5-1 illustrates the random and open pore structure of the MWCNT network within the modified film. Surface profilometry measurements showed an increase in average surface roughness from 9.5 nm rms for the UNCD (control surface) to 18 nm rms for the MWCNT thin film (*n*=3, data not shown). This result was expected since the randomly oriented 3D network of MWCNTs with open pores generated a rougher surface (***Figure 5-1 C, D***). These measurements also show that careful control of the porous structure is necessary to obtain improved chemical sensing performance. A detailed discussion concerning the electrochemical properties of the modified microelectrodes is presented in the following sections.

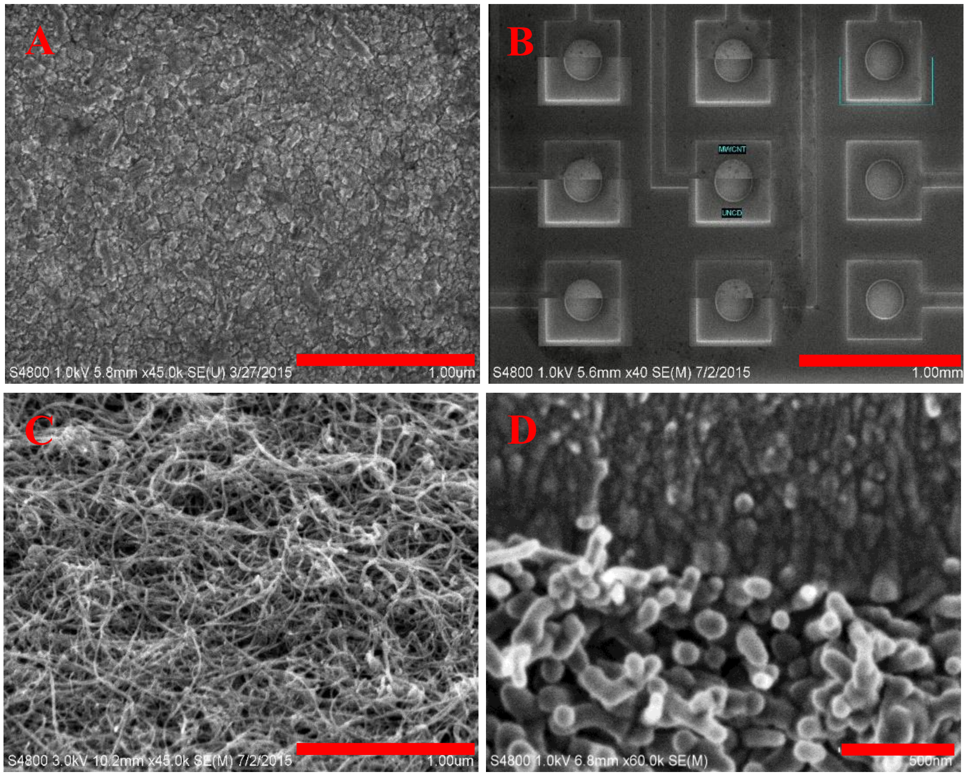

Figure 5-1. SEM images showing ***A)*** An unmodified UNCD. ***B)*** 3X3 microarray with nine individually addressable, 250 µm-diameter UNCD microelectrodes. ***C)*** Top view of MWCNT-modified UNCD microelectrode. ***D)*** Cross-sectional view of the modified microelectrode interface. Scale bars for A-D are 1 µm, 1 mm, 1 µm and 500 nm, respectively.

5.1.2 Electrochemical Performance of Modified Hybrid Electrode

Figure 5-2 shows the electrochemical response in 1X PBS (***Figure 5-2 A, B***) and 100 µM DA in 1X PBS (***Figure 5-2 C, D***) of the unmodified and MWCNT film modified UNCD microelectrodes used in this study. Based on the minimal variability in CV parameter values, excellent reproducibility in electrochemical signal strengths were observed for these microelectrodes. The % variation of the CV parameter values was 0-10% (n = 3) as derived from measuring three different MEAs (***Table 5-2***). Sensitivity is defined as $I_S/[C_{DA}\times A]$,where I_S is the forward peak current from the cyclic voltammograms at a scan rate of 100 mV/s (***Figure 5-2 C, D***); C_{DA} is the DA concentration, which is 100 µM for this study; and A is the geometrical area of the UNCD microelectrode, πR^2, where R = 125 µm is the radius of the UNCD microelectrode. Electrode reaction-kinetics data can be obtained from the peak potential separations (ΔE_p) between the forward and reverse peak currents (E_{anodic}–$E_{cathodic}$) of the redox system. Studies show ΔE_p and the associated slope of the cyclic voltammogram from inner and outer-sphere redox systems could be a reliable CV indicator to study electrode reaction rates [84, 85]. S/N ratio is defined as the ratio of I_S/I_C, where I_C is the background or charging current recorded in 1X PBS buffer solution (***Figure 5-2 A, B***).

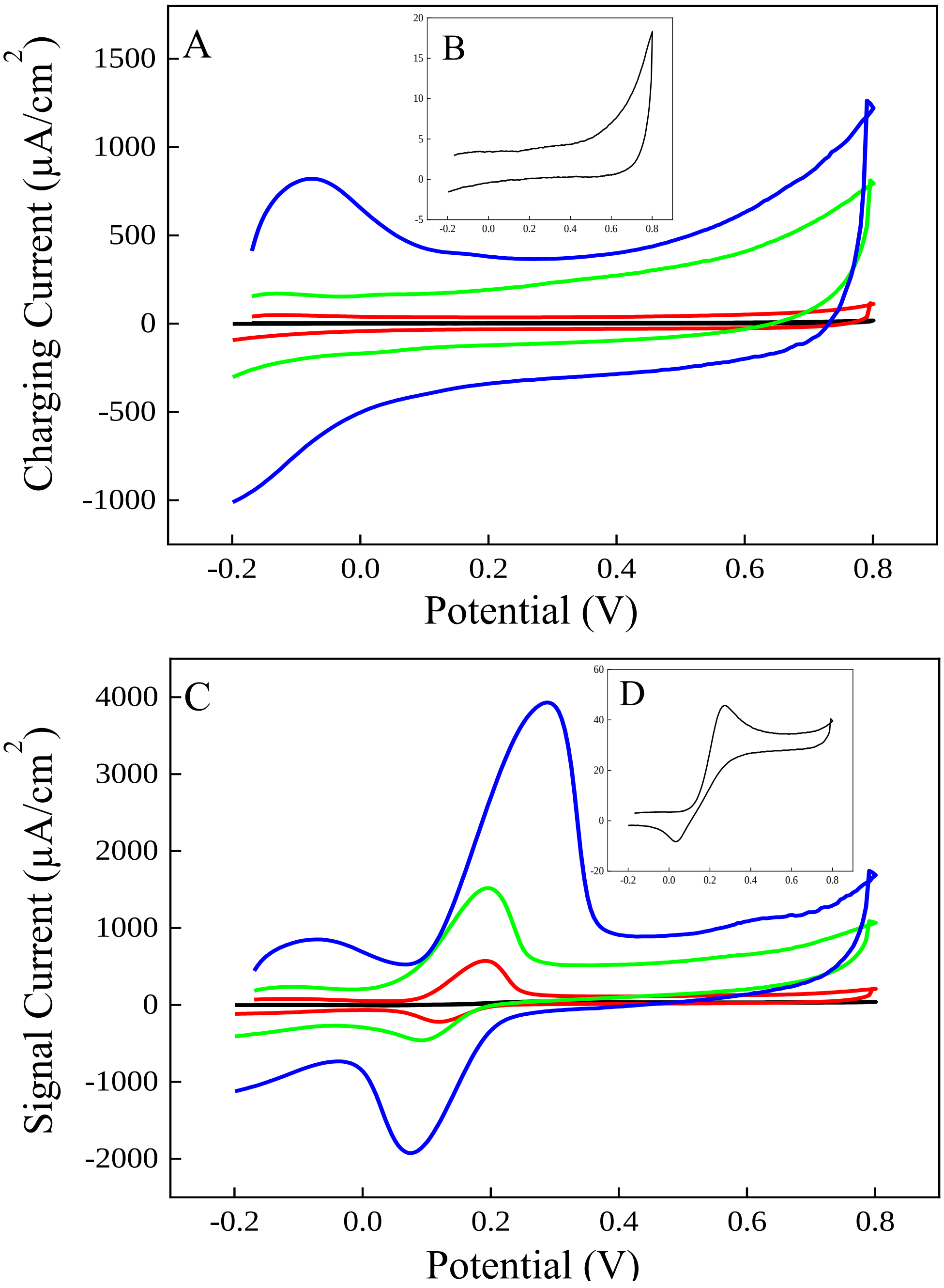

Figure 5-2. Cyclic voltammetry characterization of unmodified and MWCNT film modified UNCD microelectrodes. ***(A, B)*** Voltammograms taken in 1X PBS buffer (inset for UNCD). ***(C, D)*** Voltammograms obtained in 100 µM dopamine in 1X PBS (inset for UNCD). Legends: Unmodified UNCD (black), thin film (red), thick film (green) and thickest film (blue). Scan rate was 100 mV/s.

Table 5-2. Cyclic voltammetry data from the different MWCNT film modified UNCD microelectrodes and an unmodified UNCD (control). 100 µM DA in 1X PBS buffer or 1X PBS buffer only was used. The scan rate was 100 mV/s. The background charging current (I_c) was computed from ***Figures 5-2. A* and *B***. The dopamine signal (I_s) was computed from ***Figures 5-2. C* and *D***.

Microelectrode type	***ΔE_p(mV)***	***E_{anodic} (mV)***	***I_s (nA)***	***I_c (nA)***	***Sensitivity ($\mu A/\mu M cm^2$)***	***S/N ratio***
Unmodified UNCD (control)	200	250	13	0.9	0.3	15
Thin film	60	200	240	16.5	5	15
Thick film	85	200	650	76	14	9
Thickest film	200	280	1650	170	32	9

The sensitivity was found to be critically dependent on MWCNT film thickness. When the MWCNT thickness increased from thin (~100 nm) to thickest (~500 nm), the sensitivity increased, the S/N ratio decreased, and the electrode-reaction kinetics initially became more rapid and then slowed at increasing thickness. The charging current (I_C) that is proportional to electrode area increased from 0.9±2% nA (unmodified) to 170±3% nA (thickest film), i.e., a 200-fold increase in electrode surface area. This result is expected since MWCNT's specific surface areas are very high and more MWCNTs are expected to be deposited at longer deposition times. Secondly, the ΔE_p decreased 4-fold from 200 ±5% mV to 60±4% mV when the UNCD was modified with a thin film. The lowest ΔE_p value of 60 mV is still larger than the value corresponding to a reversible two electron redox process (which is 29.5 mV). This value slowly returned to 200 mV when the thickest film was deposited, which is the same value as that for the unmodified microelectrode. This ΔE_p dependence on film thickness was previously observed with the presence of a porous MWCNT layer on top of a planar electrode [47,48]. This observed behavior is due to the geometrical and chemical effects of the modified electrode interface. The modified surface obviously provides a more porous geometry that significantly alters the diffusion behavior of the DA because there will be a marked contribution from the thin liquid layer adjacent to the UNCD electrode surface. This makes the onset of oxidation at kinetically faster. From a chemical standpoint, the modified electrode surface is dominated by carboxylic acid and oxygen-rich functional groups that are known to influence DA adsorption behavior [49]. It is also expected that the peak current will be higher for the modified microelectrode because there is a relatively high electroactive electrode surface area within the porous MWCNT film. Thus, the peak current and ΔE_p values should depend on the film thickness for the modified microelectrode. Thirdly, the DA peak currents increased from 13±5% nA (unmodified) to 1650±8% nA (thickest film), i.e., a 127-fold increase in sensitivity even with a constant value for the geometrical surface area of the UNCD microelectrode.

5.1.3 EIS Characterization of MWCNT–Modified UNCD Microelectrodes: Effect of MWCNT Film Thickness on Interfacial Properties

The EIS spectrum of an unmodified UNCD microelectrode is fitted to a [Rs(C[R_{ct}Q])] circuit model [71](***Figure 5-3. B***). For the modified microelectrode, we developed an electrochemical pore model to describe different types of pores resulting from film modification. According to the model, the modified microelectrode is comprised of three regions, namely Region 1, Region 2 and Region 3, that have varying electrochemical activity. The total current and the corresponding electrochemical activity varied in each region due to differences in the geometrical structure of the pores. Region

3 was highly electrochemically active, Region 2 was considered to be a pure resistor, and Region 1 was a less electrochemically active region. EIS data was collected from the three modified microelectrodes, viz. thin, thick and thickest films, and fitted to these circuit models. The Nyquist plots of the impedance data for the microelectrodes are shown in ***Figure 5-3. A***. The Nyquist plot of the thin film shows an arc of a semi-circle at high frequencies followed by a straight-line at low frequencies. The model as described in ***Figure 5-3. C*** was fitted to the EIS data. The model is a combination of three circuits contributing to an overall impedance, and each RQ corresponds to the three different regions on the modified microelectrode as described above. The values of the circuit elements (***Table 5-3***) show that each region contributed to a different degree to the overall impedance (Z) values. The circuit corresponding to low impedance was due to a highly electrochemically active region, and the circuit corresponding to a very high impedance was due to the least electrochemically active region. Thus, this circuit model further validates the proposed pore model described above.

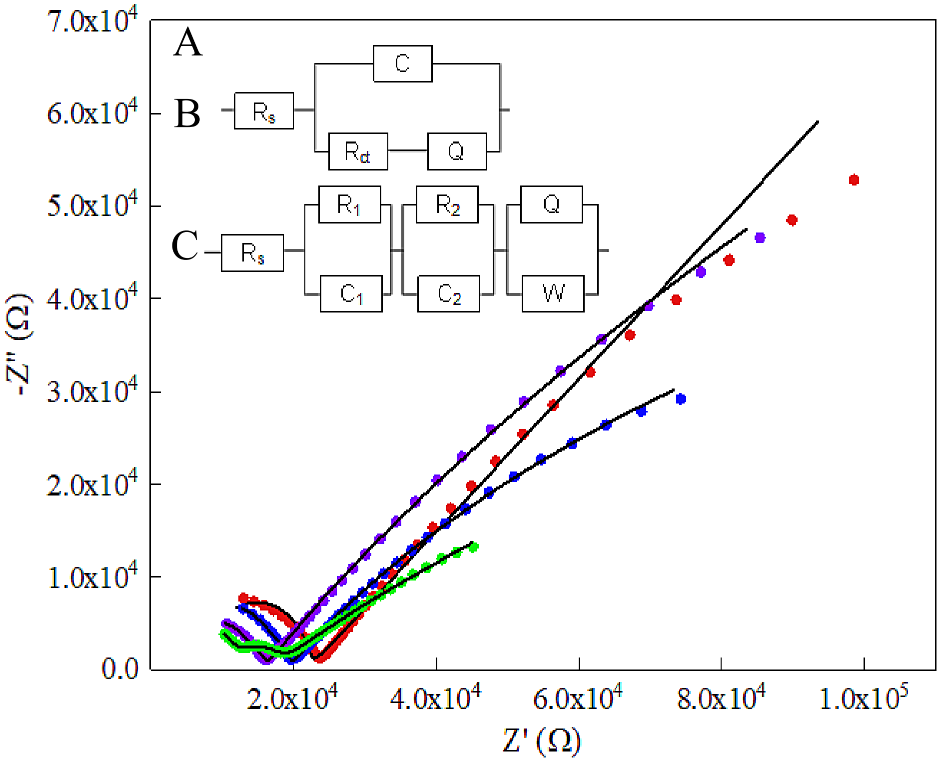

Figure 5-3. A) Nyquist plots of unmodified and MWCNT film modified UNCD microelectrodes–unmodified (red dotted), thin MWCNT film (purple dotted), thick MWCNT film (blue dotted) and thickest MWCNT (green dotted). ***B)*** The equivalent circuit of the unmodified UNCD. ***C)*** The equivalent circuit of MWCNT-modified UNCD microelectrodes. The electrolyte was 5 mM Fe (CN)$_6^{3-/4-}$ in 1M KCL. 10 mV amplitude, OCP, 0.1 Hz-100 KHz.

The impedance Z_3 contributed by the first RC circuit is described below:

$$Z_3 = \frac{R_{ct3}}{1+j\omega R_{ct3}C_3} \qquad \textbf{\textit{Eq. 5-1}}$$

The C_3 and R_{ct3} are the capacitance of the pore walls and charge transfer resistance of the pores, respectively. C_3 is of the order of nano-farads, and Rct_3 is of the order of kilo-ohms; therefore, at low frequencies, the impedance of the pores of this region is equivalent to R_{ct3}, whereas at high frequencies, the impedance of the pores is less than R_{ct3}. Thus, at low frequencies, the AC signal cannot penetrate deeply into the pores because of the IR drop, and a high impedance value for the pore walls is observed.

However, at low frequencies, the AC signal can penetrate deeply into the pores; thus, the impedance is low. This frequency-dependence behavior of the pore impedance of this region is similar to that of De Levie's pore model [86]. Further, the RC circuit for this region suggests that these pores are comprised of continuous walls with the fewest openings as C arises from a homogenous structure. The impedance of such pores is dependent on the frequency of the AC signal and corresponds to a scenario where the condition $I_{in}>I_{out}$ is satisfied in the proposed model. The capacitance described in the circuit may correspond to the total capacitance of the pore walls at low frequencies. For a thin and thick film, the impedance described above corresponds to Region 3, a highly electrochemically active region.

$$Z_2 = \frac{R_{ct2}}{1+ j\omega R_{ct2}C_2}, \qquad \textbf{\textit{Eq. 5-2}}$$

The impedance Z_2 contributed by the second RC circuit is described below: the C_2 value is of the order of picofarads, and the R_{ct2} value is of the order of kΩs. Therefore, the denominator term in the above expression for all frequencies will satisfy the following condition, 1>> $\omega R_{ct2}C_2$. Therefore, the equation can be simplified

$$Z_2 \approx R_{ct2} \text{ for all frequencies,} \qquad \textbf{\textit{Eq. 5-3}}$$

Hence, this RC circuit corresponds to a less electroactive region on the electrode where the impedance of the pores does not depend on the frequency of the signal. From the above model, the scenario $I_{in} = I_{out}$ will be satisfied because such a region behaves like a resistor. Therefore, the impedance described in Eq. 3 corresponds to Region 2 as described in the proposed model.

The third circuit comprises of impedance due to the Constant Phase Element (CPE) and the Warburg (mass transfer) impedance. The total impedance contributed by

$$Z_1 = \frac{1}{Y_Q(j\omega)^n + Y_W\sqrt{j\omega}}\,, \qquad \textbf{\textit{Eq. 5-4}}$$

this circuit is described below:

where Y_Q is the admittance of an ideal capacitor, Y_w is the admittance of diffusion, and ω is the frequency. The CPE is a consequence of the inhomogeneities in the structure of the pore walls. Therefore, diffusion has multiple paths, and the electroactive species can enter and leave a pore at different points along the length of the pore. Similarly, the AC signal can enter or leave at different points as well. If the total current entering through the pore is less than the current leaving the pore ($I_{in}<I_{out}$), this can result in an overall small current in the pores, leading to reduced electrochemical activity. This is mainly a geometrical effect, which depends on pore geometry and their surroundings. The impedance of these pores is mainly diffusion dependent, and it corresponds to Region 1. As shown in ***Table 5-3***, the values of Y_Q and Y_W of the order of µMho. This means that Z_1 will be of the order of MΩ irrespective of other factors such as frequency and the value of N. As a result, Z_1 will contribute towards a high impedance at the electrode surface.

Table 5-3. Values of interfacial parameters of MWCNT-modified UNCD microelectrodes obtained by fitting the circuit to experimental data. The errors for the circuit elements were 0-20%.

Microelectrode type	***R_s (KΩ)***	***Region 3***		***Region 2***		***Region 1***		
		C_3	***R_{ct3}***	***C_2***	***R_{ct2} (KΩ)***	***Y_{Q1} (μMho)***	***N***	***Y_W (μMho)***
Thin MWCNT-UNCD	4.3	7.1	1.8	128	9.7	4.4	0.16	10.6
Thick MWCNT-UNCD	3.7	3.8	2.4	83	13.1	9	0.15	10.6
Thickest MWCNT-UNCD	2.8	Y_Q (nMho)/N 109/0.7	6.6	85	8.5	28.7	0.24	9.8

For thick-film microelectrodes, Region 2 became slightly more resistive, the C in Region 3 was reduced by a factor of 0.5, and the admittance of Region 1 increased by a factor of 2. As shown in Eq 4, admittance was inversely related to impedance. By increasing the film thickness from thick to thickest for Region 3, the C of the circuit was replaced by a CPE, which implies that the walls of such pores became inhomogeneous. The R_{ct} in such regions increased by a factor of 3. This increase implies that as the film thickness was increased, the electroactive species inside the pores of Region 3 became saturated due to the lack of diffusion of new electroactive species and a corresponding higher R_{ct}. This increase in impedance of these pores contributed to an overall increase in charging current (I_c) “noise”. The impedance of Region 2 remained the same as that of a thin film electrode. However, the admittance of Region 1 increased by a factor of 7, presumably due to lower contact resistance between the UNCD and the overlying MWCNT film. Thus, such pores became more electrochemically active even though their walls remained inhomogeneous, and the Warburg element was equivalent. Thus, electroactive species can diffuse by multiple pathways and contribute to an overall increase in the redox current "signal" (I_s). Overall, as the film thickness increased, impedances of Region 3 increased and contributed to noise, while impedances of Region 2 were equivalent. However, in Region 1, the impedance of the pores decreased because they became more electrochemically active and contributed significantly towards the overall signal at the microelectrode. Since a high sensitivity and high S/N ratio is expected from any sensor, it is important to understand which regions and to what extent each region contributes to the signal and noise. The EIS model demonstrates that for thin film microelectrodes, Region 3 and Region 1 contributed towards the signal and Region 2 towards the noise. While, for the thickest-film microelectrodes, Region 3 and Region 2 contributed more noise, and Region 1 contributed more signal. The arc at high frequencies was suppressed. The main reason for such behavior is that the pores became more inhomogeneous due to increased film thickness. The circuit-fitting parameters incorporate this effect by adjusting the capacitance element to a CPE as shown in ***Figure 5-3.*** Therefore, this model illustrates that the sensor metrics for a given analyte can be tuned by controlling the relative thicknesses (or volumes) of the three regions in the microelectrode. This was validated here experimentally by detecting DA.

5.1.4 XPS Characterization of MWCNT–Modified UNCD Microelectrodes: Effect of Surface Functional Groups on Electrochemical Properties

XPS studies were carried out to understand the origin of the differing levels of electrochemical activity of the microelectrode regions as identified in the EIS studies. The C1s spectrum of an unmodified UNCD microelectrode (***Figure 5-4. A***) mainly consists of phase pure sp^3 hybridized diamond grains (C_2 peak) and non-diamond amorphous carbon in grain boundaries (C_0 peak). The C_3 and C_4 peaks correspond to the C−O and C=O groups along the grain boundaries. The Q and R_{ct} values obtained from the EIS spectrum were determined by which C1s and O1s peaks appear in the XPS spectrum (***Table 5-4***). The highly oxidized functional groups such as O_2 and O_5 that were present in the grain boundaries (***Figure 5-4. D***) contributed to the Q value, and the C1s and O1s peaks contributed to the R_{ct} value, respectively. In general, the presence of C1s and O1s peaks are indicative of high and low electrochemical activity regions, respectively [56, 57, 86, 87]. The [O/C+O] ratio of ~0.3 calculated from [88] core level C1(284.8eV) and O1(532eV) spectra suggests a quasi-reversible electrochemical behavior as reported previously [43, 89]. The MWCNT thin film modified microelectrode has more electrochemically active carbon functionalities, namely C_0, C_2, C_3, C_4, C_5 and C_6(***Figure 5-4. B***). C1s spectra revealed a highly ordered graphitic structure (C_2peak) accompanied by (C_0peak) originating from carbon atoms that are no longer in the regular tubular MWCNT structure [90, 91]. A lower percentage of sp^2carbon (1.0±0.16%) in the thin film resulted in a lower background current or noise and thus, a higher S/N ratio. Besides the presence of aromatic and aliphatic functionalities (C_3, C_4 peaks), the ($\pi \rightarrow \pi^*$) satellite peak that was assigned to shake up structures, increased the overall electrical conductivity of the thin film microelectrode [92]. Interestingly, the highly electroactive Region 1 observed in the EIS spectra and the high S/N ratio of >15 observed in the cyclic voltammogram could possibly be due to the presence of the satellite peak and a low sp^2content. The [O/C+O] ratio is ~ 0.8, a high abundance of carboxylic and phenolic groups (C_3, C_4, O_2, O_4 peaks) (***Figure 5-4. E***) allowed for enhanced adsorption−desorption kinetics for the dopamine−dopaminequinone redox couple, which caused DA sensitivity to increase [87]. For the thickest film microelectrode, the [O/C+O] ratio decreased to ~0.5, suggesting removal of some oxygen functional groups (e.g., carboxyl groups, etc.)[88], and there was no satellite peak. The *sp*^{2}carbon content increased (C_2 peak), and more importantly, there was a significant presence of a less electrochemically active ketone (O_3) group (***Figure 5-4. C, F***). These factors overall contributed to a more resistive electrode Region 3 as observed in EIS and a lower S/N ratio of DA detection as observed in the cyclic voltammogram. The thin-film microelectrode exhibited trace amounts (0.03 At%) of magnesium (Mg) at ~1305eV that were due to the $MgCl_2$ salt that was added to the MWCNT suspension during the EPD process [67]. The thickest-film sample showed Mg in the form of native oxide and carbonate at a much higher weight percentage (6.3At%). We assumed that these impurities could have contributed to blocking of some of the pores, which reduced the number of DA diffusion pathways, increased the R_{ct} of Region 3 and lowered the S/N to 9.

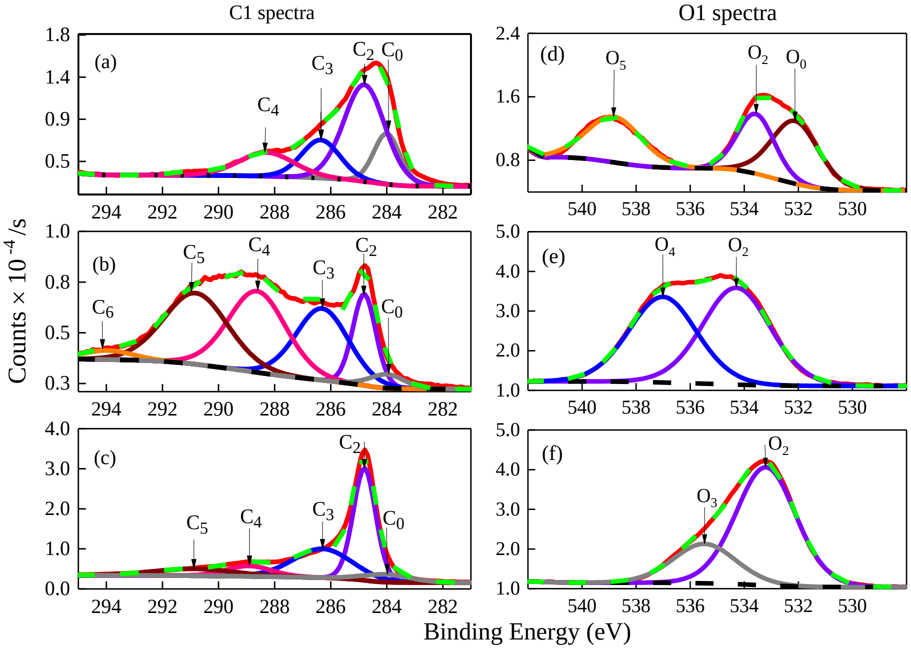

Figure 5-4. C1 and O1 XPS spectra of (a, d) unmodified, (b, e) MWCNT thin-film and (c, f) thickest-film UNCD microelectrodes. Legends: Experimental spectral (red curve), fitted spectral (green), background (black dashed). (a-c) Fitted C1 spectra consists of C_0 peak (gray), C_2 (violet), C_3 (blue), C_4 (pink), C_5 (Wine) and C_6 (orange). (d-f) Fitted O1 spectra consists of O_0 peak (wine), O_2 (violet), O_3 (gray), O_4 (blue), O_5 (orange). Surface functionality and binding energy for each C1 and O1 peak is shown in ***Table 5-4***.

Table 5-4. C1 and O1 XPS spectra of un-modified and MWCNT-modified UNCD microelectrodes.

C1 spectra	***C_0***	***C_2***	***C_3***	***C_4***	***C_5***	***C_6***
Functionality/ Binding energy (eV)	*sp^2carbon (C=C)/284*	*sp^3carbon (C-C)/ 284.8*	*aromatic (C-O) /~286*	*aliphatic (C=O), carboxyl groups/~288-289*	*carbonate (CO_3^{2-}) /~290*	*$\pi-\pi^*$ satellite peak/~291*
Unmodified UNCD (At%)	10±4	31±1	11.5±1.2	10.2±1.3	-	-
MWCNT thin film-UNCD (At%)	1±0.16	5±1	8±3	10±0.8	10±4	1±0.4
MWCNT thickest film-UNCD (At%)	3.3±0.4	20±1.5	16±1.8	4±1	5±2	-
O1 spectra	*O_0*	*O_2*	*O_3*	*O_4*	*O_5*	
Functionality/ Binding energy (eV)	*aliphatic (C-O)/ ~ 532*	*aromatic (C=O) / carbonyl group ~ 533-534*	*Ketone (-C=O) /~ 535*	*Phenolic Moieties /~ 537*	*ether (C-O-C)/ ~ 538*	
Unmodified UNCD (At%)	11.4±1.2	9±0.7	-	-	10±1.2	
MWCNT thin film-UNCD (At%)	-	33±6	-	29±3	-	
MWCNT thickest film-UNCD (At%)	-	28±0.5	10±5	-	-	

We have shown that MWCNT film modified UNCD microelectrodes provide an excellent combination of key microsensor metrics such as sensitivity, selectivity, limit of detection and S/N ratio for neurochemical detection. The complementary XPS and EIS spectra have identified three regions of varying electrochemical activity, which can be tailored to further improve the electrochemical resolution of the many brain analytes in addition to DA and 5-HT. For instance, by choosing an appropriate set of EPD process parameters and MWCNT film properties, the randomness of the pore structure within the

MWCNT film can be customized to enhance the detection performance metrics. This work demonstrates that the properties of this new class of hybrid MWCNT-UNCD microelectrode are dependent upon the MWCNT film thickness, their pore structure and their surface functionalities. There are three key benefits of the hybrid microelectrode. First, remarkable improvements in DA sensitivity (>125-fold) and limit of detection (LOD) (>180-fold) offer great promise for advancing the chemical neuroscience field. Second, MWCNTs can be selectively coated with a simple, scalable and low cost EPD process for multiplexed neurochemical sensing. Third, this work will establish a new generation of ultra-miniaturized microelectrode arrays that are highly suitable for advanced neuro electrochemical studies.

5.2 Platinum/MWCNT/Nafion Biosensor

The previous section provided a detailed discussion concerning improvement of dopamine sensing by hybrid MWCNT on top of a diamond electrode surface. However, a chip-based electrode cannot be implanted to animal tissues due to its size (16×16 mm^2). Besides, an additional exclusive layer should be applied to the electrode before any animal studies to screen interferents. In this study, Nafion was chosen and applied on top of MWCNT. This Pt/MWCNT/Nafion design not only rejected negatively charged ions like ascorbic acid; meanwhile, it provided protection to the MWCNT to avoid loss of electroactive materials due to non-specific bindings.

For the first experiment, we drop cast 4 drops of 5wt% Nafion(0.02µl) to paired electrode surfaces and then cured them at 165 °C for 5 minutes. Sensors were used from the 2nd day. Both a bare platinum electrode and a Nafion-coated platinum electrode were calibrated with 5-400 nM dopamine and 200 µM ascorbic acid. As shown in ***Figure 5-5*** and ***Table 5-5***, the bare platinum electrode had a sensitivity of 1.08±0.03 µA/µMcm^2. When a 4-drop-Nafion coating was added, the sensitivity was decreased to 0.62±0.02 µA/µMcm^2, but the coated electrode achieved a selectivity of 670±50.

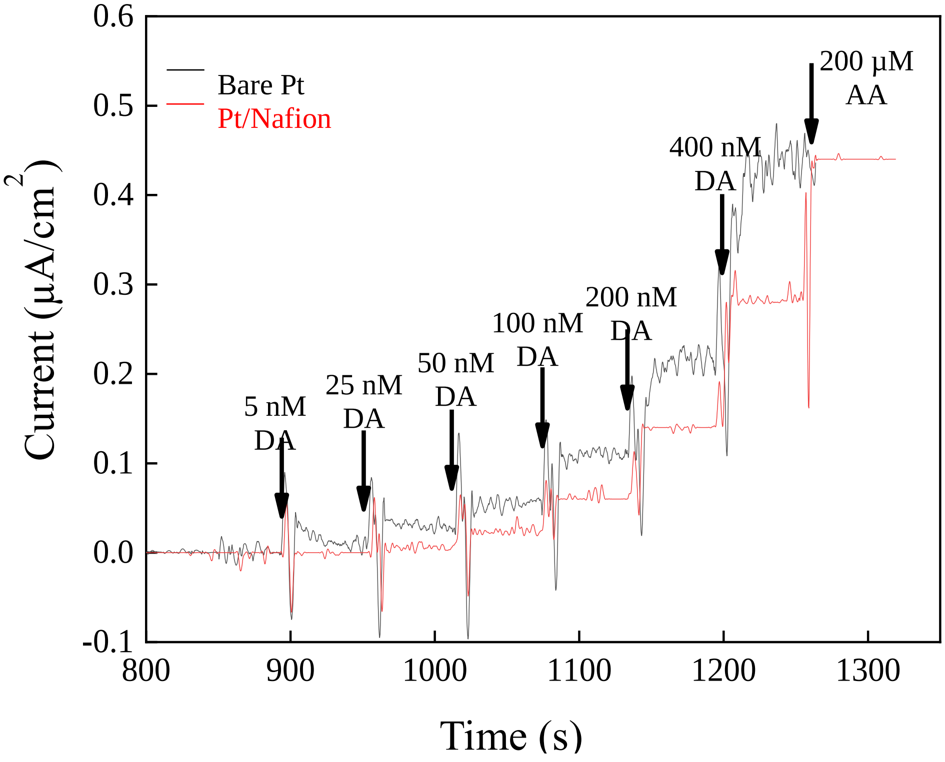

Figure 5-5. Calibration of Pt, Pt/Nafion sensor with 5, 25, 50, 100, 200, 400 nM dopamine, 200 µM ascorbic acid (concentrations after addition, left to right). Amperometry: + 0.3 V *vs* Ag/AgCl wire in a stirred 1X PBS beaker; the stir rate was 250 rpm.

Table 5-5. Performance summary from a Pt/Nafion design.

Sensor Type	***DA Sensitivity (μA/μMcm^2)***	***AA Selectivity***
Pt	1.08±0.03	N.A.
Pt/thin Nafion	0.62±0.02	670±50

There were some quite interesting findings here. First, according to ***Table 5-2***, the platinum surface has nearly a 4-fold higher sensitivity than UNCD surfaces. With an additional coating of Nafion, the Pt/Nafion design proved itself to be a sensor with both high selectivity and decent sensitivity. In addition, Pt/Nafion was sometimes used for dopamine sensing for *ex vivo* environments. Second, Pt/Nafion detected dopamine from 25 nM; however, this detection only happened in a beaker because the baseline noise was very low. In contrast, when we moved to *in vivo* use, the baseline fluctuation could be much higher; thus, we cannot claim a suitable limit of detection without improving sensitivity.

The next step was using what we learned regarding electrophoretic deposition, as described in ***Section 5.1.1.*** We electrochemically deposited (0.5mg/ml, -3 V, 300s) CNT on top of platinum electrodes to enhance the sensitivity. In this process, we found a drastic increase of more than 45 times, if comparing bare platinum to Pt/MWCNT. This difference was expected because MWCNT is known to have large surface areas that increase electroactive sites for dopamine adsorption. After CNT coating, 8 or 12 drops of Nafion were coated on MWCNT to make a thin or thick layer of Nafion. First, it is clear in ***Figure 5-6. A*** that with the coating of Nafion, the sensitivity decreased, and that selectivity increased because the AA signal got smaller. This result is consistent with our study showing that Pt/Nafion has selectivity to AA at the cost of a DA sensitivity decrease. Lost in DA sensitivity could be because a thin layer of Nafion causes a diffusion barrier for dopamine diffusion. Second, for a Pt/MWCNT surface coated with a thick layer of Nafion, the sensitivity kept decreasing, but it yielded a better selectivity.

An additional finding was that an ultra-thin Nafion layer again increased sensitivity by 10-fold, which means ultra-thin Nafion could attract dopamine by 10-fold; thus, the overall sensitivity increased to more than 400-fold (***Figure 5-6. B)***. However, this Pt/MWCNT/ultra-thin Nafion did not block AA, a phenomenon reported in earlier studies and explained as static attraction between negatively charged Nafion and positively charged dopamine. As an anionic exclusive layer, Nafion layer effectively rejects ascorbic acid while allowing penetration of dopamine. And an ultra-thin Nafion coating attracts dopamine due to electrostatic force. However, though this Pt/MWCNT/ultra-thin Nafion had super high sensitivity to dopamine, it is not marketable for *ex vivo* or *in vivo* studies because it did not impede any interferents. Still, it could be used for cell-cultures or in environments where interferents are known to not exist.

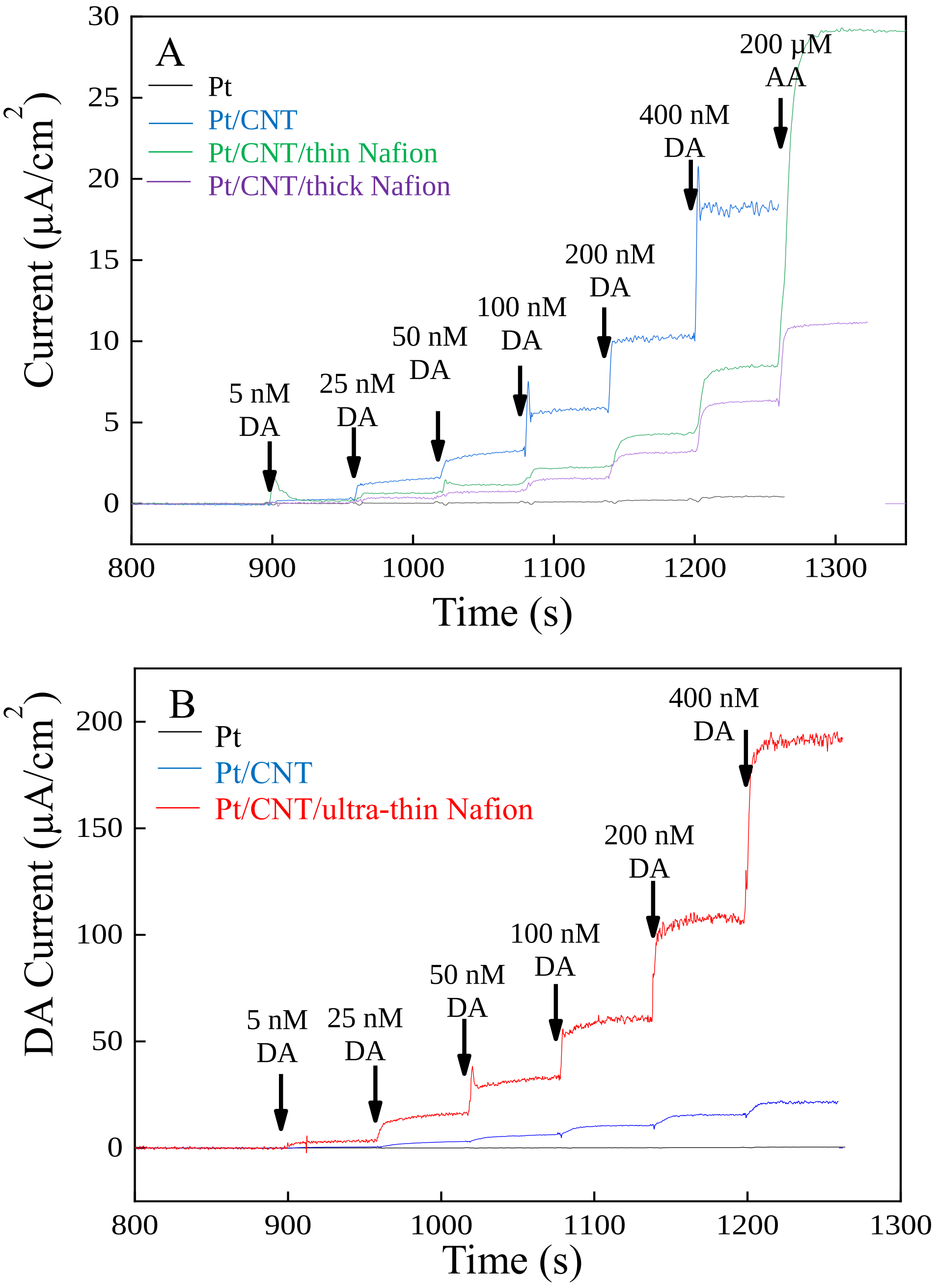

Figure 5-6. A) Calibration of Pt/CNT (blue), Pt/CNT/thin Nafion (green), Pt/CNT/thick Nafion (purple) ***B)*** Pt (black), Pt/CNT (blue), Pt/CNT/ultra-thin Nafion (red) sensor with 5, 25, 50, 100, 200, 400 nM dopamine, 200 µM ascorbic acid (concentrations after addition, left to right). Amperometry: + 0.3 V *vs* Ag/AgCl wire in a stirred 1X PBS beaker; the stir rate was 250 rpm.

Carbon fiber microelectrodes are known to have high sensitivity to dopamine due to rich edge planes and fast kinetics. However, if we compare a Pt electrode with CFM, its sensitivity is still competitive, ***Table 5-6.*** A thin-layer MWCNT and a platinum electrode modified with a thin layer of Nafion not only increased sensitivity from 0.62±0.02 to 29±5.2 μA/μMcm^2, a 47-fold increase. It also improved the limit of detection from 25 nM to 5 nM. A thick-layer of Nafion coating improved the selectivity from 235±14 to 683±17, only a 15-fold increase, but sacrificed sensitivity from 29±5.2 to 13.5±0.6 μA/μMcm^2. In considering candidates for dopamine sensing in animal studies, we would recommend either Pt/CNT/thin Nafion or Pt/CNT/thick Nafion.

Table 5-6. Summary of differently coated dopamine sensors.

Sensor Type	***DA Sensitivity (μA/μMcm^2)***	***AA Selectivity***
CFM [24]	1.1±0.06	N.A.
Pt	1.08±0.03	N.A.
Pt/thin Nafion	0.62±0.02	670±50
Pt/CNT	45.7±2.3	N.A.
Pt/CNT/Ultra-thin Nafion	433±40	N.A.
Pt/CNT/thin Nafion	29±5.2	235±14
Pt/CNT/thick Nafion	13.5±0.6	683±17

Similar to the long-term study of glutamate biosensors, we also did some experiments to explore the stability of dopamine sensors and seek the best way to store Pt/MWCNT/Nafion sensors. This sensor was used for 8 weeks, twice every week. The microelectrodes were dry stored in the box between each use. Within these two months of use, we did not find a drastic change in sensitivity or selectivity.

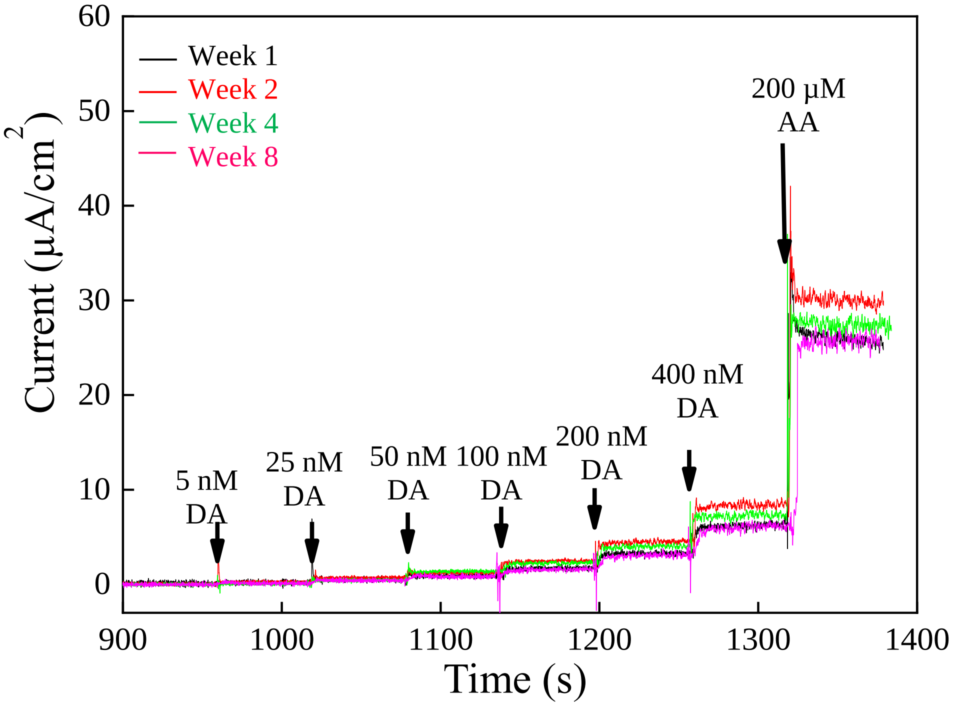

Figure 5-7. Calibration of MWCNT/Nafion modified platinum surfaces with 5, 25, 50, 100, 200, 400 nM dopamine, 200 µM AA (concentrations after addition, left to right). The platinum surfaces were coated with approximately 100 nm MWCNT and 12 drops of Nafion, approximately 0.02 µL per drop; this sensor was air dry stored if not in use. Amperometry: + 0.3 V *vs* Ag/AgCl wire in a stirred 1X PBS beaker; the stir rate was 250 rpm.

CHAPTER 6

EX VIVO AND IN VIVO EXPERIMENTS

6.1 Glutamate Level Measured in Sprague D Rats' Brain Slices After Electrical Stimulation

6.1.1 Glutamate Level from Self-referencing

Real-time detection of glutamate secreted from a hippocampal slice was accomplished by using electrical stimulation models. 100 µA unipolar stimulation pulses with varying widths were used to induce firing of neurons and thus release glutamate to the sensor surface. In this study, two channels were used, namely a glutamate site (Pt/Enzyme/mPD) and a sentinel site (Pt/BSA-GDH/mPD). The sentinel site had all the coatings the glutamate site had except GluOx, ***Figure 6-1***. Since it was an acute experiment, we used only one drop coating for both sites for a better sensitivity, and we used mPD2 as the exclusive layer for stable selectivity. Stimulation parameters were as shown in ***Table 6-1***: A-250 ms, B-50 ms, C-ten times 5 ms pulses separated by 1 ms, D-25 ms, and 1000 ms pulses (arrows) were used as a control to evaluate the activity of the slices. The data plotted in ***Figure 6-2. A*** is the raw data.

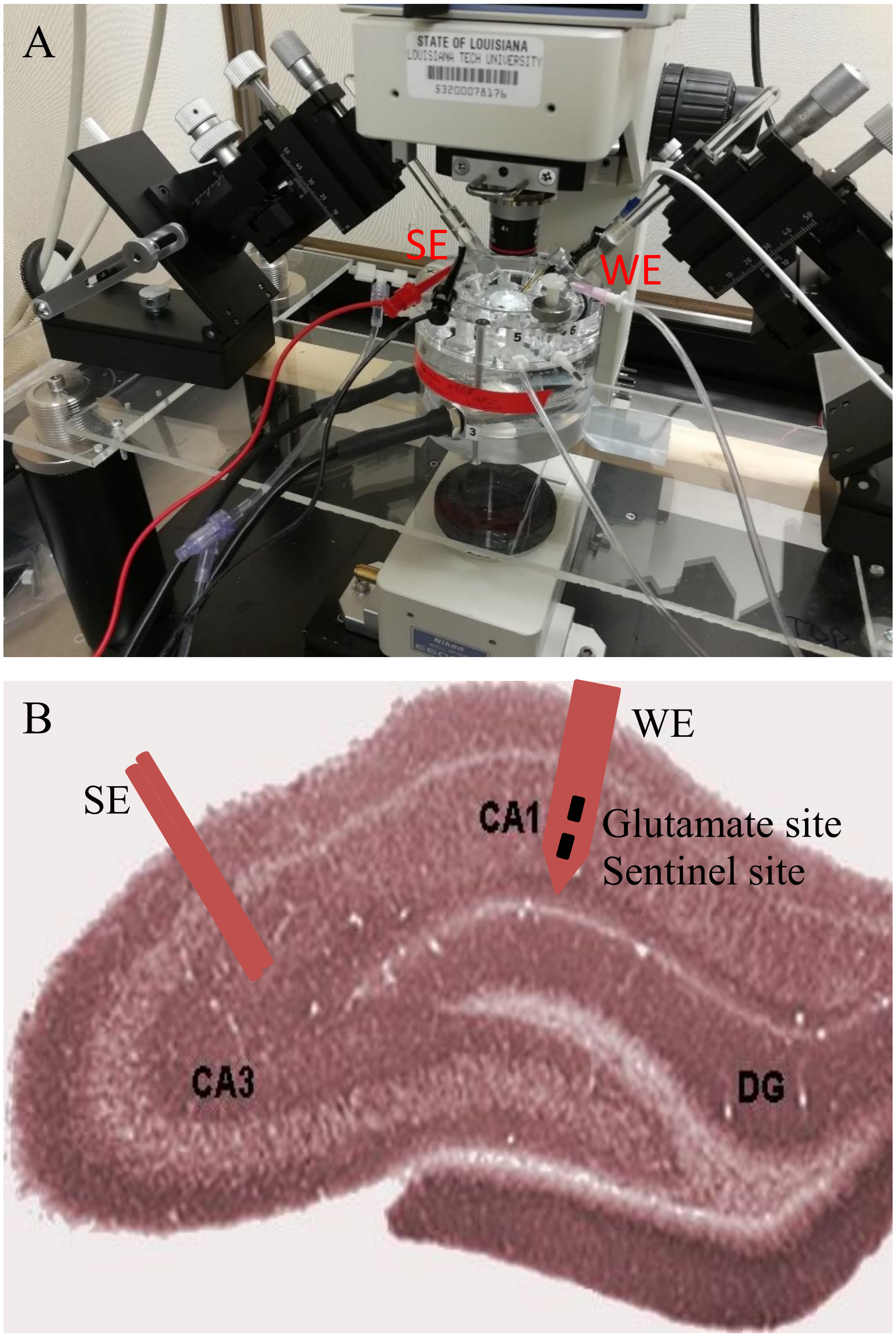

Figure 6-1. A. A picture of *ex vivo* experiments in a working chamber consisting of an 8-TRK probe as the working electrode (WE) and tungsten wire as the stimulus electrode (SE). ***B.*** Hippocampus region of a rat brain and position of WE, SE.

Thus, we subtracted the sentinel site current from glutamate site current and replotted in ***Figure 6-2. B***. Signal currents in ***Figure 6-2. B*** are defined as glutamate currents only. We again did four sets of pulse B after pulse D experiments because previous detection using pulse B generated slightly higher current from the sentinel site than the glutamate site. This difference was probably because glutamate neurons were not that active when we first did pulse B, and this fact was confirmed by observing a very low control current in arrow 2. Similarly, control currents in arrow 4,5 were higher when we performed pulse D and B. Therefore, we normalized signals between arrow 4 and 5 (pulse D and B) by normalizing control currents (arrow 4,5) with initial control currents (arrow 1,3). The corresponding glutamate concentration was calculated using a glutamate sensitivity from the linear range (1-200 μM) and rise time was calculated using $T_{10\text{-}90}$ for each parameter in ***Table 6-1,*** respectively.

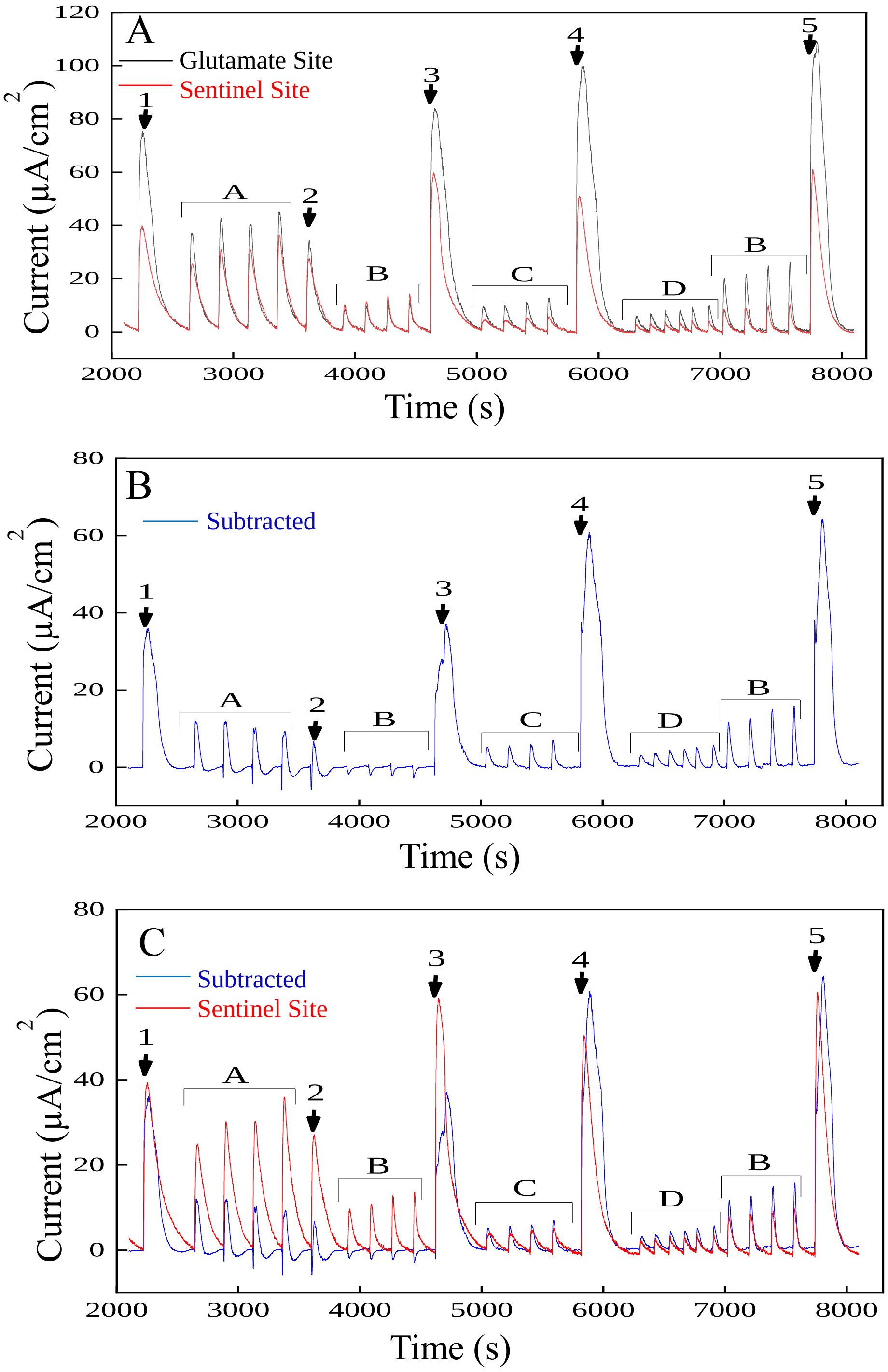

Figure 6-2. A) *Ex vivo* recording of stimulated release of Glu in rat hippocampal slice from two sites: glutamate site (Pt/Enzyme/mPD, black) and sentinel site (Pt/BSA-GDH/mPD, red). ***B)*** Glutamate current (blue) that subtracted sentinel site current from Glutamate site current. ***C)*** Glutamate current (blue) and sentinel site current (red). Amperometry: + 0.7 V *vs* Ag/AgCl wire.

Table 6-1. Stimulation parameter of pulses and corresponding glutamate current rise time.

Pulse Width	***Glu Concentration (μM)***	***Rise Time $T_{10\text{-}90}$ (s)***
Arrow-1000 ms as control	140.31±4.45	21.36±5.02
A-250 ms	41.41±2.42	8.36±1.96
B-50ms	31.05±1.95	5.34±0.16
C-5 ms×10, separated by 1 ms	23.04±1.45	7.18±0.63
D-25ms	9.53±0.94	4.47±0.46

The glutamate concentrations represented behind each stimulation parameter were within the ranges in extracellular spaces. We found that as the released glutamate concentration increased from 9.53 ± 0.94 µM (pulse D) to 140.31 ± 4.45 µM (control pulse), the rise time also increased from 4.47 ± 0.46 s to 21.36 ± 5.02 s. For the control stimulus, sometimes two phases of signal were found in the glutamate signal (arrow 3). This is probably because strong pulses affect more neurons, and it takes time for the glutamate “far away” to diffuse to the sensor surface. We have not found “two slopes” from weaker pulses Glu current or sentinel. Besides, the slow rise time was expected because it takes time for glutamate to leak out from the synapse and diffuse to the sensor surface, and the peaks we saw were “co-work” of neurons near the stimulus tungsten wire. At this point, we had successfully detected the glutamate level released from the Sprague D rats’ brain slices after electrical stimulation.

6.1.2 Signal in Sentinel Channel

There were some interesting findings here. First, we saw obvious currents, even from a sentinel site. The sentinel current was sometimes even higher than the glutamate current. This discrepancy indicated that there were some analytes our sensor was responsive to get released. This finding was not expected and was never reported in literature; however, it can be explained.

Table 6-2. Stimulation parameter of pulses and corresponding glutamate currents, sentinel current.

Pulse Width	***Glu Current (μA/cm^2)***	***Sentinel Current (μA/cm^2)***
Arrow-1000 ms as control	35.92±1.14	51.25±3.89
A-250 ms	10.60±0.62	29.9±1.83
B-50ms	7.95±0.50	8.63±0.34
C-5 ms×10, separated by 1 ms	5.9±0.37	4.23±0.24
D-25ms	2.44±0.24	3.28±0.18

It can be attributed to three factors: first, we think the main interferent source could be H_2O_2 or NO. ROS or RNS has been reported to be promoted by Ca^{2+} entry through a N-methyl-D-aspartate (NMDA) receptor, and micromolar range H_2O_2 could possibly have generated under electrical stimulations in extracellular spaces [93-96]. The functionality of our enzyme-based microsensor is relying on a high sensitivity to hydrogen peroxide, even after coating protein and mPD (***Figure 6-3.***). There is no obvious difference in H_2O_2 sensing between a glutamate site and a sentinel site when we drop cast 1 drop for each, followed by mPD2. Also, it was earlier mentioned that a platinum-based amperometry sensor has sensitivity to nitric oxide.

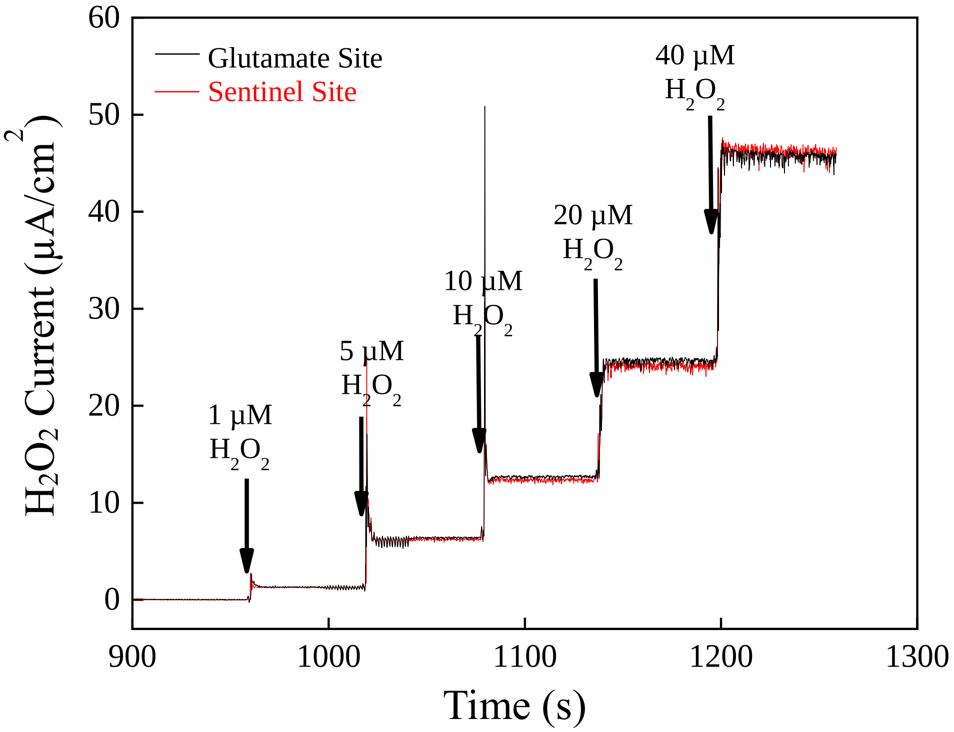

Figure 6-3. Calibration of glutamate and sentinel sites with 1, 5, 10, 20, 40 µM H_2O_2 (concentrations after addition, left to right). Amperometry: + 0.7 V *vs* Ag/AgCl wire in a stirred 1X PBS beaker; the stir rate was 250 rpm.

The H_2O_2 might have come from electrical stimulation, but we would not rule out the possibility that a small portion came from H_2O_2 diffused from the glutamate site. Though without glutamate oxidase proteins, the BSA-GDH-coated sentinel site itself did not give any current to glutamate in the beaker, but when we put such sensors (sentinel and glutamate in one pair) in a 5 ML petri dish, we did see 12.5 % H_2O_2 generated from the neighboring glutamate site diffused to the sentinel site, ***Figure 6-4.***

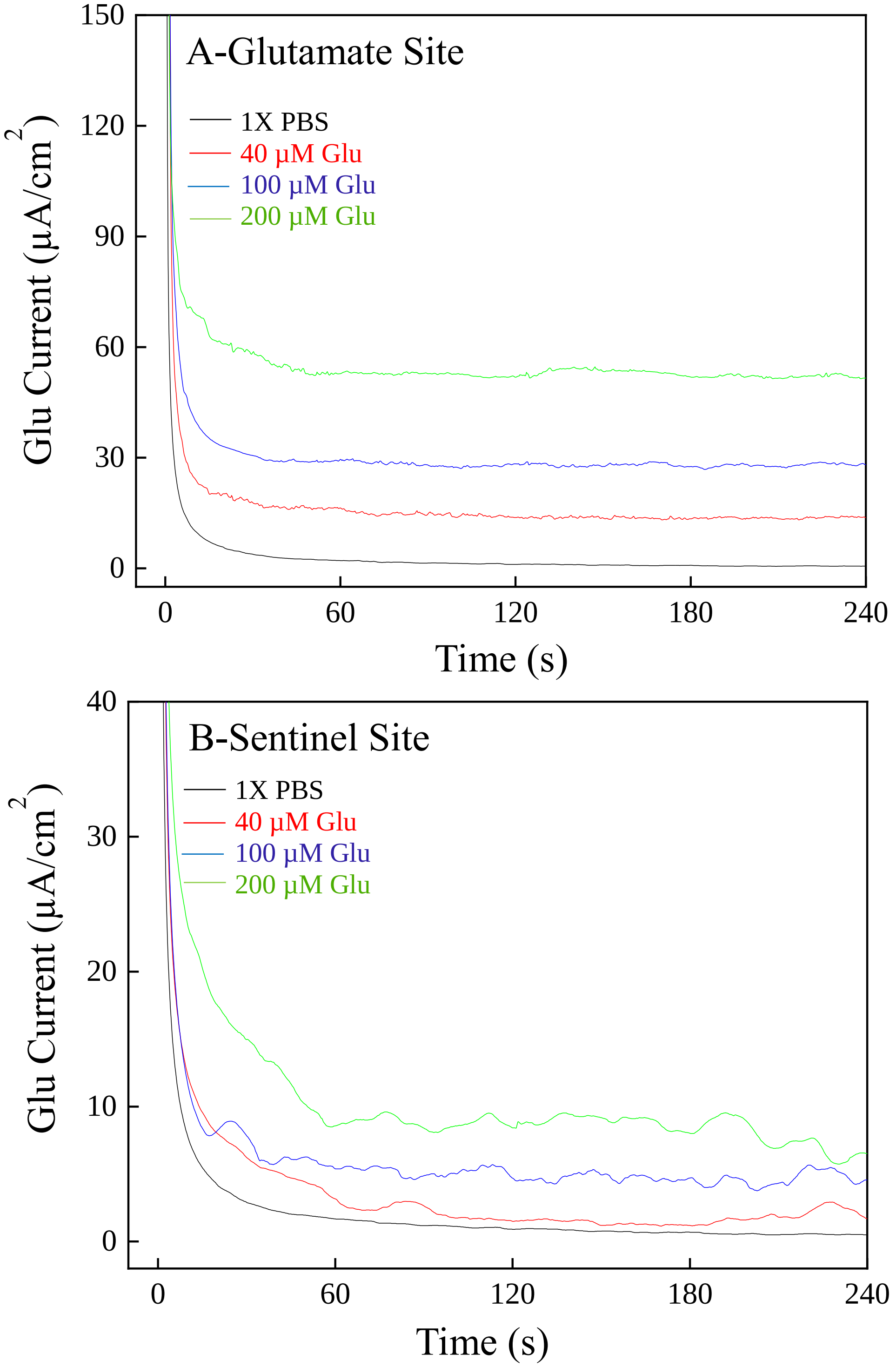

Figure 6-4. Amperometry curve of an **A**-glutamate site and **B**-sentinel site in a 5 ML petri dish containing 1X PBS (black), 40 (red), 100 (blue), 200 (green) µM glutamate, respectively. Amperometry: + 0.7 V *vs* Ag/AgCl wire.

Second, the interferent source could be due to excess release of ascorbic acid, though the sentinel site did not respond to glutamate and had a selectivity to a normal level of interferents as shown in ***Figure 6-5.*** However, the AA concentration in the extracellular environment of dentate has been reported to possibly increase by hundreds of micromolar after electrical stimulation, seen as an index for release of excitatory amino acid [97, 98]. Therefore, we expected some interferent signal from this aspect. Third, field current that generated from the ion channel opens, and flux of K^+, Na^+, Cl^- may also contribute to some small currents.

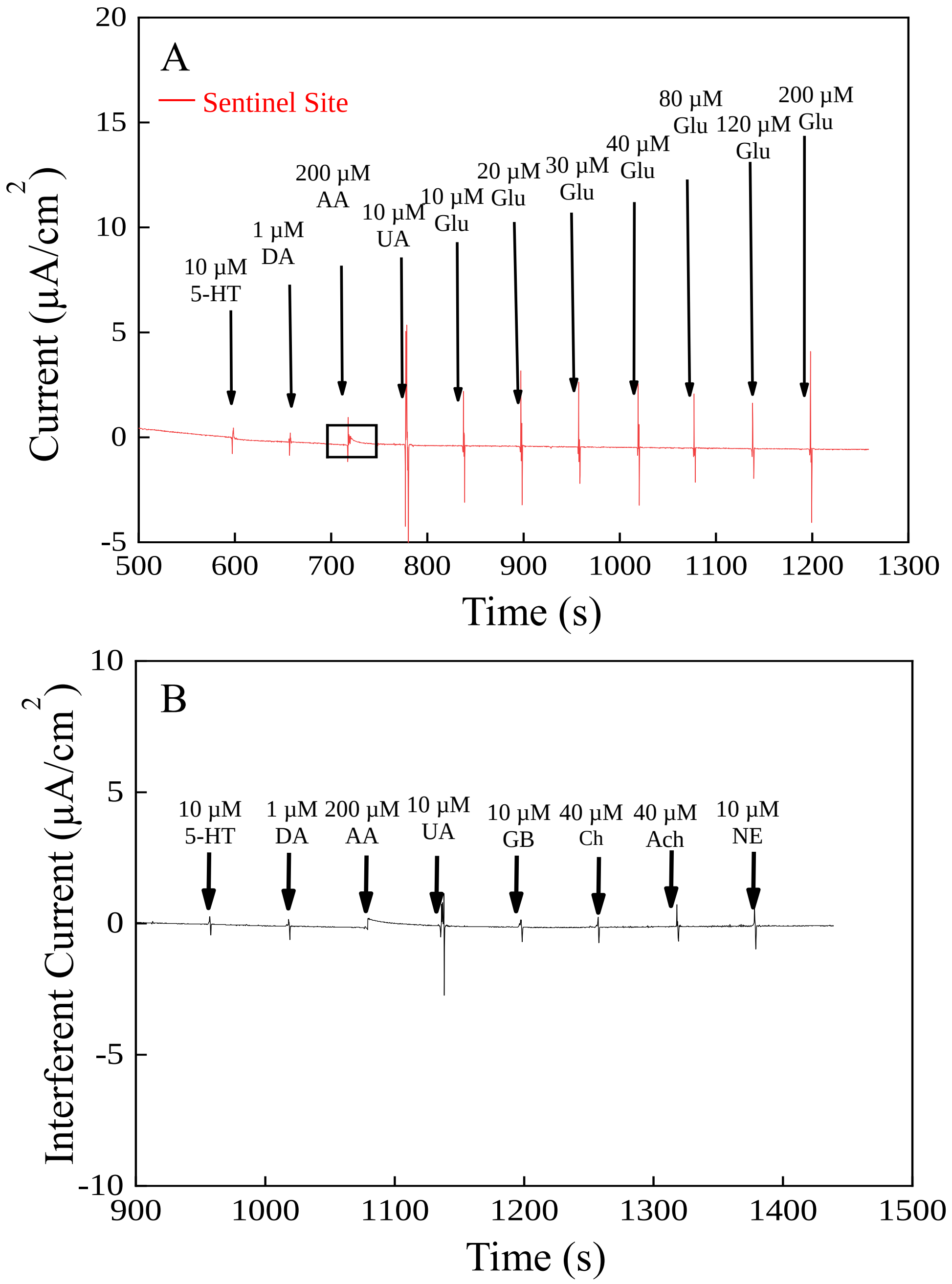

Figure 6-5. ***A)*** Calibration of a sentinel channel with 10 µM 5-HT, 1 µM dopamine, 200 µM ascorbic acid, 10 µM uric acid and 10, 20, 30, 40, 80, 120, 200 µM glutamate (concentrations after addition, left to right). ***B)*** Calibration of a sentinel channel with 10 µM 5-HT, 1 µM dopamine, 200 µM ascorbic acid, 10 µM uric acid, 10 µM GABA, 40 µM choline, 40 µM acetylcholine, 10 µM norepinephrine (concentrations after addition, left to right). Amperometry: + 0.7 V *vs* Ag/AgCl wire.

We hereby confirmed the capability of sensor used for *ex vivo* environment, established the importance of a self-referencing technique and gave proper explanations for potential interferents in the sentinel site.

6.2 Glutamate Level Measured in Awake Free-Behaving Sprague D Rats

6.2.1 Resting Glutamate Level Measured in Sprague D Rats

The 8-TRK sensors used for animal study had two coated sites, namely a glutamate site (Pt/Enzyme/mPD) and a sentinel site (Pt/BSA-GDH/mPD). The sentinel site had all the coatings a glutamate channel had except GluOx. The two sites were implanted into the hippocampus region. The stereotaxic coordinates of MEAs in the rat dentate gyrus are -5.0 mm anteroposterior, -2.3 mm mediolateral and -2.8/-3.0 mm dorsoventral from bregma.

When running the experiment, a 1000 Hz amperometry curve was recorded from the screen. One hour was given to obtain a clean, electrochemical baseline and electrophysiological signal. After plotting the sentinel and glutamate signal from this period, interestingly, we found an obvious baseline difference between the two sites. The only difference for the two MEAs was the GluOx because it was not coated on the sentinel site; otherwise, they had the same performance to all other interferents. Thus, this difference in baseline should be attributed to the basal glutamate dissolved in the extra-cellular space. Another evidence to support this conclusion occured when we did the experiment in *ex vivo* slices (aCSF). The baseline current of the glutamate and sentinel sites was the same: close to the default setting of current (28 $\mu A/cm^2$), ***Figure 6-6***. This shows that the intrinsic charging current of two sites were the same, and differences come from faradaic reactions.

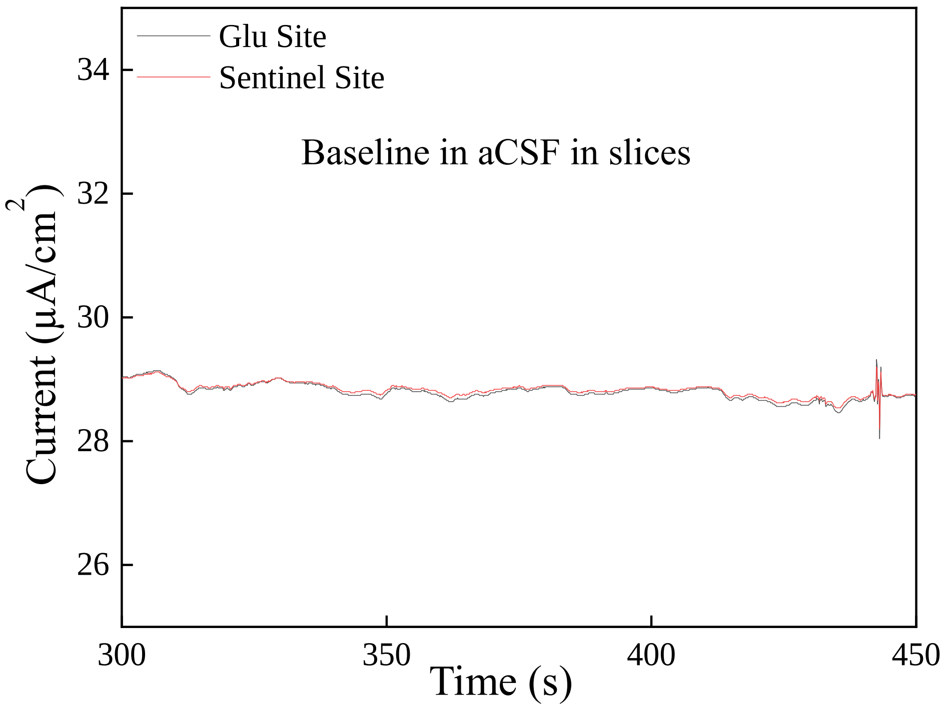

Figure 6-6. Baseline of glutamate and sentinel sites of 8-TRK probes in aCSF in a rat brain slice (CA1 area).

We plotted ***Figure 6-7***, which is the baseline of the two sites in a free-moving rat's brain at around one hour. The baseline differences that averaged from 4 sets of *in vivo* baseline data were 1.69±0.22 µA/cm^2. Since we know from pre-calibration that our glutamate channel sensitivity is 0.212 ± 4 µA/µMcm^2, the basal glutamate concentration was easily calculated and was 8 ± 1 µM. This number is consistent with previous basal-glutamate levels measured through electrochemical sensors or microdialysis coupled with high performance liquid chromatography [99, 100].

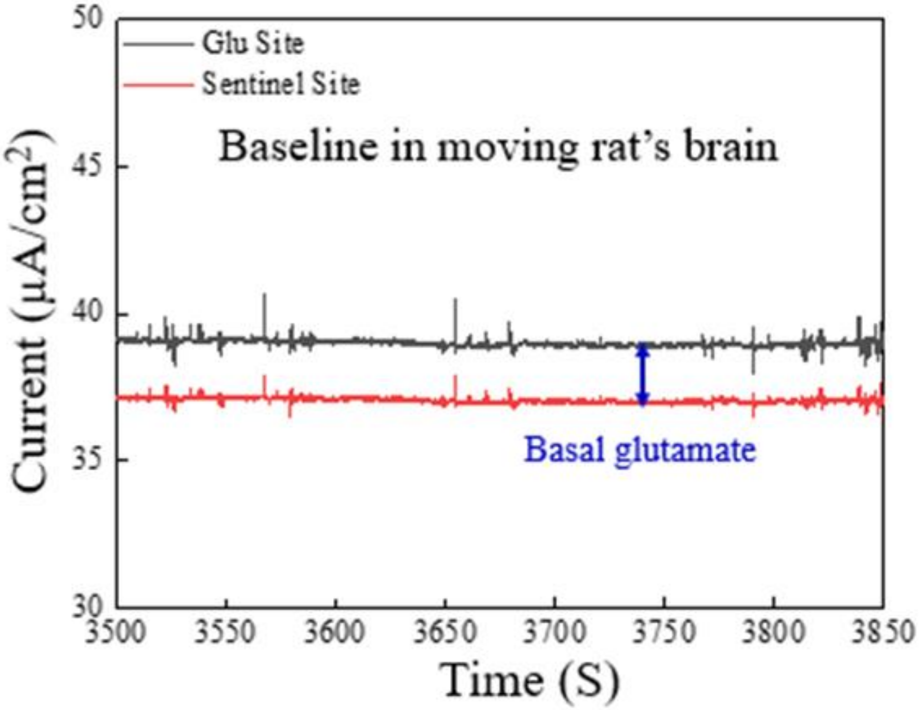

Figure 6-7. Baseline of glutamate and sentinel sites of 8-TRK probes in a rat brain (CA1 area) before any drug was given.

6.2.2 Glutamate Level Measured in Epileptic Sprague D Rats

Lithium chloride (3 M, 1 ML/Kg) was introduced to the rat 24 hours before experimental recording, pilocarpine (123 mM, 1 ML/Kg) was injected into the rat at the end of baseline recording (around 1 hr 10 min), and the signal was disturbed between 1 hr 10 min to 1 hr 20 min because there were lots of motion artifacts, and sometimes it needed reconnection. Onset of a seizure usually took around 20 min after pilocarpine, and the signal recorded for another two hours before phenobarbital and diazepam were given to stop the seizure. There were two main findings. First, we found obvious change in the sentinel current starting from the moment the seizure began, ***Figure 6-8***. This current lasted throughout the seizure. There is an initial drop in sentinel current. Then it took 400 s to slowly increase to a steady-sentinel current (56 pA, P2, ***Figure 6-9***), and again increased to second peak (40 pA, P2, ***Figure 6-9***) in 100s. After that, it took 4000 s for the sentinel current decreased to a base level. This current could possibly indicate high concentration of reactive oxidative species (ROS) (56 pA, steady current) and release of ascorbic acid (40 pA, second peak) in response to ROS. Besides, in ***Figure 6-8 B,*** the initial increase in sentinel current (steady current in phase 1, ***Figure 6-9***) suppressed glutamate signal by -8 pA (-0.75 µM), but in second increase (phase 2, @6000s), both signals hit the peak. This might involve more complicated mechanism: phase 1 and 2 represent release of H_2O_2 and ascorbic acid, respectively. Second, as for glutamate signal, after subtracting sentinel current from glutamate site, we have found a small spike that is at least 3 times higher than baseline noise (+3.02 µM Glu). H_2O_2 initially suppressed release of glutamate, but as a result of AA release, glutamate increased 32 pA (+3.02 µM Glu) in 300s and come to zero after 800s. Unlike sentinel current that finally diminished after 4000s, this glutamate spike current only lasted 800s, ***Figure 6-9***. This glutamate signal indicated the release and uptake in status-epileptic rat are slow. Beside this obvious Glu spike at 6000s, there were actually other two small currents at 8000 s and 10000s, respectively, ***Figure 6-8 B***. However, the latter currents were too small to be called “signal”. This glutamate concentration release is consistent with what has been reported earlier from an epileptic rat using lithium chloride and pilocarpine, in one-word, broad spike of glutamate. [101]

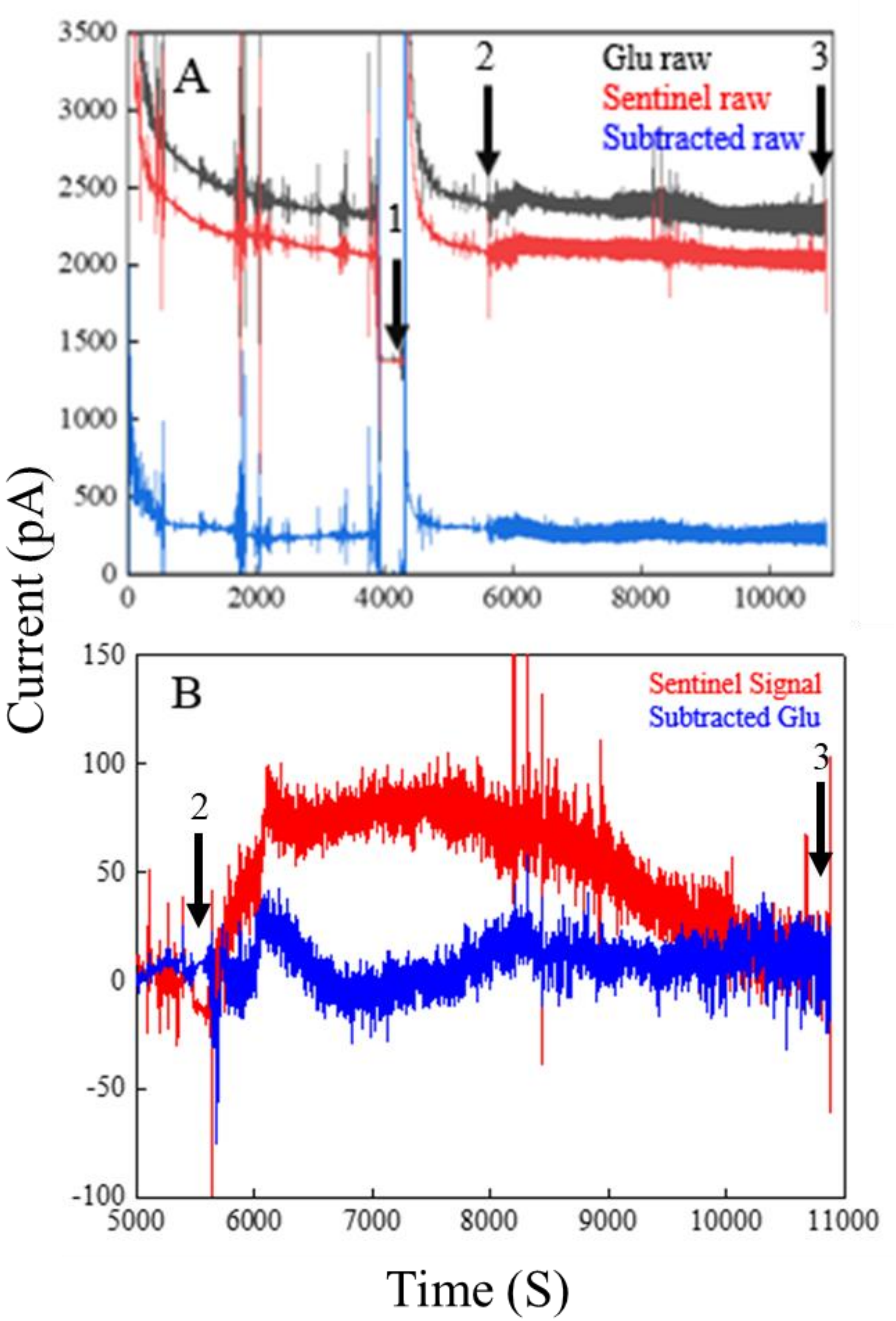

Figure 6-8. A. Raw data of glutamate and sentinel sites with arrow 1 indicating injection of pilocarpine, arrow 2 indicating onset of seizure and arrow 3 indicating the injection of the anti-epileptic drugs phenobarbital and diazepam. ***B.*** Baseline subtracted current of sentinel and glutamate signals from 8-TRK probes in a rat brain (CA1 area).

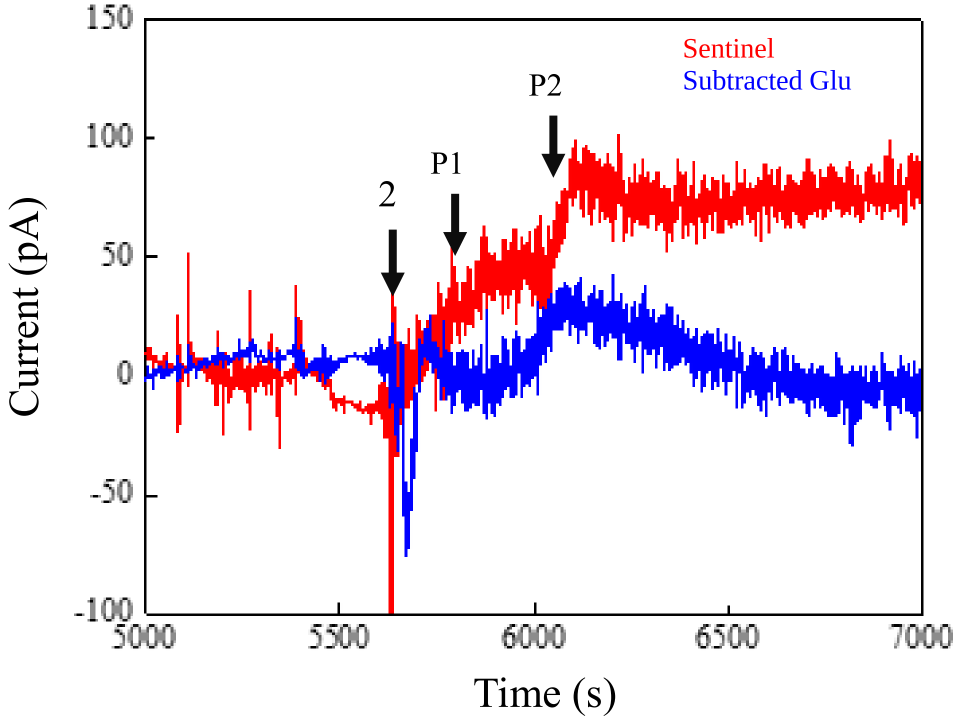

Figure 6-9. Subtracted current of glutamate site from 8-TRK probes in a rat brain (CA1 area) with arrow2 indicating the onset of seizure, P1 and P2 indicate 2 phases. Magnified segment is between 5ks and 7ks.

In addition to the signal current observed during experimental day, we also recorded the two MEAs after 2 weeks. Without any medicine given, the microelectrodes were simply run in CA1 for one hour. Post-status epilepsy could possibly develop in a rat's brain, we found interesting spikes from glutamate channel while sentinel channel gave nothing, ***Figure 6-10***. Using self-referencing technique, we plot the clean glutamate signals. We found many small spikes during the one-hour recording, which indicated the quick release of glutamate from pre-synaptic neurons to extra-cellular spaces and uptake dynamics of glutamate in astrocytes. The released glutamate concentrations were calculated and shown in ***Table 6-3***. Similar to recordings in the 1st week, released glutamate levels were still among micromolar range. The release of glutamate (0.17-0.44

s) are much faster than expected, however this can be explained by sensor surface are very close to neurons. The falling phase of peak was attributed to a comparatively slow uptake of glutamate by astrocytes that were near the probe.

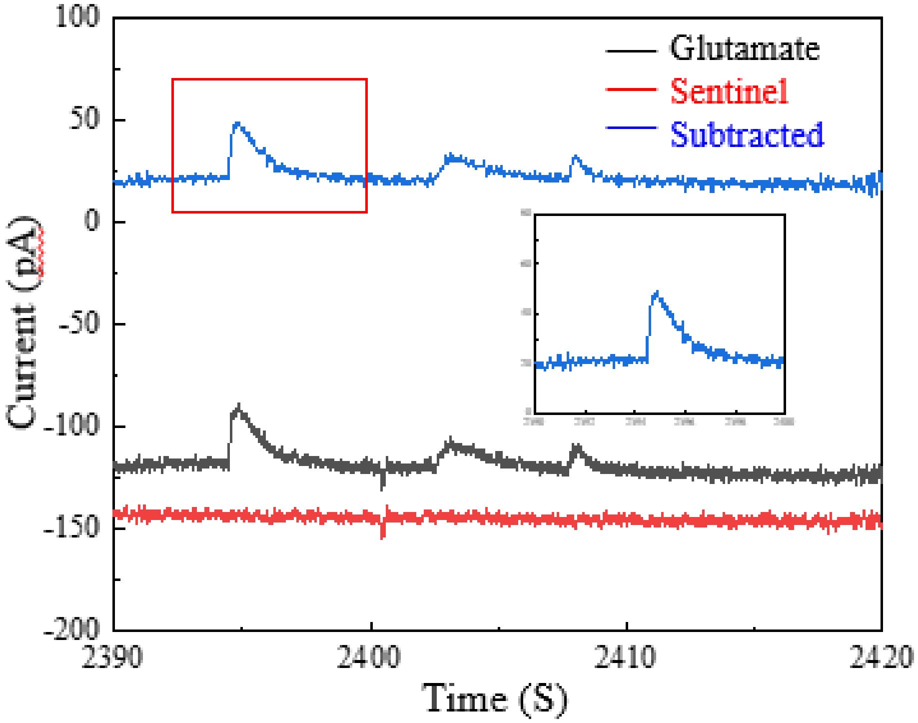

Figure 6-10. Currents from glutamate and sentinel sites in a rat brain after 2 weeks (CA1 area).

Table 6-3. Parameters of glutamate spikes observed after 2 weeks.

Time (s)	***Current (pA)***	***Glu Concentration (µM)***	***Rise Time $T_{10\text{-}90}$ (s)***	***Spike Full Time (s)***
2394.7	25.2	2.35	0.17	3.4
2403.2	12.4	1.16	0.44	4.5
2408.0	12.7	1.19	0.2	1.8

To sum up, from this *in-vivo* experiment, we tested our two-electrodes set-up (sentinel and glutamate MEAs) in a real free-moving animal. During pilocarpine-introduced convulsion (status epilepsy), we found obvious increase in sentinel and a small increase in glutamate current. Our data possibly initiated release dynamics of oxidant and antioxidant, glutamate release, and slow sentinel signal clearance. Glutamate current initially decreased by 8 pA (-0.75 µM), but then increased by 32 pA (3.02 µM) in 300s and come to zero after 800s (slow uptake or continuous relase). As for post-status epilepsy, there were occasional release of glutamate, quick (s') and small (<20 µM).

Those preliminary data possibly indicated a release of ascorbic acid, hydrogen peroxide and release of glutamate at status-epileptic rats, and only found small currents from glutamate when the rats' brain were “rewired” in post-status epilepsy after 2 weeks.

CHAPTER 7

CONCLUSIONS AND FUTURE WORK

7.1 Conclusions

In this dissertation, we have demonstrated a detailed understanding and development of enzyme-based glutamate microsensors and MWCNT-modified dopamine microsensors. Microsensors were tested for real-time monitoring of glutamate released after *ex vivo* electrical stimulations and *in vivo* recording of free-moving rats. The MWCNT-modified dopamine sensor showed increased sensitivity and limit of detection without compromising selectivity. Detailed findings are below:

1) An optimized microsensor microarray with high sensitivity (212-530 nA/µMcm^2), high AA selectivity (244-841) and low limit of detection (69-170 nM) has been developed for glutamate sensing.
2) Microsensors pre-cleaned with alcohol and electrochemically cleaned showed superiority in detecting hydrogen peroxide, a byproduct of the glutamate enzymatic reaction; pulse cleaned surfaces further enhanced sensitivity towards H_2O_2 by 53 %, which is because a porous structure formed after chemical etching, thus increasing glutamate sensitivity (25 %) after glutamate oxidase and mPD coatings.

3) Glutamate oxidase with optimal parameters was developed to pursue a excellent performance; the best glutamate oxidase concentration was 0.4 U/µl, and optimal applied potential was 0.7 V.
4) Optimal thickness for chronic use was 2.3 µm (4 drops), and for acute use, it was 0.41 µm (1 drop); glutamate sensitivity decreased with thickness.
5) An extended lifetime (>2month) for the enzyme-coated sensor was achieved if it was stored in DI water at room temperature, away from light and dust.
6) After study with a screening layer of meta-polyphenylene diamine, the microsensors displayed excellent selectivity against major interferents. A coating of mPD as an outer layer effectively impeded interferents and also decreased glutamate sensitivity but protected the enzymes. A 5 mV/s coating was more stable than 50 mV/s in the long term because it is thicker.
7) The glutamate sensor performed linearly within 1-600 µM glutamate, and it followed the Michaelis Menten equation within 8000 µM.
8) Interferents like H_2O_2, NO or AA could possibly be released after electrical stimulations, and those signal currents could not be eliminated totally; a self-referencing technique was necessary for *ex vivo* and *in vivo* glutamate experiments.
9) The basal glutamate concentration for *in vivo* study in the dentate gyrus was 8±1 µM.
10) Those preliminary data possibly indicated a release of ascorbic acid, hydrogen peroxide at the onset of seizure. Glutamate concentration was initially suppressed

but then increased by 32 pA (3.02 μM). Only found small currents from glutamate when the rats were stabilized in post-status epilepsy after 2 weeks.

11) We needed a hybrid electrode for dopamine sensing. There are three key benefits of the hybrid microelectrode. First, remarkable improvements in DA sensitivity (>125-fold) and LOD (>180-fold) compared with bare UNCD surfaces offer great promise for advancing the chemical neuroscience field. Second, MWCNTs can be selectively coated with a simple, scalable and low cost EPD process for multiplexed neurochemical electrodes. Third, complementary XPS and EIS spectra have identified three regions of varying electrochemical activity.
12) Through a facile two-step modification, a sensitivity-enhanced dopamine sensor was developed for animal studies. We used this sensor for 1 month when stored dry in the air after experiments.
13) Multi-Wall Carbon Nanotubes increased effective surface areas for dopamine adsorption and thus greatly increased sensitivity to dopamine by 45 fold. A thick layer of Nafion$^{(-)}$ impeded AA$^{(-)}$ through ionic impulsion and improved selectivity but decreased sensitivity to 13.5 fold.

7.2 Future Work

The methods and results obtained here form the foundation to launch research in development, modification and characterization of electrochemical biosensors for glutamate and dopamine detection. Based on the knowledge and experience obtained from this work, I would like to plan future work for neurochemical sensing as described below:

1. Use advanced materials for glutamate (H_2O_2) sensing. When designing our own sensor in the future, we can choose different metal materials when performing sputtering. Preliminary data showed that iridium results in an appreciably higher sensitivity to H_2O_2 sensing than platinum.
2. Use a metal pillar structure (length up to a few microns) as surfaces for glutamate sensing. Enzymes would be coated along the growth direction (perpendicular to the substrate). The advantage of this design is that instead of being lost during diffusion, H_2O_2 generated from the outer layer of enzyme could also achieve electron transfer and contribute to faradaic current.
3. Pretreat MWCNT surfaces for dopamine sensing, and further increase sensitivity by employing flame etching, laser ablation and electrochemical pretreatments (e.g., extended waveforms, overoxidation) that alter the microelectrode’s surface charge.
4. Design our own multi-array shank electrodes. The linear microelectrodes are too long in the Z-direction (>400 μm for only 2 sites). A multi-array shank electrode with circular site design would make it possible to record both from the cortex and the hippocampus, allowing us to detect more than one analyte when coating those arrays differently.

APPENDIX A

PROTOCOL FOR ENZYME FUNCTIONALIZATION OF PLATINUM MICROELECTRODE ARRAY FOR GLUTAMATE DETECTION

A. Surface cleaning of platinum (Pt) microelectrode arrays (MEAs) before modifying them with glutamate oxidase (GluOx)

1. Clean the Pt MEA surface of the probe with a polymer swab soaked with methanol. Gently rub the surface (15X) under the hood in the STL lab. (Protections are required.) Rinse probe with enough DI water, blow-dry with N_2 and store in the box.
2. Electrochemically cycle (ECC) the Pt MEA sites (two sites at a time – 45, 36, 27 and 18), using the 4-cable connector. Cycle between –0.3V and +1.0 V, 20 mV/s, 15 cycles) in 0.05 M sulfuric acid in a 2-electrode setup using the static cell (RE: Calomel). Flush with enough DI water and blow-dry with N_2. For this step, use the Gamry system.
3. CV characterize the Pt MEA sites in 1M KCL, followed by 5 mM ferro/5 mM ferri in 1M KCl solution (CV at 100 mV/s and EIS at OCP) in a 3-electrode setup using the static cell (RE: Calomel; CE: Pt wire). Follow the file name nomenclature.
4. Rinse with DI water immediately, clean the Pt MEA surface of the probe with a polymer swab soaked with DI water (15X), and rinse with DI water again. Blow-dry with N_2, and store in box.
5. Store the probe in a dry, cool place before use (drawer or cabinet).

B. GluOx preparation

1. Take the 25 units (U) GluOx powder (as received) from the –80 °C freezer (biomedical bldg. Room 220B) and transport to the lab in an ice box. Keep it in 4 °C refrigerator for 20 min. Then thaw the powder at room temperature for 30 min.
2. In the laminar flow hood (biomedical bldg. Room 240), clean the pipette tips using an IPA-soaked wipe before placing them inside the hood. Prepare the GluOx stock solution by adding sterile H_2O (from Dr. Decoster's lab) to the lyophilized GluOx. Add 25 µL of sterile H_2O to 25 units (U) of GluOx to yield 1.0 U/µL. ***The pipette tips for the transfer solution and the 200 µL microcentrifuge tubes that will be***

used should be sterilized when purchased or autoclaved and sterilized in Biomedical Engineering 2nd floor common lab.

3. Centrifuge for 30 s.
4. Split the GluOx solution into 1 μL volumes in 25, 200 μL-tubes. Transfer back to the BME, and store at –80°C until further use.
5. Prepare the bovine serum albumin (BSA)- glutaraldehyde matrix solution by transferring 13.3 mg BSA to a 1.5 mL centrifuge tube.
6. Add 980 μL DI H_20 to the 1.5 mL tube using a 1 mL pipette.
7. Mix the solution by re-pipetting (5X) using a 1 mL pipette until all the powders are dissolved. Avoid air bubbles. Microcentrifuge for 30 s.
8. Add 6.7 μL of glutaraldehyde.
9. Centrifuge for 30 s.
10. Set aside the solution for 5 min. (It should be light yellow.)
11. Add 1.5 μl of matrix solution to the thawed 200 μL centrifuge tube that contains 1 μL of 1.0 U/μL GluOx. This should form a solution of 0.8% BSA, 0.1% glutaraldehyde and 0.4 U/μL GluOx.
12. Microcentrifuge for 30 s.
13. Set aside the GluOx solution for 1 min.
14. Use the GluOx solution within 15 min.

C. GluOx coating procedure

1. Rinse a surface-cleaned Pt MEA probe with DI water, blow-dry with N_2 and put the probe in the oven at 160 °C for 5 min.
2. Use a Hamilton microsyringe (2 μL) to coat the GluOx or basal solution.
3. Rinse the syringe in IPA (3X) and then in DI H_20 (3X).
4. Pre-rinse the syringe with GluOx solution. (You can use 0.5-1 μL out of 2.5 μL in the aliquot.)
5. Fill the syringe carefully with GluOx solution to avoid entrapped bubbles.
6. Place and focus the probe horizontally on the box where it was stored under the Nikon stereomicroscope. ***(This step should be done before the GluOx solutions are ready.)***
7. Carefully dispense one bead of the solution (~0.05μL) on top of any of the two neighboring Pt sites. Do not touch the probe surface or scrape it.
8. Wait 90 s before dispensing the next drop. The total number of drops depend on need.
9. Dry or cure the coated probe by storing it in the dark at room temperature for at least 2 days (reported to be ideal for long-term by Gerhardt Group).

10. Rinse the syringe in IPA (3X) and then in DI H_2O (3X).

D. mPD coating

5. The night before experimental day, measure and dissolve 10 mM mPD in 1 M NaCl and then purge with nitrogen for 30 min.
6. Perform cyclic voltammetry scans between +0.2 V and +0.8 V, using a saturated calomel electrode as a reference electrode to form a size-exclusive mPD layer.
7. Rinse mPD coated MEAs with DI water and store dry overnight.
8. Between each use, store sensors in DI water.

APPENDIX B

PROTOCOL FOR MWCNT FUNCTIONALIZATION OF PLATINUM MICROELECTRODE ARRAY FOR DOPAMINE DETECTION

A. Preparation of MWCNT ink

1. Use as-received MWCNT ink (1 mg/mL) purchased from Nanolab, Inc (Waltham, MA) with a diameter of 15 ± 5 nm, length of 1–5 μm, and 5% COOH functionalized.
2. Dilute the MWCNT to 0.5 mg/mL by mixing 1:1 with DI water.
3. Add 5 µM $MgCl_2 \cdot 6H_2O$ salt solution to the MWCNT suspension and sonicate for 30 min. Do this to charge the MWCNT surface positively.

B. Electrophoretic deposition

1. Control 1.5 mm of space between the working electrode (WE) and the counter electrode (CE, platinum wire, Alfa Aesar). Fill the gap between the WE and CE with MWCNT suspension.
2. Apply a voltage (-3 V to -9 V) using the g\Gamry reference 600 Potentiostat (Gamry Instruments, Warminster, PA, USA) to the WE for various time (200-500 s) until MWCNT of desired thickness is deposited.
3. After the EPD process is completed, soak the WE in DI water for 5 min and then rinse for 30 s to remove any non-specifically bound MWCNTs and chloride salt residues. Finally, dry the MWCNT-modified microelectrodes in an oven at 50 °C for 45 min.

C. Nafion coating

1. To increase selectivity, apply Nafion to the MWCNT-coated surface.
2. Apply 8 drops of 5wt% Nafion (0.02µl per drop) to paired Pt/MWCNT electrode surfaces and then cure at 165 °C for 5 min.
3. Use the sensors from the second day.
4. Between each use, store the sensors to air dry.

REFERENCES

[1] Pagels, Markus, Clive E. Hall, Nathan S. Lawrence, Andrew Meredith, Timothy GJ Jones, Herman P. Godfried, CS James Pickles *et al*. "All-diamond microelectrode array device." Analytical chemistry 77, no. 11 (2005): 3705-3708.

[2] Suzuki, Ikuro, Mao Fukuda, Keiichi Shirakawa, Hideyasu Jiko, and Masao Gotoh. "Carbon nanotube multi-electrode array chips for noninvasive real-time measurement of dopamine, action potentials, and postsynaptic potentials." Biosensors and Bioelectronics 49 (2013): 270-275.

[3] Nutt, David J. "Relationship of neurotransmitters to the symptoms of major depressive disorder." The Journal of clinical psychiatry 69 (2008): 4-7.

[4] Meldrum, Brian S. "The role of glutamate in epilepsy and other CNS disorders." Neurology (1994).

[5] Nicholls, David G. "The glutamatergic nerve terminal." European journal of biochemistry 212, no. 3 (1993): 613-631.

[6] Danbolt, Niels C. "Glutamate uptake." Progress in neurobiology 65, no. 1 (2001): 1-105.

[7] Palucha, A., and A. Pilc. "The involvement of glutamate in the pathophysiology of depression." Drug news & perspectives18, no. 4 (2005): 262-268.

[8] Sandberg, Stefan G., and Paul A. Garris. "Neurochemistry of addiction: monitoring essential neurotransmitters of addiction." In Advances in the Neuroscience of Addiction, pp. 110-146. CRC Press, 2010.

[9] Featherstone, David E. "Intercellular glutamate signaling in the nervous system and beyond." ACS chemical neuroscience 1, no. 1 (2009): 4-12.

[10] Hawkins, Richard A. "The blood-brain barrier and glutamate." The American journal of clinical nutrition 90, no. 3 (2009): 867S-874S.

[11] Olney, John W. "Brain lesions, obesity, and other disturbances in mice treated with monosodium glutamate." Science 164, no. 3880 (1969): 719-721.

[12] Robinson, Michael B., and Joshua G. Jackson. "Astroglial glutamate transporters coordinate excitatory signaling and brain energetics." Neurochemistry international 98 (2016): 56-71.

[13] During, Matthew J., and Dennis D. Spencer. "Extracellular hippocampal glutamate and spontaneous seizure in the conscious human brain." The lancet 341, no. 8861 (1993): 1607-1610.

[14] Bryant, Astra S., Bojia Li, Mark P. Beenhakker, and John R. Huguenard. "Maintenance of thalamic epileptiform activity depends on the astrocytic glutamate-glutamine cycle." Journal of neurophysiology 102, no. 5 (2009): 2880-2888.

[15] Tanaka, Kohichi, Kei Watase, Toshiya Manabe, Keiko Yamada, Masahiko Watanabe, Katsunobu Takahashi, Hisayuki Iwama *et al*. "Epilepsy and exacerbation of brain injury in mice lacking the glutamate transporter GLT-1." Science 276, no. 5319 (1997): 1699-1702.

[16] Monge-Acuña, Andrea A., and Jaime Fornaguera-Trías. "A high-performance liquid chromatography method with electrochemical detection of gamma-aminobutyric acid, glutamate and glutamine in rat brain homogenates." Journal of neuroscience methods 183, no. 2 (2009): 176-181.

[17] Reinhoud, Nico J., Hendrik-Jan Brouwer, Lusi M. van Heerwaarden, and Gerdien AH Korte-Bouws. "Analysis of glutamate, GABA, noradrenaline, dopamine, serotonin, and metabolites using microbore UHPLC with electrochemical detection." ACS chemical neuroscience 4, no. 5 (2013): 888-894.

[18] Watson, Christopher J., B. Jill Venton, and Robert T. Kennedy. "In vivo measurements of neurotransmitters by microdialysis sampling." (2006): 1391-1399.

[19] Okumoto, Sakiko, Loren L. Looger, Kristina D. Micheva, Richard J. Reimer, Stephen J. Smith, and Wolf B. Frommer. "Detection of glutamate release from neurons by genetically encoded surface-displayed FRET nanosensors." Proceedings of the National Academy of Sciences 102, no. 24 (2005): 8740-8745.

[20] Hires, Samuel Andrew, Yongling Zhu, and Roger Y. Tsien. "Optical measurement of synaptic glutamate spillover and reuptake by linker optimized glutamate-sensitive fluorescent reporters." Proceedings of the National Academy of Sciences105, no. 11 (2008): 4411-4416.

[21] Okubo, Yohei, Hiroshi Sekiya, Shigeyuki Namiki, Hirokazu Sakamoto, Sho Iinuma, Miwako Yamasaki, Masahiko Watanabe, Kenzo Hirose, and Masamitsu Iino. "Imaging extrasynaptic glutamate dynamics in the brain." Proceedings of the National Academy of Sciences 107, no. 14 (2010): 6526-6531.

[22] Weltin, Andreas, Jochen Kieninger, and Gerald A. Urban. "Microfabricated, amperometric, enzyme-based biosensors for in vivo applications." Analytical and bioanalytical chemistry408, no. 17 (2016): 4503-4521.

[23] Burmeister, Jason J., and Greg A. Gerhardt. "Self-referencing ceramic-based multisite microelectrodes for the detection and elimination of interferences from the

measurement of L-glutamate and other analytes." Analytical chemistry 73, no. 5 (2001): 1037-1042.

[24] Day, B. K., F. Pomerleau, J. J. Burmeister, P. Huettl, and G. A. Gerhardt. "Microelectrode array studies of basal and potassium-evoked release of l-glutamate in the anesthetized rat brain." Journal of neurochemistry 96, no. 6 (2006): 1626-1635.

[25] Weltin, Andreas, Jochen Kieninger, Barbara Enderle, Anne-Kathrin Gellner, Brita Fritsch, and Gerald A. Urban. "Polymer-based, flexible glutamate and lactate microsensors for in vivo applications." Biosensors and Bioelectronics 61 (2014): 192-199.

[26] Özel, Rıfat Emrah, Cristina Ispas, Mallikarjunarao Ganesana, J. C. Leiter, and Silvana Andreescu. "Glutamate oxidase biosensor based on mixed ceria and titania nanoparticles for the detection of glutamate in hypoxic environments." Biosensors and Bioelectronics 52 (2014): 397-402.

[27] Zhang, Maogen, Conor Mullens, and Waldemar Gorski. "Amperometric glutamate biosensor based on chitosan enzyme film." Electrochimica acta 51, no. 21 (2006): 4528-4532.

[28] Tian, Faming, Alexander V. Gourine, Robert TR Huckstepp, and Nicholas Dale. "A microelectrode biosensor for real time monitoring of L-glutamate release." Analytica chimica acta645, no. 1-2 (2009): 86-91.

[29] Burmeister, Jason J., Verda A. Davis, Jorge E. Quintero, Francois Pomerleau, Peter Huettl, and Greg A. Gerhardt. "Glutaraldehyde cross-linked glutamate oxidase coated microelectrode arrays: selectivity and resting levels of glutamate in the CNS." ACS chemical neuroscience 4, no. 5 (2013): 721-728.

[30] Arima, Jiro, Takashi Tamura, Hitoshi Kusakabe, Makoto Ashiuchi, Toshiharu Yagi, Hidehiko Tanaka, and Kenji Inagaki. "Recombinant expression, biochemical characterization and stabilization through proteolysis of an l-glutamate oxidase from Streptomyces sp. X-119-6." Journal of biochemistry 134, no. 6 (2003): 805-812.

[31] Arima, Jiro, Chiduko Sasaki, Chika Sakaguchi, Hiroshi Mizuno, Takashi Tamura, Akiko Kashima, Hitoshi Kusakabe, Shigetoshi Sugio, and Kenji Inagaki. "Structural characterization of l-glutamate oxidase from Streptomyces sp. X-119-6." The FEBS journal 276, no. 14 (2009): 3894-3903.

[32] Bartlett, P. N., V. Q. Bradford, and R. G. Whitaker. "Enzyme electrode studies of glucose oxidase modified with a redox mediator." Talanta 38, no. 1 (1991): 57-63.

[33] Chaubey, Asha, and BlD Malhotra. "Mediated biosensors." Biosensors and bioelectronics 17, no. 6-7 (2002): 441-456.

[34] Castillo, J., Szilveszter Gáspár, Suzanne Leth, M. Niculescu, Alessia Mortari, Ibolya Bontidean, V. Soukharev, S. A. Dorneanu, A. D. Ryabov, and Elisabeth Csöregi.

"Biosensors for life quality: Design, development and applications." Sensors and Actuators B: Chemical 102, no. 2 (2004): 179-194.

[35] Ruzgas, Tautgirdas, Elisabeth Csöregi, Jenny Emnéus, Lo Gorton, and György Marko-Varga. "Peroxidase-modified electrodes: fundamentals and application." Analytica Chimica Acta 330, no. 2-3 (1996): 123-138.

[36] Ammam, Malika, and Jan Fransaer. "Highly sensitive and selective glutamate microbiosensor based on cast polyurethane/AC-electrophoresis deposited multiwalled carbon nanotubes and then glutamate oxidase/electrosynthesized polypyrrole/Pt electrode." Biosensors and Bioelectronics 25, no. 7 (2010): 1597-1602.

[37] Burmeister, Jason J., Francois Pomerleau, Michael Palmer, Brian K. Day, Peter Huettl, and Greg A. Gerhardt. "Improved ceramic-based multisite microelectrode for rapid measurements of L-glutamate in the CNS." Journal of neuroscience methods 119, no. 2 (2002): 163-171.

[38] Miller, Erin M., Jorge E. Quintero, François Pomerleau, Peter Huettl, Greg A. Gerhardt, and Paul EA Glaser. "Simultaneous glutamate recordings in the frontal cortex network with multisite biomorphic microelectrodes: new tools for ADHD research." Journal of neuroscience methods 252 (2015): 75-79.

[39] Robinson, Donita L., B. Jill Venton, Michael LAV Heien, and R. Mark Wightman. "Detecting subsecond dopamine release with fast-scan cyclic voltammetry in vivo." Clinical chemistry 49, no. 10 (2003): 1763-1773.

[40] Pihel, Karin, Q. David Walker, and R. Mark Wightman. "Overoxidized polypyrrole-coated carbon fiber microelectrodes for dopamine measurements with fast-scan cyclic voltammetry." Analytical chemistry 68, no. 13 (1996): 2084-2089.

[41] Wang, Huai-Sheng, Tian-Hua Li, Wen-Li Jia, and Hong-Yan Xu. "Highly selective and sensitive determination of dopamine using a Nafion/carbon nanotube coated poly (3-methylthiophene) modified electrode." Biosensors and Bioelectronics 22, no. 5 (2006): 664-669.

[42] Zachek, Matthew K., Pavel Takmakov, Benjamin Moody, R. Mark Wightman, and Gregory S. McCarty. "Simultaneous decoupled detection of dopamine and oxygen using pyrolyzed carbon microarrays and fast-scan cyclic voltammetry." Analytical chemistry 81, no. 15 (2009): 6258-6265.

[43] Dutta, Gaurab, Shabnam Siddiqui, Hongjun Zeng, John A. Carlisle, and Prabhu U. Arumugam. "The effect of electrode size and surface heterogeneity on electrochemical properties of ultrananocrystalline diamond microelectrode." Journal of Electroanalytical Chemistry 756 (2015): 61-68.

[44] Strand, Andrew M., and B. Jill Venton. "Flame etching enhances the sensitivity of carbon-fiber microelectrodes." Analytical chemistry 80, no. 10 (2008): 3708-3715.

[45] Nemes, Peter, and Akos Vertes. "Laser ablation electrospray ionization for atmospheric pressure, in vivo, and imaging mass spectrometry." Analytical chemistry 79, no. 21 (2007): 8098-8106.

[46] Arumugam, Prabhu U., Hua Chen, Shabnam Siddiqui, Jarret AP Weinrich, Ayodeji Jejelowo, Jun Li, and M. Meyyappan. "Wafer-scale fabrication of patterned carbon nanofiber nanoelectrode arrays: a route for development of multiplexed, ultrasensitive disposable biosensors." Biosensors and Bioelectronics 24, no. 9 (2009): 2818-2824.

[47] Li, Jun, Jessica E. Koehne, Alan M. Cassell, Hua Chen, Hou Tee Ng, Qi Ye, Wendy Fan, Jie Han, and M. Meyyappan. "Inlaid multi-walled carbon nanotube nanoelectrode arrays for electroanalysis." Electroanalysis: An International Journal Devoted to Fundamental and Practical Aspects of Electroanalysis 17, no. 1 (2005): 15-27.

[48] Kovach, Paul M., Andrew G. Ewing, Robert L. Wilson, and R. Mark Wightman. "In vitro comparison of the selectivity of electrodes for in vivo electrochemistry." Journal of neuroscience methods 10, no. 3 (1984): 215-227.

[49] Rand, Emily, Adaikkappan Periyakaruppan, Zuki Tanaka, David A. Zhang, Michael P. Marsh, Russell J. Andrews, Kendall H. Lee, Bin Chen, M. Meyyappan, and Jessica E. Koehne. "A carbon nanofiber-based biosensor for simultaneous detection of dopamine and serotonin in the presence of ascorbicacid." Biosensors and Bioelectronics 42 (2013): 434-438.

[50] Huang, Jianshe, Yang Liu, Haoqing Hou, and Tianyan You. "Simultaneous electrochemical determination of dopamine, uric acid and ascorbic acid using palladium nanoparticle-loaded carbon nanofibers modified electrode." Biosensors and Bioelectronics 24, no. 4 (2008): 632-637.

[51] Salimi, Abdollah, Kamaleddin Abdi, and Gholam-Reza Khayatian. "Amperometric detection of dopamine in the presence of ascorbic acid using a nafion coated glassy carbon electrode modified with catechin hydrate as a natural antioxidant." Microchimica Acta 144, no. 1-3 (2004): 161-169.

[52] Sainio, Sami, Tommi Palomäki, Sneha Rhode, Minna Kauppila, Olli Pitkänen, Tuula Selkälä, Geza Toth *et al*. "Carbon nanotube (CNT) forest grown on diamond-like carbon (DLC) thin films significantly improves electrochemical sensitivity and selectivity towards dopamine." Sensors and Actuators B: Chemical 211 (2015): 177-186.

[53] Hočevar, Samo B., Joseph Wang, Randhir Prakash Deo, Mustafa Musameh, and Božidar Ogorevc. "Carbon nanotube modified microelectrode for enhanced voltammetric detection of dopamine in the presence of ascorbate." Electroanalysis: An International Journal Devoted to Fundamental and Practical Aspects of Electroanalysis 17, no. 5-6 (2005): 417-422.

[54] Li, Suwen, Jing Guo, Mansun Chan, and Jie Yuan. "Multi-walled carbon nanotube coated microelectrode array for high-throughput, sensitive dopamine detection." In The

9th IEEE International Conference on Nano/Micro Engineered and Molecular Systems (NEMS), pp. 643-646. IEEE, 2014.

[55] Habibi, Biuck, Mojtaba Jahanbakhshi, and Mohammad Hossein Pournaghi-Azar. "Simultaneous determination of acetaminophen and dopamine using SWCNT modified carbon–ceramic electrode by differential pulse voltammetry." Electrochimica Acta 56, no. 7 (2011): 2888-2894.

[56] Luong, John HT, Keith B. Male, and Jeremy D. Glennon. "Boron-doped diamond electrode: synthesis, characterization, functionalization and analytical applications." Analyst 134, no. 10 (2009): 1965-1979.

[57] Suzuki, Akane, Tribidasari A. Ivandini, Kenji Yoshimi, Akira Fujishima, Genko Oyama, Taizo Nakazato, Nobutaka Hattori, Shigeru Kitazawa, and Yasuaki Einaga. "Fabrication, characterization, and application of boron-doped diamond microelectrodes for in vivo dopamine detection." Analytical chemistry 79, no. 22 (2007): 8608-8615.

[58] Arumugam, Prabhu U., Hongjun Zeng, Shabnam Siddiqui, Dan P. Covey, John A. Carlisle, and Paul A. Garris. "Characterization of ultrananocrystalline diamond microsensors for in vivo dopamine detection." Applied physics letters 102, no. 25 (2013): 253107.

[59] Xie, Songtao, Geoffrey Shafer, Christopher G. Wilson, and Heidi B. Martin. "In vitro adenosine detection with a diamond-based sensor." Diamond and related materials 15, no. 2-3 (2006): 225-228.

[60] Koehne, Jessica E., Michael Marsh, Adwoa Boakye, Brandon Douglas, In Yong Kim, Su-Youne Chang, Dong-Pyo Jang *et al*. "Carbon nanofiber electrode array for electrochemical detection of dopamine using fast scan cyclic voltammetry." Analyst 136, no. 9 (2011): 1802-1805.

[61] Xiao, X., J. Birrell, J. E. Gerbi, O. Auciello, and J. A. Carlisle. "Low temperature growth of ultrananocrystalline diamond." Journal of Applied Physics 96, no. 4 (2004): 2232-2239.

[62] Krauss, A. R., O. Auciello, D. M. Gruen, A. Jayatissa, A. Sumant, J. Tucek, D. C. Mancini *et al*. "Ultrananocrystalline diamond thin films for MEMS and moving mechanical assembly devices." Diamond and Related Materials 10, no. 11 (2001): 1952-1961.

[63] Halonen, Niina, Aatto Rautio, Anne-Riikka Leino, Teemu Kyllonen, Géza Toth, Jyrki Lappalainen, Krisztián Kordás *et al*. "Three-dimensional carbon nanotube scaffolds as particulate filters and catalyst support membranes." Acs Nano 4, no. 4 (2010): 2003-2008.

[64] Luo, Junxin, Yong Wu, and Shen Lin. "Recent Developments of Carbon Nanotubes Hybrid Assemblies for Sensing." Am. J. Nano Res. Appl 3 (2015): 23-28.

[65] Kong, Jing, Alan M. Cassell, and Hongjie Dai. "Chemical vapor deposition of methane for single-walled carbon nanotubes." Chemical Physics Letters 292, no. 4-6 (1998): 567-574.

[66] Chhowalla, Manish, K. B. K. Teo, C. Ducati, N. L. Rupesinghe, G. A. J. Amaratunga, A. C. Ferrari, D. Roy, J. Robertson, and W. I. Milne. "Growth process conditions of vertically aligned carbon nanotubes using plasma enhanced chemical vapor deposition." Journal of applied physics 90, no. 10 (2001): 5308-5317.

[67] Zhao, Haifeng, Hang Song, Zhiming Li, Guang Yuan, and Yixin Jin. "Electrophoretic deposition and field emission properties of patterned carbon nanotubes." Applied surface science 251, no. 1-4 (2005): 242-244.

[68] Burmeister, Jason J., Karen Moxon, and Greg A. Gerhardt. "Ceramic-based multisite microelectrodes for electrochemical recordings." Analytical chemistry 72, no. 1 (2000): 187-192.

[69] Talauliker, Pooja M., David A. Price, Jason J. Burmeister, Silpa Nagari, Jorge E. Quintero, Francois Pomerleau, Peter Huettl, J. Todd Hastings, and Greg A. Gerhardt. "Ceramic-based microelectrode arrays: recording surface characteristics and topographical analysis." Journal of neuroscience methods198, no. 2 (2011): 222-229.

[70] Burmeister, J. J., T. D. Coates, and G. A. Gerhardt. "Multisite microelectrode arrays for measurements of multiple neurochemicals." In The 26th Annual International Conference of the IEEE Engineering in Medicine and Biology Society, vol. 2, pp. 5348-5351. IEEE, 2004.

[71] Siddiqui, Shabnam, Zhenting Dai, Courtney J. Stavis, Hongjun Zeng, Nicolaie Moldovan, Robert J. Hamers, John A. Carlisle, and Prabhu U. Arumugam. "A quantitative study of detection mechanism of a label-free impedance biosensor using ultrananocrystalline diamond microelectrode array." Biosensors and Bioelectronics 35, no. 1 (2012): 284-290.

[72] Naguib, Nevin N., Jeffrey W. Elam, James Birrell, Jian Wang, David S. Grierson, Bernd Kabius, Jon M. Hiller *et al*. "Enhanced nucleation, smoothness and conformality of ultrananocrystalline diamond (UNCD) ultrathin films via tungsten interlayers." Chemical Physics Letters 430, no. 4-6 (2006): 345-350.

[73] McCreery, Richard L. "Advanced carbon electrode materials for molecular electrochemistry." Chemical reviews 108, no. 7 (2008): 2646-2687.

[74] Zeng, Hongjun, Andrew R. Konicek, Nicolaie Moldovan, Filippo Mangolini, Tevis Jacobs, Ian Wylie, Prabhu U. Arumugam, Shabnam Siddiqui, Robert W. Carpick, and John A. Carlisle. "Boron-doped ultrananocrystalline diamond synthesized with an H-rich/Ar-lean gas system." Carbon 84 (2015): 103-117.

[75] Song, Chuanzhe, Teresa A. Murray, Ryoichi Kimura, Makoto Wakui, Kevin Ellsworth, Sam P. Javedan, Syndia Marxer-Miller, Ronald J. Lukas, and Jie Wu. "Role of

α7-nicotinic acetylcholine receptors in tetanic stimulation-induced γ oscillations in rat hippocampal slices." Neuropharmacology 48, no. 6 (2005): 869-880.

[76] Pajkossy, Tamás. "Impedance of rough capacitive electrodes." Journal of Electroanalytical Chemistry 364, no. 1-2 (1994): 111-125.

[77] Barsoukov, Evgenij, and J. Ross Macdonald. "Impedance Spectroscopy Theory, Experiment, and Applications, A John Wiley & Sons." Inc., Publication, USA (2005): 13-20.

[78] Lasia, Andrzej. "Impedance of porous electrodes." In Electrochemical Impedance Spectroscopy and its Applications, pp. 203-250. Springer, New York, NY, 2014.

[79] Martin, M. H., and A. Lasia. "Influence of experimental factors on the constant phase element behavior of Pt electrodes." Electrochimica Acta 56, no. 23 (2011): 8058-8068.

[80] Kerner, Zsolt, and Tamás Pajkossy. "On the origin of capacitance dispersion of rough electrodes." Electrochimica Acta 46, no. 2-3 (2000): 207-211.

[81] Aaronson, Barak DB, Chang-Hui Chen, Hongjiao Li, Marc TM Koper, Stanley CS Lai, and Patrick R. Unwin. "Pseudo-single-crystal electrochemistry on polycrystalline electrodes: Visualizing activity at grains and grain boundaries on platinum for the Fe2+/Fe3+ redox reaction." Journal of the American Chemical Society 135, no. 10 (2013): 3873-3880.

[82] McMahon, Colm P., Gaia Rocchitta, Pier A. Serra, Sarah M. Kirwan, John P. Lowry, and Robert D. O'Neill. "The efficiency of immobilised glutamate oxidase decreases with surface enzyme loading: an electrostatic effect, and reversal by a polycation significantly enhances biosensor sensitivity." Analyst 131, no. 1 (2006): 68-72.

[83] Jerkiewicz, Gregory, Gholamreza Vatankhah, Jean Lessard, Manuel P. Soriaga, and Yeon-Su Park. "Surface-oxide growth at platinum electrodes in aqueous H2SO4: Reexamination of its mechanism through combined cyclic-voltammetry, electrochemical quartz-crystal nanobalance, and Auger electron spectroscopy measurements." Electrochimica Acta49, no. 9-10 (2004): 1451-1459.

[84] Bennett, Jason A., Jian Wang, Yoshiyuki Show, and Greg M. Swain. "Effect of sp2-bonded nondiamond carbon impurity on the response of boron-doped polycrystalline diamond thin-film electrodes." Journal of The Electrochemical Society 151, no. 9 (2004): E306-E313.

[85] Bard, Allen J., Larry R. Faulkner, Johna Leddy, and Cynthia G. Zoski. Electrochemical methods: fundamentals and applications. Vol. 2. New York: wiley, 1980.

[86] Notsu, Hideo, Ichizo Yagi, Tetsu Tatsuma, Donald A. Tryk, and Akira Fujishima. "Introduction of oxygen-containing functional groups onto diamond electrode surfaces by oxygen plasma and anodic polarization." Electrochemical and solid-state letters 2, no. 10 (1999): 522-524.

[87] Duo, I., C. Levy-Clement, A. Fujishima, and Ch Comninellis. "Electron transfer kinetics on boron-doped diamond Part I: Influence of anodic treatment." Journal of Applied Electrochemistry 34, no. 9 (2004): 935-943.

[88] Tu, Yudi, Takashi Ichii, Toru Utsunomiya, and Hiroyuki Sugimura. "Vacuum-ultraviolet photoreduction of graphene oxide: Electrical conductivity of entirely reduced single sheets and reduced micro line patterns." Applied Physics Letters 106, no. 13 (2015): 133105.

[89] Wang, Mei, Nathalie Simon, Gaelle Charrier, Muriel Bouttemy, Arnaud Etcheberry, Musen Li, Rabah Boukherroub, and Sabine Szunerits. "Distinction between surface hydroxyl and ether groups on boron-doped diamond electrodes using a chemical approach." Electrochemistry Communications 12, no. 3 (2010): 351-354.

[90] Datsyuk, V., M. Kalyva, K. Papagelis, J. Parthenios, D. Tasis, A. Siokou, I. Kallitsis, and C. Galiotis. "Chemical oxidation of multiwalled carbon nanotubes." Carbon 46, no. 6 (2008): 833-840.

[91] Ago, Hiroki, Thomas Kugler, Franco Cacialli, William R. Salaneck, Milo SP Shaffer, Alan H. Windle, and Richard H. Friend. "Work functions and surface functional groups of multiwall carbon nanotubes." The Journal of Physical Chemistry B 103, no. 38 (1999): 8116-8121.

[92] Lascovich, J. C., and S. Scaglione. "Comparison among XAES, PELS and XPS techniques for evaluation of sp2 percentage in aC: H." Applied surface science 78, no. 1 (1994): 17-23.

[93] Kulagina, Nadezhda V., and Adrian C. Michael. "Monitoring hydrogen peroxide in the extracellular space of the brain with amperometric microsensors." Analytical chemistry 75, no. 18 (2003): 4875-4881.

[94] Riquelme, Denise, Alvaro Alvarez, Nancy Leal, Tatiana Adasme, Italo Espinoza, Juan Antonio Valdés, Natalia Troncoso *et al.* "High-frequency field stimulation of primary neurons enhances ryanodine receptor-mediated Ca2+ release and generates hydrogen peroxide, which jointly stimulate NF-κB activity." Antioxidants & redox signaling 14, no. 7 (2011): 1245-1259.

[95] Gunasekar, P. G., A. G. Kanthasamy, J. L. Borowitz, and G. E. Isom. "NMDA receptor activation produces concurrent generation of nitric oxide and reactive oxygen species: implications for cell death." Journal of neurochemistry 65, no. 5 (1995): 2016-2021.

[96] Ferreira, Nuno R., C. F. Lourenco, Rui M. Barbosa, and João Laranjinha. "Coupling of ascorbate and nitric oxide dynamics in vivo in the rat hippocampus upon glutamatergic neuronal stimulation: a novel functional interplay." Brain research bulletin 114 (2015): 13-19.

[97] O'Neill, Robert D., Marianne Fillenz, Lars Sundstrom, and J. Nicholas P. Rawlins. "Voltammetrically monitored brain ascorbate as an index of excitatory amino acid release in the unrestrained rat." Neuroscience letters 52, no. 3 (1984): 227-233.

[98] Cammack, Jon, Behman Ghasemzadeh, and R. N. Adams. "The pharmacological profile of glutamate-evoked ascorbic acid efflux measured by in vivo electrochemistry." Brain research 565, no. 1 (1991): 17-22.

[99] Li, Ziyue, Yilin Song, Guihua Xiao, Fei Gao, Shengwei Xu, Mixia Wang, Yu Zhang *et al*. "Bio-electrochemical microelectrode arrays for glutamate and electrophysiology detection in hippocampus of temporal lobe epileptic rats." Analytical biochemistry 550 (2018): 123-131.

[100] Burmeister, Jason J., Erin R. Hascup, Kevin N. Hascup, Verda Davis, Seth R. Batten, Francois Pomerleau, Jorge E. Quintero *et al*. "REAL-TIME IN VIVO NEUROTRANSMITTER MEASUREMENTS USING ENZYME-BASED CERAMIC MICROELECTRODE ARRAYS: WHAT WE HAVE LEARNED ABOUT GLUTAMATE SIGNALING." Compendium Of In Vivo Monitoring In Real-time Molecular Neuroscience-Volume 1: Fundamentals And Applications 18 (2014): 113.

[101] Li, Ziyue, Yilin Song, Guihua Xiao, Fei Gao, Shengwei Xu, Mixia Wang, Yu Zhang *et al*. "Bio-electrochemical microelectrode arrays for glutamate and electrophysiology detection in hippocampus of temporal lobe epileptic rats." Analytical biochemistry 550 (2018): 123-131.